Temporal and Spatial Nanobiomaterials for Tissue Engineering and Drug Delivery

by

Yasmine Renee Doleyres

A dissertation submitted in partial fulfillment
of the requirements for the degree of
Doctor of Philosophy
(Macromolecular Science and Engineering)
in the University of Michigan
2020

Doctoral Committee:

Professor Jinsang Kim, Co-Chair
Associate Professor Kenichi Kuroda, Co-Chair
Professor Joerg Lahann
Research Associate Professor Suhe Wang

Yasmine R. Doleyres

doleyres@umich.edu

ORCID iD: 0000-0002-2319-7411

Dedication

This dissertation is dedicated to my parents, Jean Evans Doleyres and Danielle Lominy Doleyres, for loving and guiding me all of these years and to my dear sister, Dr. Helene Majisha Doleyres, whom I love so much. We share the same “title” now and no one can take that away from us, even if we change paths!

And to everyone whose light I have been able to enjoy over these 30 years of life and have added to my life and this journey in one way or another. This is yours too!

Acknowledgements

Despite how challenging and long the past 7.5 to almost 8 years have been during this PhD journey, I feel very privileged and blessed to have been on this path at the University of Michigan and a part of the Macromolecular Science and Engineering (Macro) Program. I thank the Lord for always ordering and guiding my steps throughout my life. I am especially thankful for the people that have been put in my life. I know none of it was an accident. There are very many, and I apologize if I forgot anyone. Your presence and light in my life is not forgotten, even if it was at the moment of writing this.

In guiding and helping me decide to go on to graduate school when I was very unsure and hesitant, **Dean Christopher Jones** at MIT (at the time) first took the time and helped me really understand what graduate school was all about, how to transition from being a "sponge to a source", how to learn to pay attention to cues on your performance from others, and that I could pursue graduate school. Thank you for taking the time to meet with me multiple times and get connected when I decided on Michigan!

Next, I would like to acknowledge my committee members. Thank you **Prof. Peter X. Ma** for letting me grow over the past 7.5 years in the lab. I have valued your lessons, time, and many stories. I'll never forget the day you told me I'm finally "thinking life a scientist" not too soon after this plan to wrap up was put in motion. Thank you to my co-chairs, **Prof. Kenichi Kuroda** and **Prof. Jinsang Kim** for stepping up and helping me get to this finish line. It has been a whirlwind finish, but I literally could not have gotten to this point without your time and

patience. Thank you **Prof. Joerg Lahann** for the enjoyable classes, feedback that I wish I sought more of, and support in my work. Finally, thank you **Prof. SuHe Wang**. I am so thankful Prof. Ma decided that I should collaborate with you during my PhD. I am so grateful for your care, genuine support, ambition, snacks, excitement for everything happening, and all around mentorship. You would say often how me stopping by your office brightened your day, but you have no idea how much you did the same for me.

There are numerous people that have helped my work/research and time at Michigan go smoothly. I would like to thank **Jesse Chen** for being a flow cytometry expert, being so patient through all of the different trials we had to run to get things just right, and listening to my latest crisis. It has been great working together. Thank you to **Dr. Owen Neill** at EMAL for all of your SEM help and hellos in passing, and **Jim Windak** for your help with so many instruments in the Chemistry building. Within the Dental Building, I would like to thank **Prof. David Kohn** for his mentorship and stories, **Amy Koh** for helping us secure valuable mice and your always sunny character, **Dr. Rajani Bhat** for your research advice and hellos in passing, the **BMS office** and **Office of Research (TEAM)** for making everything happen smoothly, our **delivery men**, the **nighttime facilities** team behind the scenes, and everyone around that made the day to day better. A thank you also to the old **Graduate Education office** that had the best staff, was incredibly helpful, and made volunteering for different activities so fun. And of course, thank you to the Macro administrative assistants over the years (**Nonna Hamilton**, **Adam Mael**, and **Julie Pollak**) who go above and beyond for our program and always have the answers.

The **Ma Lab** has been a unique place to work and fun community to be a part of over these 8 years. I have had so many labmates over the years and have been very fortunate to develop a good friendship and working relationship with almost everyone. A big thank you to all

of my past and present labmates, since there are just too many to name! I hope life gives us the opportunity to meet again, since we're so spread out around the world. Thank you for the skills and knowledge I was able to learn from you, for the good conversations and celebrations, for your friendship, for motivating each other, and for putting up with me when I wasn't in the best mood, especially towards the end. I would like to say a special thank you to soon-to-be **Dr. Renato 'Sam' Navarro**. Thank you for being my right-hand in the lab. Working so closely each day has made for some tense moments here and there, but beyond that there is so much I appreciate. Thank you for the fun collaborations we've come up with and the many that didn't work, for being able to learn from each other on a daily basis, for commiserating on the hard days, for always being excited about the little and big things even when I didn't want to get too excited, for always looking out for me, and for your friendship. I would also like to say a special thank you to **Dr**. **Kunal Rambhia** for your upbeat character and support throughout our collaborations and throughout my PhD overall, but especially towards in this "wrapping up" process. Thanks for reminding me "the best thesis is a done thesis"! Thank you to the undergraduate students who have worked alongside me: **Andrea Mathew**, **Clarence Womack**, **Amani Strong**, and **Mohamad Awada**. I truly valued your time and patience with me as we tried to figure things out.

I often tell people that I feel that I meet the best of the best people no matter where I am. A great number of people contribute to this sentiment, and I am so thankful for the eclectic and cool group of friends I've made and people I've met and been able to enjoy Ann Arbor with. To: my starting Macro cohort, Macro Program friends-especially my mentees, the UMich capoeiristas, the women in GradCru Bible studies, GradCru friends especially my dear **Dianne Roeper**, the UMich Haitians (Vin Lakay), the St. Thomas usher, and my "MIT@UMich"

friends, thank you so much for your friendship and great memories! Thank you to my roommates while I've been at Michigan: **LaPorscha Frazier**, **Violet Sheffey**, **Lauren Birks**, and **Dr. Ciara Sivels** (my longest roommate ever!) for always making "home" feel like home and for the many laughs and stories in bedroom doorways and apartment living rooms. Following these women, I would like to thank the amazing group of women that paved the way and also completed their PhDs (or are just about to) during my time here; they know who they are. I am always in awe of what you are all up to and how you balance life so gracefully. Thank you to my BBBS Little Sis, **KeShon Williams** and family for keeping me young and hip during the stresses of grad school. **Seth and Rachel Booth**: I am so thankful you guys moved to Michigan a little after I started and that our friendship was able to continue growing since 2007! Our Wednesday lunches became such a highlight of each week. Your love, time, meals during the really crazy times, and sharing you families with me will always mean so much! Thank you **Dr. Karis Buford** and the Stevenson family for all of your love and friendship as well and always taking care of me! I know my visits were far and few between, but they were always so much fun. To some additional life-long friends: **Dr. Arlyne Simon** (my sister-friend who first made Macro feel like it could be home), soon-to-be **Dr. Lydia Atangcho**, **Dr. Chukwuka "Chuky" Mbagwu**, soon-to-be **Dr. Astrid Raisanen**, **Mick Wollman**, **Dr. Ibrahim Boulares**, **Dr. Alan Teran**, **Dr. Jonathan Las Fargeas**, **Yingying Zeng**, **Nisha Hollingsworth**, **Shuyu Long**, **Prof. Diana Louis**, and soon-to-be **Dr. Genevieve "Genny" Romanowicz** (match maker extraordinaire ;-) and the greatest lab neighbor)—unfortunately I cannot write a whole dissertation to each of you, but I'll simply say you are all so dear to me and contributed to this journey in special ways. Hopefully I can keep reminding each of you this for many, many years to come. Remember Rush?! And to some more dear sisters for life: **Kerry Box**, **Dr. Razaz Mageid**, **Joy Ekuta**,

Breanna Berry, **Kristyn "Kiki" Berry**, **Rachel Empensando**, **Meagan Byrne**, **Dr. Olivia Beaubrun**, **Dr. Sarahjean Kerrole**, and **Jennifer Dorsey**—thanks for always making time to chat and catch up no matter how long it's been. I'm so thankful that I've been able to grow and change with all of you!

Finally, to my dear family. This really would not have been possible without you because you have set my foundation long before this PhD journey. Mom and dad (**Evans and Danielle**), thank you for always being my pillars and always pushing me and entertaining everything I've wanted to pursue in life. Yes, it all began with a postcard that I put in the trash and look how far we've come since then. I am so happy to complete this degree for you two as a testament to your sacrifices, love, support, and so much more. Thank you for also bearing with me when I didn't call home after it had already been a few days! **Maji**, my amazing big sister. I have always loved being able to follow in your footsteps. It seems like our conversations have gotten longer and longer as the years pass, and I enjoy every second of them. Thank you for always listening to me, encouraging me, and teaching me so much, although I know you won't think so. Thank you for teaching and modeling the biggest lesson of all—continued resilience—because life will always be challenging. And my dear nainaine, **Marie Lominy**, my second mom. The story wouldn't be complete without you! Thank you for your constant love, support, energy, and phone calls.

Last, but not least, my biggest silver lining through this long journey, my fiancé, soon-to-be **Dr. Wenshley Henry**. My love, I don't think my words will ever be eloquent enough to express my thanks to you. Meeting at the beginning of my sixth year was the greatest gift. I cannot picture what the end of my time at Michigan would have been like without you and the person you are; your visits and smiles throughout the working days are something I'll cherish forever because I'm not sure we'll have that working setup ever again! Thanks for being by my

side, wiping my tears, talking through things with me, and even running many, many samples for me late into the night with soon-to-be **Dr. Timothy Tamas** (thank you, Tim!!). Life is going to be so grand moving on from here with you! Thank you also to my sweet soon-to-be family that constantly has me lifted in prayer.

For all the prayers, thoughts, love, smiles, hugs, laughs, care packages, lunches, dinners, midday breaks, texts, videochats, visits, and just time—I'm so thankful!

I would also like to acknowledge the Rackham Merit Fellowship and T-32 Tissue Engineering and Regeneration Training Grant (TEAM) for funding my graduate studies.

Table of Contents

List of Tables

List of Figures

List of Appendices

Abstract

The intersection of materials science, biology, and nanotechnology has allowed for the development of advanced nanobiomaterials for tissue engineering and drug delivery. With more knowledge of how physical and chemical properties of a biomaterial influence cell function and response, it is important to impart different characteristics to materials with which cells will interact. Characteristics to consider for tissue engineering and/or drug delivery applications include: biocompatibility, mechanical properties, surface area, and ligand presentation. As foreign materials that are placed into the body and are not necessary permanently, these materials should also be biodegradable. Previous biomaterials have fallen short in many ways (i.e. lack of degradability, poor modulus matching, lack of porosity), as it is difficult to design a material with all necessary attributes. The more biomimetic and tailorable a material is, the better suited it is for these applications. New chemistries and approaches must be considered to incorporate all necessary characteristics. This work introduces two new materials that are characterized and evaluated for biomaterials applications and successfully overcome the temporal and spatial shortcomings of previous research.

2-methylene-1,3,6-trioxocane (MTC) is a hydrophobic monomer that is crosslinked with poly(ethylene glycol) diacrylate, a hydrophilic crosslinker, at varying crosslinker concentrations and molecular weights. In this work, with respect to tissue engineering, the materials' morphological changes, swelling, degradation, and elastic modulus properties are all assessed. Tunability is found in these properties as the crosslinker is adjusted and a hydrophobic-hydrophilic balance dictates many behavioral properties, including an atypical increase in

swelling as crosslinker concentration is increased. The biocompatibility is assessed with MTC formulations with 575 Da and 2 kDa crosslinker at 1.0% crosslinker concentrations exhibiting moderate swelling (<100%) and modulus of ~100 kPa showing good biocompatibility and utility for soft tissue engineering applications.

As a drug delivery system (DDS), crosslinked MTC samples were evaluated in terms of tunability and kinetics of drug release behavior. Drug release was tested for three different types of drugs: small molecule hydrophobic, small molecule hydrophilic, and a protein. From the 10-week studies, MTC hydrogels importantly demonstrated suitability for controlled release of the small molecule hydrophobic drug, with constant zero order kinetics displayed across crosslinker variations at physiological pH; the model protein, exhibited first order behavior and increasing drug release as crosslinker concentration increases. Rapid, 1 minute subcutaneous *in situ* gelling was also demonstrated in a mouse, making MTC advantageous as an injectable DDS.

Finally, polymeric nanoparticle functionalization is explored to improve drug targeting/internalization to treat HER2+ breast cancer. This strategy is tested by (1) comparing nanoparticles fabricated from a linear PEGMA-PLGA copolymer versus a novel palm-tree PEGPET-PLGA copolymer chemistry and (2) testing a new targeting peptide sequence and its modified targeting-internalization sequences through the addition of the TAT cell penetrating peptide sequence. Through early experiments, more than 2 times the binding affinity was measured *in vitro* for multi-functionalized nanoparticles compared to linear nanoparticles, showing that the increased peptide presentation on the nanoparticles' surface fabricated with the PEGPET-PLGA copolymer helps enhance cell targeting. Select combination peptide sequences with TAT also show evidence of increased HER2+ affinity.

From this thesis, contributions are made to the field of biomaterials by not only providing new materials and chemistries available for varied biomaterials use, but most critically, provides commentary on their necessity, methods to modulate these nanobiomaterials temporally and spatially and appropriate characterization, and their ongoing use.

Chapter 1. Introduction to Nanobiomaterials in Tissue Engineering and Drug Delivery

1.1. Necessity of nanobiomaterials in the field of medicine

The merging of the fields of biology, materials science, and nanotechnology has led to the advent of numerous solutions and strategies particularly in the field of medicine over the past few decades[(1)]. These traditional disciplines combined have formed the multidisciplinary area of nanobiomaterials[(2)]. Through nanobiomaterials approaches such as surface patterning techniques, biosensor fabrication, and nanoparticle development, strategies have been pursued that span the areas of prevention, diagnosis, treatment, and repair of numerous diseases and various injuries or defects sustained to the body. For this reason nanobiomaterials, or nanotechnology-derived biomaterials, encompasses a wide range of biomedical applications including their use for organ regeneration through a tissue engineering approach, as materials in drug delivery systems, and as nanomaterials used for medical imaging and sensing within the body. The ability to manipulate materials on this small scale, temporally and spatially, is extremely important in the applications listed, and a unifying focus of the work explored in this dissertation. Development of such ability is desired in order to fabricate improved materials, continue to advance the field, and produce results that are biomimetic. Manipulating materials can be approached in numerous ways, which generally include (1) spatial modifications through altering the surface topography, nanofeatures, mechanical properties, surface area/ processability, and adding functionalization, and (2) temporally by controlling the rate at which a material degrades or how slowly or quickly drug a drug is released, for example. Within the field, there is the need to continue developing and

advancing materials in these ways mentioned as new opportunities in nanobiomaterials can be achieved as the limitations of nanotechnology are surpassed.

Nanobiomaterials are defined in the literature as materials that support or aid biological function in the body with structures or components that are at the nanoscale (1-100nm) in at least one dimension or component, although less than 1000 nm is still classified as being on the nanoscale[1,3–5]. Materials at this size range are of interest because they exhibit a number of properties that differentiate them from larger bulk materials and make them advantageous for use in tissue engineering and drug delivery. These advantageous properties include: (1) greater homogeneity and purity in overall material composition and structure as reactions are taking place on the nanoscale, (2) a significant increase in surface area which allows for greater surface reactivity in both larger scaffold materials and smaller nanoparticles, (3) improved mechanical properties in overall bulk materials (i.e. high ductility and high yield strength of scaffolds and substrates) due to characteristics of their composition (i.e. increased grain boundary sliding and short-range diffusion), and (4) superior magnetic, optical, and electrical properties also due to the structural composition of a material[1]. With regard to their use as biomaterials, nanomaterials offer other characteristics that are not only beneficial but also necessary for superior interaction and performance in biological environments with cells and tissues. The first attractive characteristic of nanobiomaterials is that their chemical and structural compositions are able to show strong similarities to nanoscale hierarchical components of natural tissues, organs, and cells. For example, nanomaterials made from bio-based polymers for bone tissue engineering have been engineered to contain calcium phosphate, collagen, and glycosaminoglycans (GAGs), which are all components that help the scaffold mimic the nanostructure of native bone[6–8]. Similar examples can be found across multiple tissue types including: cartilage, skin, and cardiac

tissue among others[9–12]. Another attractive characteristic of nanobiomaterials is the ability to tailor the features or components of the materials to a size comparable to the biomolecules and structures being mimicked in the fabricated microenvironment. For example, nanofibrous scaffolds and microspheres have been developed and used for drug delivery and tissue engineering applications to enhance the growth of bone and cartilage tissues[13–15]. The fibers that comprise these drug delivery devices and cell carriers have fibers that range in size from 50-500nm in diameter and have been found to improve cell attachment as well as stimulate cell proliferation and differentiation. This phenomenon is hypothesized to take place because of how the fibers are able to recapitulate the extracellular matrix (ECM) architecture and promote advantageous cell-matrix interactions[14]. Finally, understanding the chemical and physical properties of nanomaterials allows them to be tailored to have specific physical and surface properties, providing the necessary spatial control needed to develop nanobiomaterials to which cells and the body respond well. Previous researchers have shown that the stiffness or rigidity of biomaterials can affect cell response and that the presence of different topographies and functional groups on the material surface can affect cell behavior and response[16–19].

While the detailed mechanisms of interaction between nanomaterials and biological systems, namely cells and tissues, are currently still being investigated, it is generally accepted that materials' surface and bulk properties dictate cell and tissues responses *in vitro* and *in vivo*[1,12,20]. The greatest take away for the field, and one that highlights the importance of nanobiomaterials and the continued work presented in these chapters, is that to be effective, biomaterials must incorporate physical and chemical properties that ultimately mimic native tissue, enhance cell interaction, or helps control the cell microenvironment in a temporal manner[21]. The types and ways in which nanobiomaterials have been used for biomaterial

applications for tissue engineering and drug delivery purposes are presented in the remainder of this chapter.

Part 1:

1.2. Nanobiomaterials for tissue engineering

The field of tissue engineering has developed as a way to overcome issues that are faced when tissues and organs must be replaced and/or repaired due to age, disease, or trauma. In general, the majority of organs and tissues within the human body innately face limited regenerative potential[22]. While some organs can self-regenerate, overtime as people age, cells and tissues often lose the ability to self-repair as the population and quality of progenitor stem cells decreases, limiting the healing capacity of tissues. Along the same lines, individuals who suffer a traumatic injury or develop a disease may necessitate tissue engineering or regenerative medicine approaches to heal certain defects[21,23]. Organ transplantation allows for damaged or diseased organs to be replaced by healthier organs, but this of course requires a donor organ or donor tissue, which is not always readily available. Organ transplantation also often commits patients to taking life-long immunosuppressants and carries the risk complications if the organ does not perform well after surgery[24,25]. Tissue engineering approaches aim to apply "the principles of engineering and of life science towards the development and biological substitutes that restore, maintain, or improve tissue or organ function" [24].

Tissue engineering, often interchangeably called regenerative medicine, involves the use of three major components, which are: (1) isolated cells, usually stem cells, to replace those that no longer function, (2) specific growth or differentiation factors to induce stem cells toward the desired tissue lineage, and (3) a three-dimensional, porous scaffold[26–28]. These components

altogether have been called the tissue engineering triad **(Figure 1.1)**. Many factors must be considered when choosing the appropriate cells and biological chemicals/ cues to include in a tissue engineering system; this dissertation, however, focuses on the different nanobiomaterials and novel biomaterials approaches that have been and continue to be developed for tissue engineering.

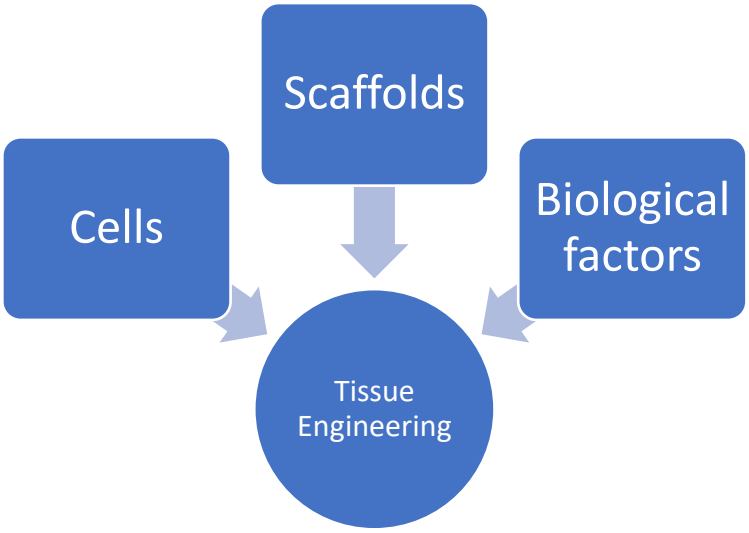

Figure 1.1: Components of tissue engineering triad.

Tissue engineering scaffolds, as the name implies, are materials that provide support for growing cells and act as a template for tissue formation. Scaffolds may be seeded with cells and/ or growth factors and cultured *in vitro* to allow for tissue growth in a dish or a more dynamic environment, such as a bioreactor, and subsequently implanted into the body; scaffolds can also be directly implanted *in vivo* with or without cells or growth factors to use the body's own mechanisms to support tissue growth[27]. The type of tissue that is being regenerated and whether it is a soft tissue or hard tissue dictates the type of nanobiomaterial that is appropriate as a scaffolding material, with a poor choice in material being detrimental to the expected tissue's growth. Scaffolding materials can be made from natural or synthetic materials and range from

self-assembled structures (i.e. peptides and polyelectrolyte multilayer assemblies), to polymers, ceramics, metals, semiconductors, and carbon nanostructures[1]. Polymers are arguably the most versatile of all these material types, and their versatility as a material to fabricate nanobiomaterials for tissue engineering and drug delivery (Part 2) is discussed here. An overview of common polymers used to develop tissue engineering scaffolds and scaffold design requirements and methods is presented in the next section.

1.2.1. Spatial and temporal requirements and fabrication of polymeric tissue engineering scaffolds

When considering 3D polymer scaffolds and the polymers that are ideal for their fabrication, there are multiple design requirements that should be incorporated to engineer the optimal tissue engineering substrate[27,28]. The first requirement is that the scaffold architecture must be considered and the scaffold must have high porosity with adequate pore size and interconnectivity. Porosity allows for cell migration throughout the scaffold and eventually cell proliferation and tissue formation. This is important whether cells are first seeded onto the scaffold *in vitro* or the scaffold is implanted *in vivo* and native cells are left to attach and move throughout the scaffold to form new tissue, blood vessels (vascularization), and nerves. Pores also allow for nutrient and waste exchange throughout the scaffold, which is critical for cell and tissue survival. The next requirement is that scaffolds should have high surface area; the nature of 3D porous scaffolds allows them to readily fulfill this requirement. A high surface area is critical as cells must attach to a surface in order to survive and many developing tissues require a high cell number and good cell-cell contact for survival and growth, which can only be achieved through a high surface area structure. As new tissue needs to form in the place of the scaffold,

the third requirement is biodegradability. Scaffolds must degrade at a suitable rate to match tissue formation so as not to inhibit tissue growth and extracellular matrix formation. If the scaffold degrades too slowly tissue formation will be prevented, and a scaffold which degrades too rapidly leads to a lack of cell guidance. An additional aspect of this requirement is that the intact scaffold and the degradation by-products should have good biocompatibility. This means that all components and degradation products should be non-toxic and should not interfere with the function of any organs or be adversely immunoreactive. The final requirement, and one that is difficult to achieve, is developing a scaffold with good mechanical properties that mimic the tissue that is being replaced. The scaffold should be mechanically sound to allow for easy handling and implantation, have good mechanical integrity which can be difficult to maintain once pores are introduced into the substrate, and have a modulus that matches that of the native tissue being regenerated. As was alluded to previously, substrate stiffness and how proteins and cells are able to interact with the scaffold affect proliferation and differentiation[29,30]. Finally, as it pertains to the future of tissue engineering and translation of materials into the clinic, it should be possible to scale-up the production of scaffolds made at the bench and this process should be cost-effective. Along with this, the length and ease of storage and whether off-the shelf availability is possible should be considered. By meeting all of these design criteria, scaffolds should allow for good cell adhesion, growth, migration, and differentiation leading to the formation of stable and healthy tissues.

Many natural and synthetic polymers and polymeric blends of both types of polymers are able to satisfy all of the requirements discussed above, especially synthetic polymers. The most commonly used synthetic polymers in tissue engineering are linear aliphatic polyesters, namely poly(glycolic acid) (PGA), poly(lactic acid) (PLA), and copolymers of both called poly(lactic-

co-glycolic acid) (PLGA)[28,31]. Synthesized through the ring-opening polymerization of cyclic dimers, these polymers are recognized as biocompatible and degrade via hydrolysis into components, lactic acid and/ or glycolic acid, that the body is able to process. These polymers are also Food and Drug Administration (FDA) approved, which makes them ideal for clinical use. PGA has the simplest chemical structure and is the most hydrophilic, which makes its degradation rate rather short, ranging 2-4 weeks, depending on the molecular weight. PLA, which varies from PGA by the presence of a pendant methyl group, is more hydrophobic and therefore undergoes hydrolysis less readily than PGA and can take months to years to degrade also depending on the molecular weight. The copolymer of PGA and PLA, PLGA, is often used to achieve intermediate degradation rates. Different ratios of glycolic acid and lactic acid are used in the copolymer (i.e. 85:15, 75:25, 50:50, 25:75, and 15:85) in order to achieve an ideal degradation rate as well as mechanical properties when developing a scaffolding material. The degradation rate of these copolymers is a balance between two factors, (1) the hydrophobicity and hydrophilicity and (2) the stereoregularity/ crystallinity of the copolymer, which is disrupted when different repeated units are introduced[28]. Other linear aliphatic polyesters that are biocompatible and biodegradable are used in the field, such as polycaprolactone (PCL), poly(hydroxybutyrate) (PHB), and poly(glycerol sebacate) (PGS). PCL is a semicrystalline polymer with a very low glass transition temperature of -62°C and is therefore always in a rubbery state. PHB is produced via fermentation and is a highly crystalline and brittle polymer. Both PCL and PHB degrade at significantly slower rates than PGA, PLGA, and PLGA on the timescale of years, which makes them less attractive for use in developing tissue engineering scaffolds. PGS, on the other hand, is a polyester synthesized via a two-step polycondensation and cross-linking reaction of glycerol and sebacic acid, two inexpensive and FDA approved

components. The mechanical properties of PGS can be tuned by changing the curing time, curing temperature, and component concentrations. Unique from all of the polymers mentioned, PGS exhibits thermoset elastomeric properties, which makes it particularly useful for soft tissue applications[31]. However, it is difficult to solubilize in traditional organic solvents and a challenge to process due to its tackiness, which makes it not ideal for scaffold fabrication[32].

Besides meeting the requirements of biocompatibility, biodegradability, and mechanical tunability through composition changes, the synthetic polymers mentioned can be processed into 3D porous scaffolds. One of the ways in which 3D scaffolds are made is using 3D printing. In 3D printing, a computer-assisted-design (CAD) file is prepared and used to directly print structures made from biodegradable polymers. Multiple layers of polymer are printed and they are bound together using an added binding material. While very attractive as a technique and advantageous in the precise control and reproducibility provided, 3D printing is limited in the size of features that can be produced which is limited to hundreds of micrometers as there is a pixel/ resolution limit. Smaller features have been printed using two-photon laser printing where an infrared laser polymerizes precise areas in a monomer solution that is mixed with a photoinitiator. While this laser technique provides good resolution on the nanometer scale, this technology is still rather costly due to the specialized equipment needed. This laser technique also has limited materials selection and produces heterogeneity within the structure due to ranges in the materials' particle size. Another alternative method for creating complex 3D scaffolds involves patterning through lithography[33]. This technique, however, faces the same limitations as 3D printing as far as equipment needed, resolution, and scaffold heterogeneity.

Creating interconnected, porous scaffolds has been done using a widely used reverse fabrication process originally developed in the Ma lab. In this process, a porogen is used to

create interconnected spherical pores[34–37]. Paraffin spheres, followed by sugar spheres that decrease the process time and eliminates the need for organic solvents during the porogen dissolution step, are produced and put into a 3D mold where they are then slightly melted together through a heat treatment process. Polymer is then cast into the paraffin or sugar template. Once the polymer is set, the porogen-polymer construct is put into an organic solvent or distilled water to dissolve the paraffin or sugar, respectively. Using different sets of sieves, 3D scaffold disks with pores in the range of 250-400µm, 125-250µm, and 60-90µm have been developed **(Figure 1.2)**. Synthetic polymers have been used extensively in tissue engineering approaches using the techniques mentioned as well as many other techniques that have not been discussed (i.e. gas foaming, etc.[38–40]) to regenerate or support the repair of numerous soft and hard tissues[1]. These polyester polymer blends are well suited to be processed in this way and form high surface area, 3D scaffolds with nanofeatures and good mechanical properties which arise from their intrinsic chemical properties and ability to achieve sufficiently high molecular weights.

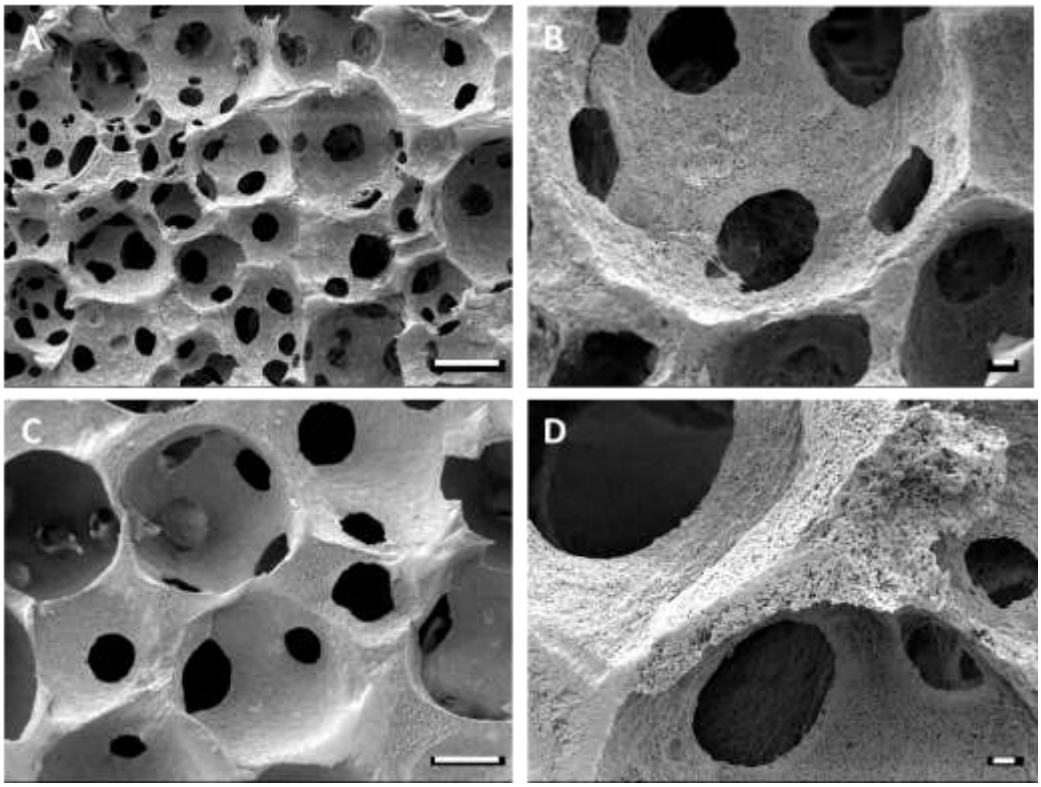

Figure 1.2: Interconnected, porous 3D scaffolds made with sugar porogen. Scanning Electron Microscopy (SEM) images show poly(L-lactic acid) scaffolds with **(A)** 125-250 µm pores at 150x, **(B)** 125-250 µm pores at 500x, (C) 250-400 µm pores at 150x, and **(D)** 250-400µm pores at 500x (Scale bar= 100 µm in **(A)** and **(C)**; Scale bar=10 µm in **(B)** and **(D)**.

1.2.2. Designing hydrogels as tissue engineering scaffolds

An important class of polymeric scaffolds that are used in tissue engineering is hydrogels. Hydrogels, which were first synthetically developed with the advent of contact lenses in the 1950-60s, are 3D crosslinked networks of polymer that are crosslinked through covalent bonds formed via ultraviolet/radical polymerization, click chemistry, thermal gelation, and radical polymerization or through physical intramolecular or intermolecular forces such as ionic bonding, hydrogen bonding, and hydrophobic interactions[41–44]. Unique compared to the polymers previously mentioned, hydrogels absorb large amounts of water anywhere from hundreds to thousands of times their dry weight, swell without dissolving or losing their structure

immediately, and generally have a soft and rubbery appearance in their swollen state. Hydrogels have gained attention over the years as scaffolds for tissue engineering application because of numerous attractive characteristics. These include their more hydrophilic nature and likeness to biological tissues largely comprised of water, their injectability which makes them ideal for filling irregularly shaped defects and performing minimally invasive procedures, and their ease of modification which allows cells, growth factors, and ligands to be incorporated into the precursor hydrogel material. The hydrophilic nature of hydrogels in solution has other advantages when compared to traditional polymeric scaffolds in that they provide an aqueous environment that can protect cells and encapsulated drugs as well as aid in transport of nutrients and wastes to and from cells[42]. Similar to the more hydrophobic polymers previously mentioned, hydrogels can be natural, synthetic, or a composite of both naturally occurring and synthetic hydrogel materials. Natural hydrogels are made from naturally occurring macromolecules found in the body and in nature such as polynucleotides, polypeptides, and polysaccharides[41,45]. Some well-known natural hydrogels include chitosan, collagen, silk, and alginate. These hydrogels have a number of benefits including intrinsic biocompatibility, cell-mediated degradability, and innate cell binding and interaction motifs. Their disadvantages for use in tissue engineering lie in that they have high batch to batch variation and exhibit a limited range of mechanical properties, especially after processing for reuse as a biomaterial. Synthetic hydrogels, on the other hand, can be made with more precise control in chemistry, structure, and function[45]. This control allows hydrogels with specific mechanical properties to be fabricated. By adjusting the amount of crosslinker or controlling the crosslinking density, hydrogel stiffness can be tuned, which is a critical advantage of synthetic hydrogels and makes them a more versatile material to create tissue engineering scaffolds.

To perform as a tissue engineering construct, hydrogel scaffolds must meet many of the same requirements listed for non-hydrogel scaffolds, mainly (1) they must be biocompatible, (2) biodegradable, (3) have high porosity and high surface area, (4) have good mechanical properties for the tissue being regenerated, and (5) be cost effective and easily scaled up in production for future translation into the clinic. The biggest issue with many hydrogels developed in the literature is that they lack biodegradability, have weaker mechanical properties than desired, and tend to be non-adhesive to cells. An example of this would be poly(ethylene glycol) (PEG), which is widely used as a bulk material to create synthetic hydrogels[28,43]. PEG is recognized as a chemically and biologically inert material in the field of biomaterials and is often used to prevent cell and protein adhesion. When PEG is used in tissue engineering scaffolds, however, it is often functionalized by using PEG derivatives with functional groups that can attach various adhesion ligands and peptides that help with cell attachment. PEG derivatives are also often used as a crosslinker rather than the bulk hydrogel material. While PEG is FDA approved and its use has many benefits, the greatest disadvantage is that PEG is not degradable. PEG must be manipulated either through copolymerization with degradable polymers such as PGA and PLA mentioned earlier, or by adding matrix-metalloproteinase (MMP)-degradable linkages off of the PEG backbone. This latter process allows PEG constructs to be broken down by enzymes *in vitro* or *in vivo*.

Two more commonly used polymers for hydrogel fabrication and tissue engineering purposes are poly(2-hydroxyethyl methacrylate) (PHEMA) and poly(vinyl alcohol)[43,46]. PHEMA is characterized by its permeability and hydrophilicity, and with suitable crosslinker, PHEMA is used for contact lenses and other ophthalmic applications. Poly(vinyl alcohol) (PVA) is produced from poly(vinyl acetate) and its hydrophilicity and solubility can be controlled by

adjusting the molecular weight. PVA is fashioned into hydrogels by physically crosslinking most commonly with glutaraldehyde. Similar to PEG, PHEMA and PVA are also chemically and biologically inert materials that require functionalization and the incorporation of biologically active motifs. While bioinertness is often seen as a disadvantage of synthetic hydrogels, it can be advantageous when it allows for more control in the type and amount of bioactive ligands that are added to the hydrogel which helps regulate cell attachment and behavior. Hydrogel scaffolds can also void or minimize the amount of non-specific protein absorption and protein fouling, which helps these bioinert materials avoid the foreign body response when implanted *in vivo*. Overall, these hydrogels are more tailorable and can be more precisely designed for specific use. The benefits of hydrogel scaffolds in tissue engineering work and the ability to manipulate hydrogels as a nanobiomaterial is explored throughout this dissertation by characterizing a novel hydrogel material and assessing its biocompatibility and applicability for future tissue engineering goals. The monomer class, specific monomer examples, and the monomer selected to form a novel hydrogel in this work is introduced in the next section.

1.2.3. Introduction to cyclic ketene acetals, MDO and MTC

The monomer 2-methylene-1,3-dioxepane (MDO) and its "second generation" molecule, 2-methylene-1,3,6-trioxocane (MTC) are two of the most basic cyclic or ring monomers from a class of polymers known as cyclic ketene acetals (CKAs) **(Figure 1.3)**. First developed in the 1980s, CKAs are a unique class of polyesters that have not been as heavily explored as traditional aliphatic polyesters[47,48]. Unlike cyclic esters such as lactide, glycolide, and ε-caprolactone which undergo ring-opening polymerization, CKAs undergo a radical ring-opening polymerization (RROP) process, which takes places because of a radical addition process at the

vinyl bond[49,50] **(Figure 1.4)**. This addition is followed by a molecular rearrangement that is exclusive to CKAs and leads to the formation of an ester linkage in the polymer backbone. Ester linkages are advantageous, especially as it pertains to biomaterials, because through hydrolysis they impart degradability to a material. CKAs are an exclusive class of monomers because they are the only ones that allow for the synthesis of poly(vinyl-co-ester) materials, and through RROP, the synthesis of functionalized polyesters and degradable vinyl polymers. MTC is slightly more hydrophilic than MDO due to the addition of an oxygen molecule in its ring structure, making it more ideal as a biodegradable material. With a chemical structure nearly mimicking that of the previously mentioned polymer PCL, early work alluded to the possible use of this polymer as a biomaterial. The low molecular weights achieved during polymerization, however, has limited MTC's utility for fabrication into robust scaffolding constructs for cell testing and subsequent tissue engineering use[51–53]. By taking advantage of the MTC monomer chemistry, these issues can be overcome by forming a crosslinked hydrogel, which is of infinite molecular weight and holds its shape in solution[54]. Novel MTC hydrogels are characterized on the nano/micro- and macroscale and are tailored to meet the requirements of a hydrogel for tissue engineering as described in the previous section.

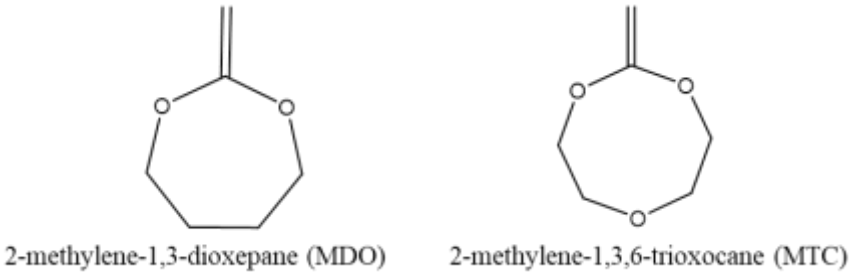

Figure 1.3: Cyclic ketene acetal (CKA) monomer rings for MDO and MTC.

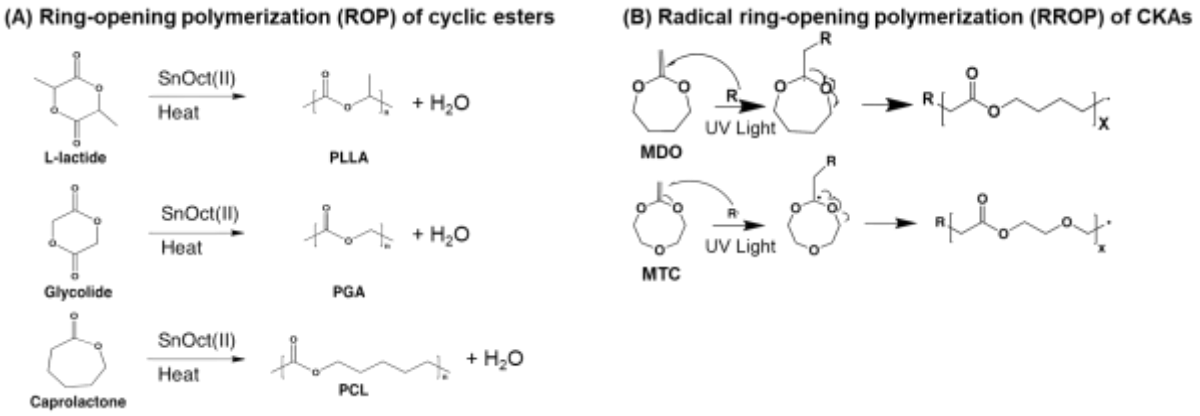

Figure 1.4: Illustration of ring-opening polymerization (ROP) versus radical ring-opening polymerization (RROP). (A) ROP of cyclic ester monomers and (B) RROP of cyclic ketene acetal (CKA) monomers.

Part 2:

1.3. Nanobiomaterials for drug delivery

In addition tissue engineering, nanobiomaterials are essential to the field of drug delivery and the larger field of nanomedicine. As the name suggests, the goal of developing drug delivery systems are to serve as effective delivery strategies of therapeutic drugs and agents to specific sites of the body, usually in a controlled and/or targeted manner[55]. Today, a number of drugs are being developed to treat various diseases faced by the general population of the United States such as cancer, cardiovascular, inflammatory, and microbial diseases. These drugs are costly, and from initiation of development through completion of clinical trials, can cost upwards of $1 billion dollars while spanning a decade or longer to produce[56]. Along with the high costs and time that goes into producing these drugs, many fail to reach the end of clinical trials due to biocompatibility or toxicity issues, and fewer make it to the marketplace due to known severe side effects[55,57]. Some of the current issues with many drug compounds include poor: *in vivo* stability, bioavailability, drug solubility, absorption in the body, and issues with toxicity. An additional issue is the difficulty in controlling delivery of the therapeutic agent to a specific site

of the body Along with off-target effects, the greatest issue with traditional drugs in pill or injection form is that, even when taken as prescribed, dose-related toxicity issues often arise due to constant fluctuations in drug concentration in the blood[58]. Nanobiomaterials strategies developed over the last 40 years have allowed some of the challenges associated with the delivery of therapeutics to the body to be overcome. These challenges have been overcome particularly by creating materials-based drug delivery systems, to more effectively help cells interact with the varying pharmaceutical agents.

There are a number of advantages that are afforded by combining nanotechnology and the field of drug delivery/ nanomedicine[59,60]. The greatest benefit of drug delivery, outside of allowing more drugs to be viable treatment options due to increased drug solubility and bioavailability, is an increase in the efficacy of the many different drug molecules that can be delivered using similar drug delivery strategies. Some of the more challenging molecules to deliver include DNA, RNA, and some cancer therapy agents; this is difficult due to their propensity to become denatured or be cleared by the body, and thus, need adequate protection to travel and reach their target sites[3]. Through encapsulation, drug delivery vehicles are able to form a protective shell that better protects these drugs from harsh conditions such as the highly acidic environments of the stomach and lysosomes or enzymes and proteases traveling within the bloodstream that breakdown many drugs. Another advantage of nanobiomaterials is the ability to deliver drug agents to areas of the body that were once impossible to reach with conventional methods such as the blood brain barrier (BBB)[61,62]. The BBB is comprised of a dense and tight network of vasculature from the central nervous system that acts as a physical barrier to protect the brain. Many drugs including antibodies, chemotherapeutic agents, and peptides are inhibited from passing through the vessels and capillaries of the BBB. Treating diseases that arise in the

brain requires strategies which allow passage through this challenging network. Along with helping to maintain doses of drug at a constant therapeutic level for a longer period of time within the body, another crucial advantage of drug delivery systems is reducing the instances of drug-induced toxicity. Through using these drug delivery methods, more of the drug delivered is able to get to the intended site of action and perform its function. Because of this, a lower initial dosage of drug can be administered to the patient because a smaller proportion of the drug is lost during transit. Having a lower amount of drug released throughout a patient's system and away from intended site leads to decreased systemic toxicity and diminished side effects. Diminished instances of drug-induced toxicity will inevitably lead to fewer deaths due to drug complications and milder side effects. Further, reduced instances of complications due to systemic toxicity have the potential for improving patient compliance.

The possibilities for creating drug delivery systems are numerous due to the availability of different materials that can be used and nanotechnology techniques which can be employed. Generally, nanocarriers are within the size range of 1-1000nm and can be classified into two classes: inorganic and organic carriers[60]. With a focus on polymeric drug delivery systems, different categories of organic carriers will be discussed in the next section.

1.3.1. Types of organic nanocarriers and polymers used for fabrication

Drug delivery nanocarriers are fabricated with many variables in mind including the choice in ideal chemistry or material that should be used and the form or geometry that the carrier should take[1]. Options for chemistry range from polymers, semiconductors, sol-gels, and self-assembled structures made from proteins and DNA. The different geometries or forms that nanocarriers can take include various shapes such as nanorods, nanoparticles, and nanoscaffolds. The most

common type of nanocarrier is the nanoparticle. Nanoparticles offer many benefits as a drug delivery vehicle, many of which are based on the principles of nanotechnology and nanomaterials. With a small size and round shape, nanoparticles have a higher payload-to-mass ratio, are easy to mass produce, and are injectable, making their delivery minimally invasive. The small size of nanoparticles also makes them good at achieving long circulation times within the body, by avoiding macrophage uptake, and allows them to circulate relatively quickly[63]. Nanoparticles can pass through very small blood vessels and capillaries and, as a result, can be easily uptaken by target cells through endocytosis. Many subclasses of nanoparticles exist and those used most often are discussed here. Included as subclasses of nanoparticles are polymeric nanoparticles, micelles, polymeric liposomes (also called polymersomes), and dendrimers.

Polymeric nanoparticles are most commonly used in drug delivery strategies published throughout the literature. Based on the polymer that is used to form these particles, polymeric nanoparticles can be designed to tailor the release profile of the encapsulated drugs and thus creating a controlled drug delivery system. The drug release profile from these subcellular-sized particles is based on the degradation rate of the polymer and can often be adjusted by increasing or decreasing the molecular weight of the selected polymer. The synthesis and encapsulation of drugs into nanoparticles can be done through different nano-formulation methods such as emulsion, diffusion, solvent evaporation, nanoprecipitation, homogenization, sonication, and dropwise addition processes among others. These methods of encapsulation can be summarized as either a process that (1) entraps the drug into a particle core (nanocapsule) or within a polymeric matrix (nanosphere) or (2) a surface adsorption process **(Figure 1.5)**. The most commonly used synthetic polymers to fabricate polymeric nanoparticles include poly(lactic-co-glycolic acid) (PLGA), PLA, PCL, and poly-alkyl-cyanoacrylates[64]. These polymers have been

used to encapsulate and/or physically adsorb onto the particle surface a wide variety of drugs and molecules including anticancer drugs, insulin, antibiotics, anti-inflammatory drugs, and hormones among others.

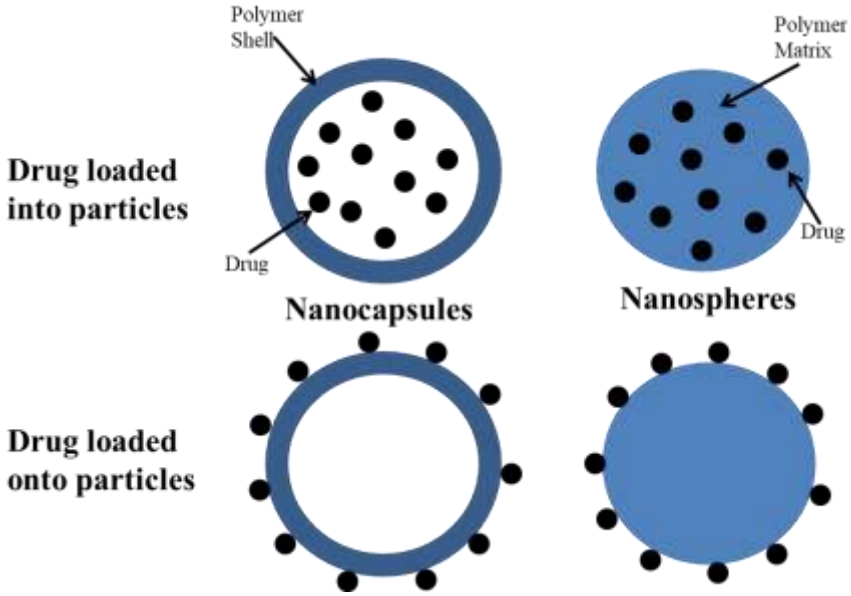

Figure 1.5: Two main classes of polymeric nanoparticles.

Within the class of polymeric nanostructures that are developed for controlled release drug delivery applications, there are specific nanoparticle architectures that have been developed to take advantage of different chemistries and load drugs with different properties. The three most commonly used architectures include micelles, dendrimers, and polymer liposomes (polymersomes). Polymeric micelles are nanospheres that are formed by using amphiphilic block copolymers that self-assemble when fabricated in a hydrophilic aqueous environment, with the hydrophilic portion forming the outside of the particle and the hydrophobic segment forming the inner region of the particle[3,57,59,65,66]. Generally, the hydrophobic core surrounds and encapsulates the added drug and the hydrophilic shell functions to increase both the drug and particle solubility. Release of the drug is achieved by disrupting the micelle's chains, which can

be done through a change in pH, temperature, or another stimulus at the target site. The most common amphiphilic di-block copolymers used to fabricate micelles are composed of a hydrophobic block of PLGA grafted to a hydrophilic PEG block or another derivative of PEG based block copolymer. These micelles that are formed tend to be around 100 nm in diameter. This size allows them to escape the clearance mechanisms of the renal and reticulo-endothelial systems, circulate throughout the body with greater residence times *in vivo*, and take advantage of the leaky vasculature which is often found in tumors. Micelles have been used extensively in research to encapsulate chemotherapeutic drugs with doxorubicin, paclitaxcel, and cisplatin being the preeminent examples.

Similar to micelles, polymersomes are also made of amphiphilic block copolymers, but unlike micelles, these block copolymers form a bilayer structure analogous to the phospholipid bilayer structure that makes up the membrane of cells in the human body[(67)]. Different from micelles, the inner cores of polymersomes form an aqueous hydrophilic core rather than a hydrophobic core. Because of this structure, there is greater variability and versatility in the type of drugs that can be loaded into this architecture. For instance, a hydrophilic drug can be loaded into the hydrophilic core or a hydrophobic drug can be entrapped within the hydrophobic bilayer chains. Similar to the previous particle types, polymersomes have been used to encapsulate and delivery hydrophobic and hydrophilic drugs, especially chemotherapeutics[(68,69)].

Lastly, dendrimers are another major group within the category of polymeric nanocarriers. Dendrimers are hyperbranched spherical structures where the branches originate from a central core[(59)]. They are attractive for use in drug delivery because their structure provides the ability to hold drugs in the core microenvironment formed by the surrounding branches and allows for packing within the spaces of the multiple branches. Depending on the

dendrimer chemistry, the dendrimer surface can be highly functionalized, with end groups dictating the macroscopic properties of the dendrimer[70]. Similar to the particle types previously mentioned, dendrimers have been used to deliver varying drugs such as common anticancer therapeutics named earlier. Polyamidoamine (PAMAM), a classically used dendrimer polymer, has been employed in drug delivery to conjugate doxorubicin through amide and hydrazone linkages for photochemical release of the drug inside cancer cells and has also been used as a non-viral vector for DNA gene delivery[71,72]. While the hyperbranched structure of dendrimers may be desirable and allow for a high degree of functionalization, drugs loaded into dendrimers are often released quickly and fail to achieve long-term release due to the lack of encapsulation of the drug by dendrimers[73,74]. Choosing an ideal nanocarrier or drug delivery system relies on thorough knowledge of the physical and chemical properties of the drug being loaded as well as the encapsulation and release kinetics of the different particle systems mentioned. This allows better decisions to be made on the most advantageous particle system for efficient delivery of different therapeutic agents.

1.3.2. Hydrogels for drug delivery

Along with the polymeric nanoparticles that have been developed as drug delivery systems, hydrogels, previously mentioned for their utility in tissue engineering, have also been utilized in the drug delivery space to create controlled drug delivery systems[75,76]. Hydrogels are crosslinked networks of homopolymers or copolymers that are formed into three-dimensional structures and are highly biocompatible due to the high water content of these systems[77–79]. The crosslinks within these constructs help provide the overall structure and physical and chemical integrity to hydrogels. When placed in an aqueous environment, hydrogels exhibit a swelling

behavior that is not only dependent on the chemical structure and degree of crosslinking, but can also be dependent on the environmental conditions such as temperature, electromagnetic field, pH, and presence of ions.[80]. The characteristic physical properties of hydrogels make them particularly useful for drug delivery use as they are generally highly porous and form an internal mesh, which can be tuned by adjusting the crosslink density and changing the swelling dynamics. This mesh network and porosity allows for drugs to be loaded directly into the gel matrix or into polymeric nanoparticles that are subsequently loaded into the gel matrix. Drug is then released at a diffusion rate that is also dependent on the hydrogel swelling rate and degradation rate, which must tested and tuned depending on the desired release behavior. Similar to the polymeric nanoparticles previously described, many different therapeutic molecules have been delivered using hydrogels including small molecule hydrophilic drugs and more fragile biomacromolecules such as peptides, protein, and DNA, which are often harmed by the degradation byproducts of polymeric nanoparticles. Many hydrogels fail to meet the ability to release small molecule hydrophobic drugs in a controlled manner, which highlights a need for hydrogels that meet this criterion[81]. Nevertheless, encapsulating these hydrophilic drug agents has been done by fabricating hydrogels into nanoparticles, microparticles, coatings, thin films, and standalone drug reservoirs. A number of synthetic polymers have been explored for hydrogel drug delivery purposes including poly(hydroxyethyl methacrylate) (HEMA), poly (*N*-isopropylacrylamide) (PNIPAAM), PVA, PEG block copolymers with PLGA, PLA and other hydrophobic segments, and poloxamer/ Pluronic based block copolymers comprised of poly(ethylene oxide) and poly(propylene oxide)[76–78]. There are a number of design criteria when developing an ideal drug formulation. Taking into account transport properties (crosslink density, polymer-drug interactions, hydrogel degradation rate), physical properties (component

concentrations and molecular weights, temperature, pH, ionic strength), and biological properties (component and construct biocompatibility) is crucial in designing the most efficient hydrogel system[75]. This topic is further explored within this dissertation.

1.3.3. Targeted drug delivery

In designing drug delivery system using nanobiomaterials strategies, one of the greatest considerations that must be made is whether the system will be a passive targeting system or an active targeting system[64,82–87]. Passive targeting refers to drug delivery approaches that take advantage of natural properties of the developed system and phenomena within the body to help nanoparticles accumulate at an intended site of action. Passive targeting simply refers to a nontargeted system that relies on the particle size and surface charge to aid in transport through the body. By achieving long term circulation in the body based on these parameters, particles can increase uptake into tumors or disease areas simply due to concentration gradients. Specific to solid tumors, particles can achieve high accumulation in the tumor mass due to the enhanced permeability and retention (EPR), which happens when a rapidly growing tumor forms a leaky vasculature network and develops inefficient lymphatic drainage system[87,88]. While nanotechnology is beneficial in this scenario and is more effective than systemic delivery of the free drug, it is not the best delivery approach.

Active targeting, on the other hand, takes passive or nontargeting drug delivery systems and chemically attaches or physically adsorbs a targeting agent to the surface of the nanocarrier[3,59,89]. The targeting agent must have high affinity and be specific to a tissue or cell ligand, helping to home particles to a site of action. This active targeting strategy increases the efficacy of the nanoparticle itself and, in turn, that of the loaded drug. Active targeting is

particularly useful in treating different cancers and similar diseases where a ligand is overexpressed and/or not present on healthy cells[86]. There are a couple factors that contribute to how well an actively targeted approach works including the conjugated ligand's density, the size of the nanoparticles, and the charge on the nanoparticle surface. The greatest consideration, however, is the choice of targeting ligand presented on the particle surface. A recent study has shown that many particles fail to reach their target sites, with only 0.7% of administered particles reaching their target tumor cells, due to multiple factors, including poor ligand selection, affinity, and particle internalization[90]. The choice of ligand includes small molecules such as vitamins, sugars, and aptamers (nucleic acids), but most commonly are proteins, antibodies, or peptides[83,86,89]. Proteins have been considered in creating actively targeted drug delivery systems because of their great affinity for various targeting receptors[83]. Overall the use of whole proteins is not ideal, however, due to their large size and the complexity involved in attaching them to the surface of nanocarriers. Monoclonal antibodies have also been conjugated to the surface of nanoparticles and take advantage of specific antibody-antigen interactions to help treat a disease. The mechanism of action of these monoclonal antibodies conjugated to a particle surface include interfering with another antibody- antigen interaction, or binding itself to the antigen on the cell surface to suppress protein expression. Antibodies have been used widely within research over the past couple decades. The most well-known antibody targeting treatments would be for the targeting of epidermal growth factor receptor (EGFR/HER2). Since EGFR is involved in cell proliferation, antibodies are often used to block EGFR activation using an antibody-interference strategy. Other strategies, such as the use of the drug trastuzumab, which is a monoclonal antibody, actively work to kill HER2 overexpressing (HER2+) cancer cells. While the use of antibodies allow for high specificity in targeting, their use also carries

notable disadvantages. The disadvantages of using antibodies include the exorbitant cost associated with their development, modification, and research which leads to expensive drug production, their propensity to trigger immune responses in humans, and their poor ability to penetrate tumors due to the large size and bulkiness of the antibody-particle conjugate.

Similar to antibodies, peptide sequences take advantage of ligand-receptors. Peptides are short 10-15 amino acid sequences (no longer than 50 amino acids) and are essentially fragments of antibodies and proteins. Peptides can be screened using phage display analysis to create libraries of peptide sequences that have high affinity to specific cell types. Through phase display technology, a number of peptide sequences have been identified such as the arginine-glycine-aspartic acid (RGD) sequence that has been recognized as a cell adhesion peptide because of its affinity to integrins found on many cell surfaces[91–93]. Targeting peptides have been used in research to treat diseases ranging from immune system diseases to multiple cancer types including glioma, prostate, lung, ovarian, and breast cancers[83,94,95]. The use of peptides in targeting strategies is advantageous over the use other targeting moieties because they have a smaller size, a simple 3D structure which leads to improved stability *in vivo,* and are cheaper and easier to synthesize and conjugate to nanocarriers[86]. Targeting peptides and their efficacy is explored in this dissertation, specifically for improving HER2+ breast cancer targeting. A recently identified HER2+ peptide is incorporated into a nanoparticle drug delivery system exploring modifications that can be made to both the peptide and the nanoparticle to increase nanoparticle binding and internalization into HER2+ breast cancer cells.

1.3.4. Motivation for HER2+ breast cancer targeting

According to the National Cancer Institute at the National Institute of Health, since 2006 there have been more than 200,000 new cases each year of breast cancer in women with more than 41,760 estimated deaths alone in 2019 [96,97]. Breast cancer is the most commonly diagnosed cancer in women and currently the third most common cause of cancer deaths in women. Within all the different breast cancer subtypes, 15-20% of breast cancers overexpress the human epidermal growth factor receptor (HER)-2. HER2+ breast cancers tend to have very poor outcomes for patients due to the aggressive nature of the cancer, their propensity to metastasize, and resistance to endocrine therapy owing to decreased expression of estrogen receptors[96,98,99]. The push for early breast cancer screening and the introduction of the monoclonal antibody trastuzumab when used in conjunction with chemotherapy has improved the prognosis of patients with HER2+ breast cancer slightly. Nevertheless, a large population of HER2+ patients fail to respond to trastuzumab and other treatments completely, and a significant fraction of patients that initially respond to treatment tend to relapse within 1-5 years of initial treatment[99]. The recurrence, progression, and eventual metastasis of the disease often lead to patient death.

Treatment approaches to breast cancer depend on the specific disease type, staging, and progression. Treatment may include a combination of surgery, radiotherapy, and systemic doses of chemotherapy, endocrine therapy, and/ or biologic therapy[100]. Despite the great deal of research that has gone into treatment and therapies for breast cancer, these "gold standard" approaches have not changed significantly in a number of decades. These approaches also have significant disadvantages in that they are invasive and can become quite extensive if lymph nodes are involved, with regards to surgery, and are systemic, leading to severe side effects in the case of chemotherapy, radiation, and other therapy options. Instead of systemic treatment,

drug delivery techniques can be employed to develop focused and more efficacious therapeutic options, which would ultimately help decrease the number of HER2+ breast cancer recurrences and deaths. Improving the efficacy and reducing the invasive and systemic nature of current treatments is an overarching goal of cancer drug delivery and can be achieved by combining and building on the nanotechnology and drug delivery strategies mentioned here.

1.4. Dissertation Overview

This dissertation is divided into two main parts. Part 1 (Chapter 2) focuses on tissue engineering and how properties can influence a material's suitability as a tissue engineering scaffold or biomaterial. Part 2 (Chapters 3 and 4) focuses on two different drug delivery strategies and how varied drug delivery approaches may be to achieve goals such as controlled release or active targeting. Chapter 2 presents a novel hydrogel biomaterial made by crosslinking the CKA monomer MTC, previously introduced, with poly(ethylene glycol) diacrylate (PEGDA). As discussed in the introduction, biomaterials must be designed with spatial and temporal considerations in mind. Polymeric and hydrogel scaffolds have been developed that either lack the mechanical properties needed for specific tissue regeneration, degradability over time, or processability that are desired to make an improved tissue engineering scaffold. The hydrogel scaffold developed here addresses these issues specifically and characterizes this novel material for biomaterials use generally. Multiple hydrogel compositions of MTC and PEGDA crosslinker are fabricated by changing the crosslinker concentration and length to determine how this chemistry and variations in the crosslinker affect properties such as wettability, degradation, stiffness, and structural changes on the nano/micro and macroscales. The processability of this hydrogel fabricated from a hydrophobic bulk material is also explored to determine the

biocompatibility of the hydrogel compositions and how this relates to the hydrogel and scaffold requirements presented in the introduction and overcomes the hydrogel disadvantages discussed. Chapter 3 extends the utility of this novel hydrogel material to determine how the release of drugs with different properties (i.e. small molecule hydrophobic, small molecular hydrophilic, and proteins) are released from this hydrogel material. The issues with tuning and tailoring hydrogel systems for controlled drug release as well as the lack of versatility of drug loading in traditional hydrogel systems that are only suitable for hydrophilic drugs are addressed. The injectability of the MTC material and ability to crosslink *in situ* is also assessed. The crosslinker lengths and concentrations are varied more drastically to determine if release trends change with greater changes in the crosslinker concentration. Chapter 4 shifts to a nanoparticle targeting strategy using an identified HER2 targeting peptide followed by combination targeting and internalizing peptide sequences that pivoted from the initial targeting sequence. Two different PEG spacer chemistries are also tested and compared to evaluate if increased peptide presentation leads to greater targeting and/or uptake by HER2+ breast cancer cells, combining some of the nanotechnology and biomaterials strategies previously mentioned. Through these approaches, HER2+ targeting is tackled to improve the selectivity and internalization ability of drug-loaded polymeric nanoparticles to overcome the systemic issues (nonselectivity and harsh side effects) of current chemotherapy administration. Finally, Chapter 5 provides insight for future work and specific ways in which the MTC hydrogels can be applied to for both tissue engineering and drug delivery application, and how the HER2+ targeting nanoparticles will be robustly tested in a clinically relevant transgenic *in vivo* mouse model.

Chapter 2. Hydrogels with Unique Swelling Properties as a Biomaterial for Tissue Engineering Application

Prepared for publication in *Chemistry of Materials* with co-authors: Navarro R*, Zhang Z, Xiang Y, Awada M, Adler N, and Ma PX., "Hydrophobic hydrogels with reverse swelling and tunable properties as a biomaterial for tissue engineering application." *Both authors contributed equally to this work.

2.1. Introduction

Hydrogels have been widely used in industry and by biomaterial scientists since the late 1950s for many applications, including as tissue engineering substrates to regenerate tissues and organs[42,46,101–110]. Made from natural and/or synthetic polymers, hydrogels are hydrophilic polymer networks that have the ability to absorb up to thousands of times their dry weight when placed in water. To be suitable for tissue engineering applications and help cells perform their function, hydrogel scaffolds should meet a number of requirements, including (1) being biocompatible, (2) being biodegradable, (3) having high surface area, and (4) having mechanical properties that are compatible with the tissue that is being regenerated[27,28]. A number of hydrogels developed fail to meet one or more of these requirements, and especially lack biodegradability and/or have weak mechanical properties as exemplified in many of the typical materials used for hydrogel formation such as polyethylene glycol (PEG) and polyvinyl alcohol (PVA). The best scaffolds for tissue engineering also have high porosity and interconnectivity

between the pores[28]. Achieving this in hydrogels is often done through methods such as photolithography, freeze drying, and gas foaming, which are challenging and costly. Advancing the types of scaffolds available, specifically by improving hydrogels to meet the listed requirements above by developing novel materials with different properties, continues to be a goal of tissue engineering.

2-methylene-1,3,6-trioxocane (MTC) is a ring monomer from a class of polyesters known as cyclic ketene acetals (CKAs). CKAs are unique because they undergo a molecular rearrangement upon radical ring-opening polymerization (RROP)[47–50,111,112]. RROP leads to the formation of a hydrolysable ester linkage in the hydrophobic polymer backbone that imparts degradability into the structure, overcoming the lack of biodegradability found in many hydrogel systems. Furthermore, this extraordinary chemistry lends itself to crosslinking through the radical produced and a diacrylate crosslinking molecule. The greatest hurdle using MTC to develop tissue engineering scaffolds has been polymerizing to high molecular weights, which has been previously attempted through traditional radical polymerization schemes in the presence of solvent[111,113]. The loosely crosslinked MTC gels that polymerized in these instances resembled weak elastomers instead of intact hydrogels. These gels overall exhibited poor mechanics, low degrees of swelling, and relied on added enzymatic degradation. Because MTC is difficult to polymerize to high molecular weights, a necessity for robust scaffold fabrication, the issue of low molecular weight is overcome in this work by crosslinking MTC into a hydrogel with high (infinite) molecular weight. In this way, the MTC chemistry, degradability, and hydrogel properties could all be taken advantage of.

Through chemical (covalent) crosslinking, a robust hydrogel can be formed. PEG and its derivatives such as poly(ethylene glycol) diacrylate (PEGDA) have been used not only to form

bulk hydrogel materials, but also as a crosslinker. PEGDA is beneficial for use as a crosslinker due to its neutral charge, hydrophilicity, good biocompatibility, resistance to protein absorption, and functionality[76,114–118]. Taking advantage of these strengths and the chemical structure of MTC previously mentioned, it was hypothesized that MTC could be covalently crosslinked with PEGDA to form a new, degradable, and tunable highly crosslinked hydrogel material. It was also hypothesized that a reverse hydrogel system such as this one, composed from a hydrophobic bulk material and a hydrophilic crosslinker, would display unique properties, especially as it pertains to the swelling behavior.

In this work, a series of MTC hydrogels were developed by varying the crosslinker length and molar concentrations to determine the different properties of PEGDA crosslinked MTC hydrogels and examine how MTC gels can change from non-swelling to swelling. It was found in this MTC hydrogel system that an increase in swelling is observed as the crosslinking density is increased, where generally a decrease in swelling is seen as the number of crosslinked points are increased within traditional hydrogels[75,119]. Finally, a notable characteristic of the MTC monomer is that it exists in a liquid state at room temperature that is miscible with its PEGDA crosslinker and does not need added water or solvent for crosslinking, which allowed for scaffold processing that is generally not possible with traditional aqueous hydrogel solutions. Capitalizing on this advantage, a one-pot reaction is used to fabricate hydrogels with an interconnected and porous morphology. The hydrogels were fabricated for the first time using a facile previously developed sugar porogen method[34,35,37]. Combining all of the advantages of the MTC monomer and desired hydrogel properties, MTC gel/hydrogel compositions were characterized and, based on ideal mechanics and swelling behavior, the biocompatibility of this novel hydrogel material as a tissue engineering scaffold was assessed.

2.2. Results and Discussion

2.2.1. Effect of changing MTC concentration and varying crosslinker percent and length on structure of dry and swelled crosslinked MTC

Through the modified MTC synthesis reactions described in the methods section as well as depicted in the reaction scheme, a greater yield of MTC monomer was achieved with an overall yield of 25-30% compared to the 10% yield previously achieved by Undin et al., which may be due to higher vacuum during the distillation steps and preventing the monomer from degrading during heating[51] **(Figure 2.1a)**. Using this ultrapure monomer (purity ~99.5%), a series of gels and hydrogels were fabricated according to the radical ring opening polymerization (RROP) and crosslinking schemes illustrated **(Figure 2.1b and 2.1c)**. Through the MTC monomer molecular rearrangement and subsequent reaction through the C=C bond in poly(ethylene glycol) diacrylate (PEGDA), a crosslinked network is quickly formed with the addition of DMPA UV initiator and 365 nm wavelength UV light source. Unique to cyclic ketene acetals, this molecular rearrangement is significant because it leads to the formation of a desired ester linkage in the polymer backbone and degradability to the forming polymer. Degradability is a beneficial feature of tissue engineering scaffolds as scaffolds degrade over a specific time range in order to allow cells to remodel their environment, form new tissue, and deposit extracellular matrix[120,121].

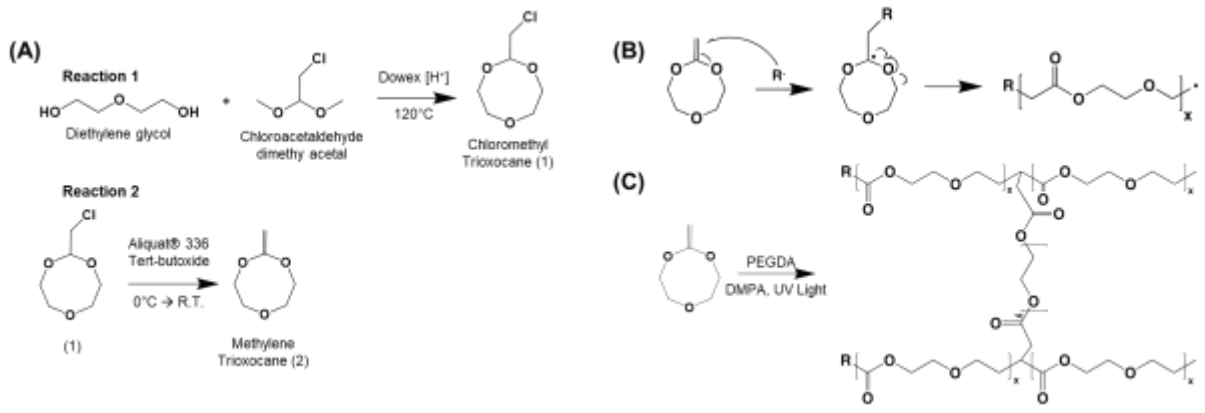

Figure 2.1: 2-methylene trioxocane (MTC) reaction steps, ring opening, and UV crosslinking schemes. (A) Reaction 1 forming MTC intermediate chloromethyl trioxocane and Reaction 2 forming MTC cyclic monomer. (B) Radical ring-opening polymerization forming linear chain with primary radical. (C) Gel/hydrogel network formed through crosslinking of MTC and PEGDA.

First, a notable change in the overall diameter of gel/hydrogel samples is observed in the sample disks following initial gelation under UV light and after allowing the samples to swell for just 24 hours in water. Throughout this paper, gels will refer to crosslinked samples that do not swell significantly (less than 100%), while hydrogels will refer to crosslinked samples that have a percent swelling of 100 or greater. Differences in the degree of swelling are seen as the mole ratios of MTC monomer and crosslinker, which is calculated with respect to the moles of MTC monomer, and the crosslinker length are varied. An example can be seen for the changes that occur in the diameter of MTC disks for two different mole percents of crosslinker (0.25% and 1.0%) as well as with varying the crosslinker length **(Figure 2.2)**. This swelling phenomenon supports the notion that this hydrogel system may show unique swelling properties and will be more robustly examined and quantified in the next section.

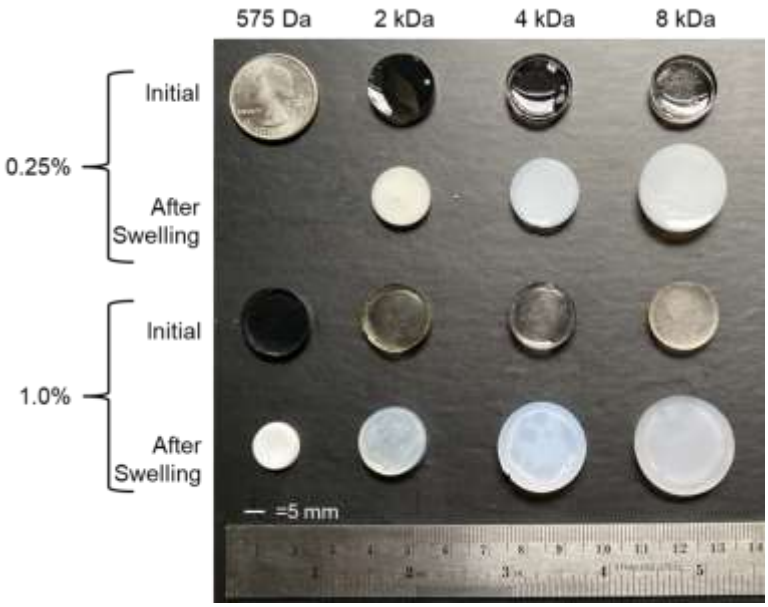

Figure 2.2: Effect of changing crosslinker concentration (mole percent) and length on gel/hydrogel swelling.

Along with this observed gross macroscopic change, changes on the microscopic level are also observed for the gel/hydrogels compositions. Using scanning electron microscopy, cross-sections of MTC gels/hydrogels were prepared and imaged after gelation as well as after submersion in water (swelling) and subsequent lyophilization. While the images immediately after crosslinking tend to show a typically smooth surface or rippled appearance due to the tight, enclosed pores, the more classical hydrogel mesh can be seen after submerging the gel/hydrogel disks in water for 3 days **(Figure 2.3)**. There is also an interconnected porous morphology that forms through the gels/hydrogels, with pores that range from 1-10 μm in size. MTC samples crosslinked with the shortest PEGDA crosslinker (575 Da) show the same morphology before and after swelling, as seen in **Appendix A**. An increase in mesh size can be seen as the crosslinker mole percent increases from 0.25% to 2.5% (relative to moles of MTC monomer) and as the PEGDA length is increased from 2 kDa to 8 kDa. Increasing the PEGDA molecular weight from 575 Da to 8 kDa increases the hydrophilicity of the MTC gels/hydrogels. Likewise,

increasing PEGDA mole ratio also shows an increase in gels/hydrogels hydrophilicity. With an increase in hydrophilicity, these hydrogels are able to draw more water throughout the crosslinked MTC network and swell. Apparent in the SEM images and found in some hydrogels is the fibrous architecture that is observed upon swelling across the different MTC gel/hydrogel compositions, especially with the 1.0% and 2.5% MTC gels/hydrogels. A nanofibrous architecture has been found to mimic the extracellular matrix and help promote increased cell attachment and differentiation on synthetic polymer scaffolds[37,122–124].

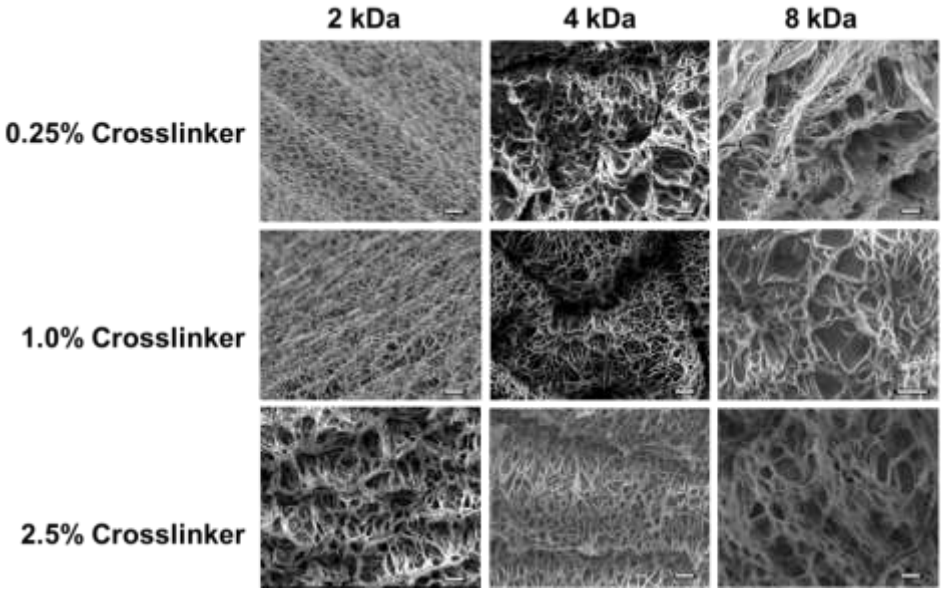

Figure 2.3: Effect of varying percents of MTC and PEGDA crosslinker as well as PEGDA length on structure of MTC samples after swelling. All samples were visualized using scanning electron microscopy after submerging sample in water for 3 days and subsequently lyophilizing before imaging. (Scale bar= 10 µm).

2.2.2. Effect of varying MTC concentration and crosslinker percent and length on swelling and degradation (mass loss) behavior of MTC gel/hydrogel samples

The swelling and degradation behaviors of the MTC gels/hydrogels were assessed and quantified as the crosslinker length and percent were changed. The behavior of the different samples was examined over a period of up to 11 weeks **(Figure 2.4)**. From the graphs produced, MTC

hydrogel samples with 2.5% percent PEGDA have the greatest swelling percent overall compared to gel/hydrogel samples fabricated with 1.0% and 0.25% PEGDA. MTC hydrogels prepared with 8 kDa 2.5% PEGDA swelled nearly 800% times their original dry mass and could be appropriately described as hydrogels. Similarly, MTC samples with 4 kDa 2.5%, 2 kDa 2.5%, 8 kDa 1.0%, and 4 kDa 1.0% achieved swelling percents between 100-500%, showing behavioral characteristics consistent with these samples' classification as hydrogels. The remaining samples, however, fail to show substantial swelling (575 Da 2.5%, 2 kDa 1.0%, 575 Da 1.0% and all 0.25%) as the hydrophobic nature of sample supersedes the hydrophilic components and can more fittingly be described as gels as they do not absorb much water.

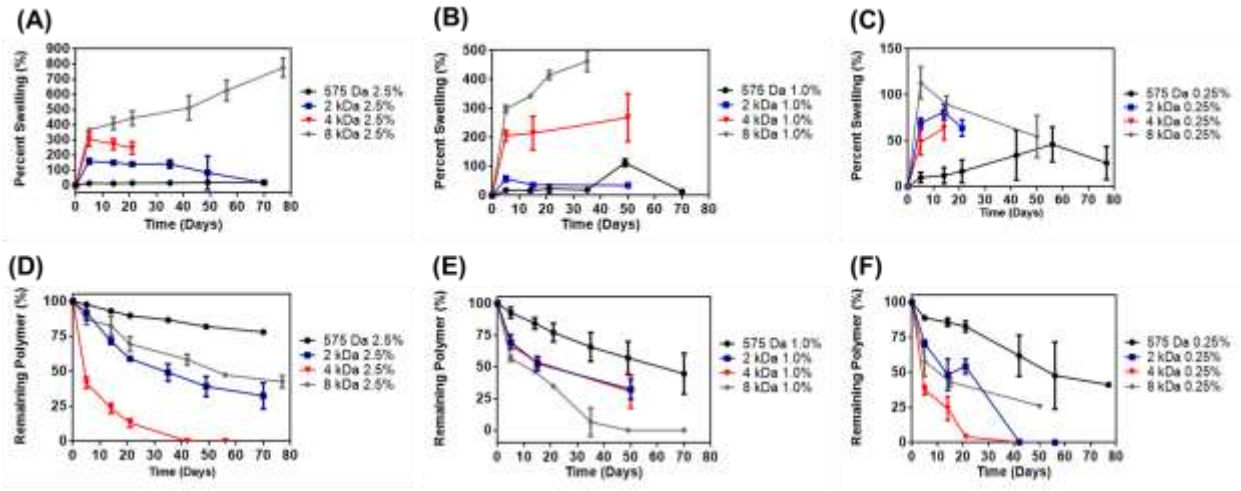

Figure 2.4: Effect of varying MTC concentration and crosslinker percent and length on swelling and degradation (mass loss) behaviors of MTC gel/hydrogel samples. Swelling (A-C) and degradation (D-F) studies were performed for up to 10 weeks in pH 7.4 PBS at 37 °C for the varying MTC gel/hydrogel samples. Data are presented as mean ± standard deviation (n=3).

The percent of mass loss over time is shown for the crosslinked gel/hydrogel disks as well **(Figure 2.4)**. MTC samples crosslinked with variable percents of 575 Da PEGDA always have the slowest rate of mass loss when compared to samples with the same percent of crosslinker. A minor decrease in the ratio of MTC to crosslinker leads to gels/hydrogels which

show an increase in rate of mass loss over time. The only true exception to this trend would be for the MTC samples crosslinked with 8 kDa 2.5% PEGDA, where the overall mass of PEGDA at 2.5 mole percent is greater than the mass of MTC. As mentioned in the introduction, PEGDA is not degradable and, because of this, the samples maintain their mass comparatively.

Along with the tunability of this hydrogel system, it can be concluded from the swelling and mass loss behavior that the hydrophobicity and hydrophilicity affect the degree of swelling and the rate at which mass decreases for the MTC gels/hydrogels. This is truly distinctive in the case of swelling with respect to the crosslinker percent because generally as the percent of crosslinker is increased in hydrogel systems, there is a decrease in swelling and mesh size[75,119,125]. Instead, there is a consistent increase in swelling as the percent of crosslinker is increased throughout this work. This suggests that the more hydrophilic a sample is, either because of higher concentration (mole percent) of PEGDA or, more traditionally, higher PEGDA molecular weight, the more a sample swells or the faster a sample degrades as more water is brought into the MTC sample. This is despite more crosslinking within the sample, which usually restricts swelling. These two effects were further studied with additional data to reflect each condition separately. First, the effect of changing the crosslinker length was isolated by keeping the mass of both MTC and the mass of crosslinker constant amongst the different samples and observing the swelling behavior over a one-week period **(Figure 2.5a)**. The effect of crosslinker length is clear as the samples rapidly swell as crosslinker molecular weight increases. Similar to the complete swelling tests previously discussed, samples with fixed mole percents of crosslinker relative to moles of MTC monomer were prepared at 2x (0.5% to 1.0%) and 5x (0.5% to 2.5%) concentrations **(Figure 2.5b, Figure A.4)**. In line with the previous swelling test and gross image of the samples, an increase in swelling is seen as the hydrophilic

PEGDA crosslinker ratio is increased in the gel/hydrogel samples. This hydrophilicity-hydrophobicity balance is able to overcome the physical limitation placed on water absorption that traditional hydrogels are restricted by with regards to swelling behavior. For hydrogels, this is truly unique and has yet to be described in previous hydrogel systems.

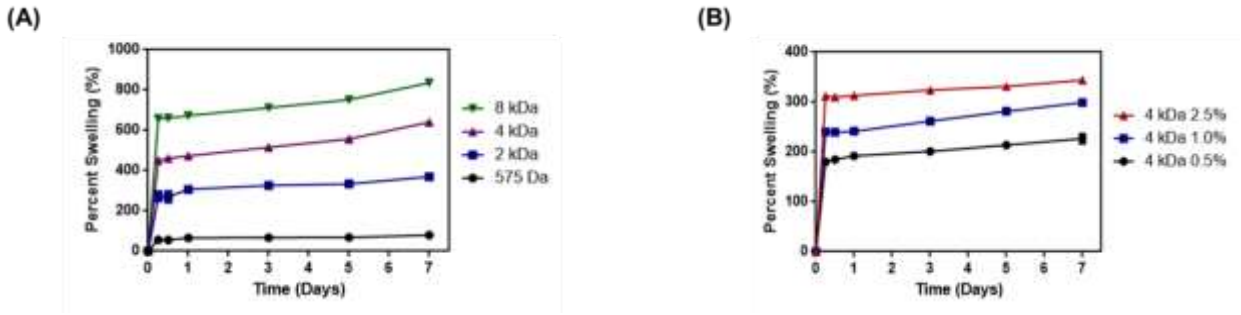

Figure 2.5: MTC gel/hydrogel swelling with fixed MTC and PEGDA masses and fixed mole percents to determine hydrophilic effect on swelling behavior. (A.) Fixing the mass at 0.9 g MTC and 0.1 g PEGDA crosslinker, samples were prepared and left to swell over 7 days in PBS pH 7.4. (B.) Fixing the mole percents of 4 kDa PEGDA crosslinker with respect to moles of MTC monomer and measuring the degree of swelling over 7 days in PBS pH 7.4. All values reported as mean ± SD (n=3). Error bars are smaller than size of markers on graph.

2.2.3. Correlating relative degree of crosslinking as MTC and crosslinker ratio are varied and crosslinker length increases using differential scanning calorimetery (DSC)

Through the experiments performed, the change in glass transition temperature (T_g) of the gels/hydrogels was determined using the second cycle heating curves and inflection point analysis. For the first time ever, the glass transition temperature of MTC polymerized by itself was also found and used as a reference for the crosslinked samples. Through a standard bulk polymerization reaction using Cumene hydroperoxide as an initiator, polymerized MTC achieved a molecular weight of 11,534 g/mol. Through DSC, the T_g was found to be -66.81 °C. This T_g is comparable to that of PCL, which MTC mimics in structure. The backbone of MTC, however, exhibits added flexibility with the addition of oxygen throughout the structure making the T_g of MTC lower than that of PCL. An examination of how changing the crosslinker length

and ratio within the MTC hydrogels was done for the range of crosslinker lengths and percents previously mentioned. From the data summarized in **Figure 2.6a-d**, it is generally seen that the longer the crosslinker (4 kDa and 8 kDa PEGDA), the lower the T_g, and when the crosslinker length is shorter (575 Da and 2 kDa), the T_g is higher. The small range in the amount of crosslinker used in this work does not show a clear trend according to the DSC data collected. However, a slight positive slope in the FTIR graph suggests that more PEGDA crosslinker is incorporated into the gel/hydrogels samples **(Figure 2.6e)**. This data was found by measuring the area under the curve of the 3000 cm^{-1} ($-CH_2$ stretching from PEGDA backbone) and 1750 cm^{-1} (C=O ester stretch from MTC) peaks to form a ratio of [PEGDA]/[MTC].

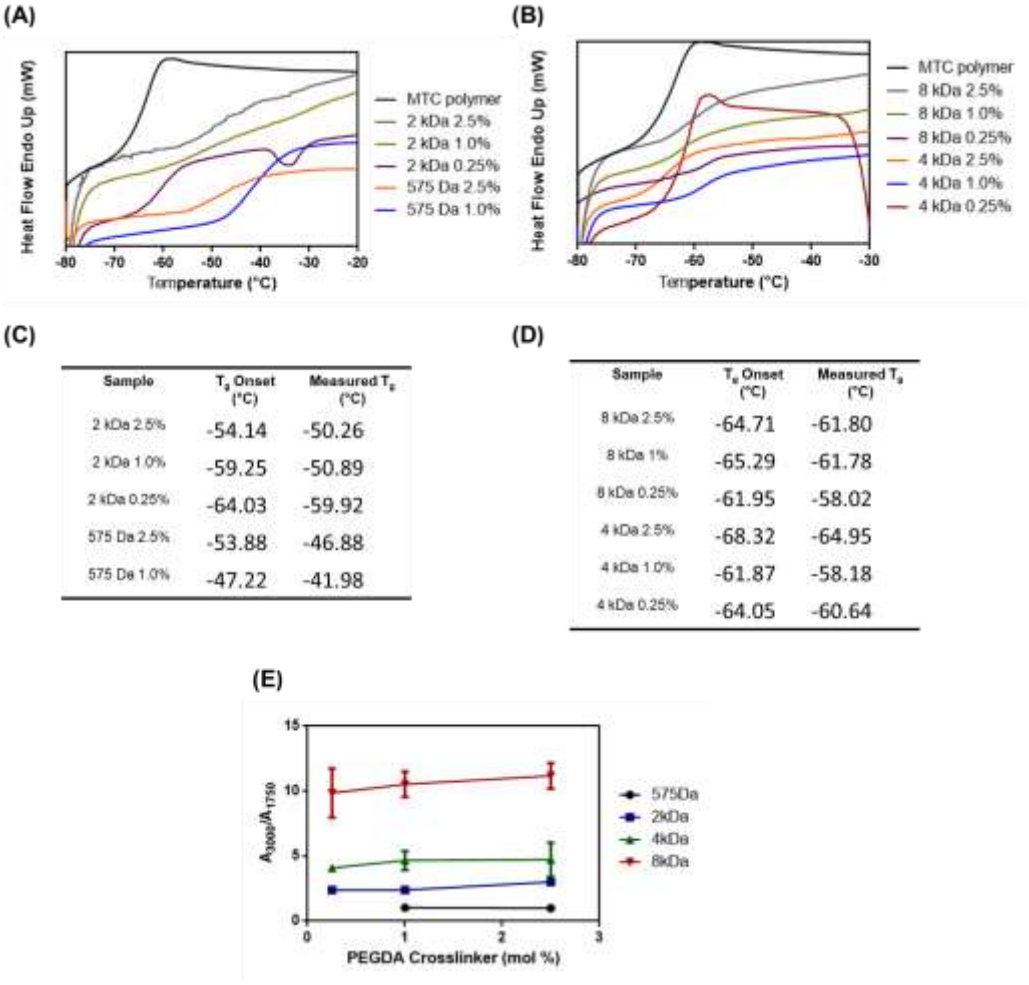

(C)

Sample	T_g Onset (°C)	Measured T_g (°C)
2 kDa 2.5%	-54.14	-50.26
2 kDa 1.0%	-59.25	-50.89
2 kDa 0.25%	-64.03	-59.92
575 Da 2.5%	-53.88	-46.88
575 Da 1.0%	-47.22	-41.98

(D)

Sample	T_g Onset (°C)	Measured T_g (°C)
8 kDa 2.5%	-64.71	-61.80
8 kDa 1%	-65.29	-61.78
8 kDa 0.25%	-61.95	-58.02
4 kDa 2.5%	-68.32	-64.95
4 kDa 1.0%	-61.87	-58.18
4 kDa 0.25%	-64.05	-60.64

Figure 2.6: Determining glass transition temperature (T_g) of polymerized MTC and MTC gel/hydrogel compositions to evaluate differences upon varying MTC-PEGDA concentration and PEGDA molecular weight (length). (A) and (C) T_g of 575 Da and 2 kDa PEGDA crosslinked MTC samples; (B) and (D) T_g of 4 kDa and 8 kDa crosslinked MTC samples; (E) FTIR analysis showing the ratio of $A_{3000\ cm^{-1}}/A_{1730\ cm^{-1}}$ or the relative amount of [PEGDA]/[MTC] incorporated into samples. The T_g onset and $T_{g,inflection}$ were found for the samples.

The literature has previously reported that the T_g is a function of the degree of crosslinking and that the higher the T_g, the greater the degree of crosslinking[126–128]. As the number of crosslinks is increased overall, the mobility of the polymerized gel/hydrogel becomes restricted and the temperature to relieve this chain restriction increases. With this information, a smaller crosslinker length leads to a higher degree of crosslinking within the fabricated MTC gels. On the other hand, a longer PEGDA crosslinker leads to a lower degree of crosslinking

within the MTC samples. This information concurs with the swelling behavior previously discussed. It can also justify, along with the hydrophobicity and hydrophilicity of the gels/hydrogels, why a larger mesh or pore size is seen as the crosslinker length is increased, as previously it was determined that as the degree of crosslinking increases, the amount of water penetration and an increase in mesh size and swelling is hindered[129]. The relative degree of crosslinking as determined from the T_g is also useful in predicting a trend in mechanical properties presented in the next section.

2.2.4. Effect of varying MTC concentration and crosslinker percent and length on elastic modulus (G') of MTC gel/hydrogel samples immediately after gelation and after swelling and the correlation to degree of crosslinking

It was investigated how varying the ratio of MTC monomer to crosslinker percent and changing the crosslinker length changes the elastic modulus of the crosslinked MTC gels/hydrogels. The elastic modulus is a critical parameter in characterizing the crosslinked MTC samples and dictates future applications, especially as it pertains to use as a biomaterial for tissue engineering. The elastic moduli were measured immediately after crosslinking and following 3 days of submersion in water (swollen). Using a rheometer, G' is summarized as crosslinker percent and length are varied at a static frequency and is also shown according to the 3 different crosslinker percents of samples across a frequency sweep **(Figures 2.7 and 2.8)**. All of the gels/hydrogels exhibited strong elastic solid like behavior and did not show overwhelming viscoelastic behavior with relatively low G'' behavior (not shown). When samples were measured immediately after gelation in their initial dry state, it was found that increases in the PEGDA crosslinker concentration and length both led to pronounced increases in the elastic modulus. A greater

difference in the modulus values is also seen among each group of fixed crosslinker percents, although fairly constant modulus values were measured as frequency is increased. From the permutations of gels/hydrogels fabricated by varying the PEGDA mole percent and length, different moduli were measured in the range of approximately 100 kPa for the more robust 1.0% and 2.5% crosslinked samples and in the range of 1.5 kPa for the more lightly crosslinked samples. As mentioned, an increase in G' is seen for the samples measured in the initial dry state as crosslinker length is increased. This decreased ability to resist deformation and therefore greater elasticity (G'), can be explained through properties of Rubber Elasticity Theory[119]. An increase in the modulus as crosslinker concentration and length are increased is not only attributable to an increase chain entanglements and viscosity as more and longer crosslinker is incorporated in a dry, packed state, but can also be related to the degree of crosslinking[130]. G' and crosslinking density have been correlated through the equation[131]:

$$G' = \nu RT,$$

where ν is the number of crosslink sites per unit volume, R is the universal gas constant, and T is the temperature. After standing in water for a few days, the samples have similar elastic moduli values, especially as crosslinker length is increased, and have a narrow range in the measured moduli. The most obvious change in moduli between the initial (dry) and wet samples can be observed in those crosslinked with 8 kDa PEGDA, where a longer crosslinker, and greater uptake of water as seen in the swelling behavior, can be attributed to a decrease in elastic modulus as water acts as a plasticizer in this instance[131]. This reversal in modulus values can be seen across all 3 crosslinker percents, though on a more subtle scale for the lower crosslinker molecular weights.

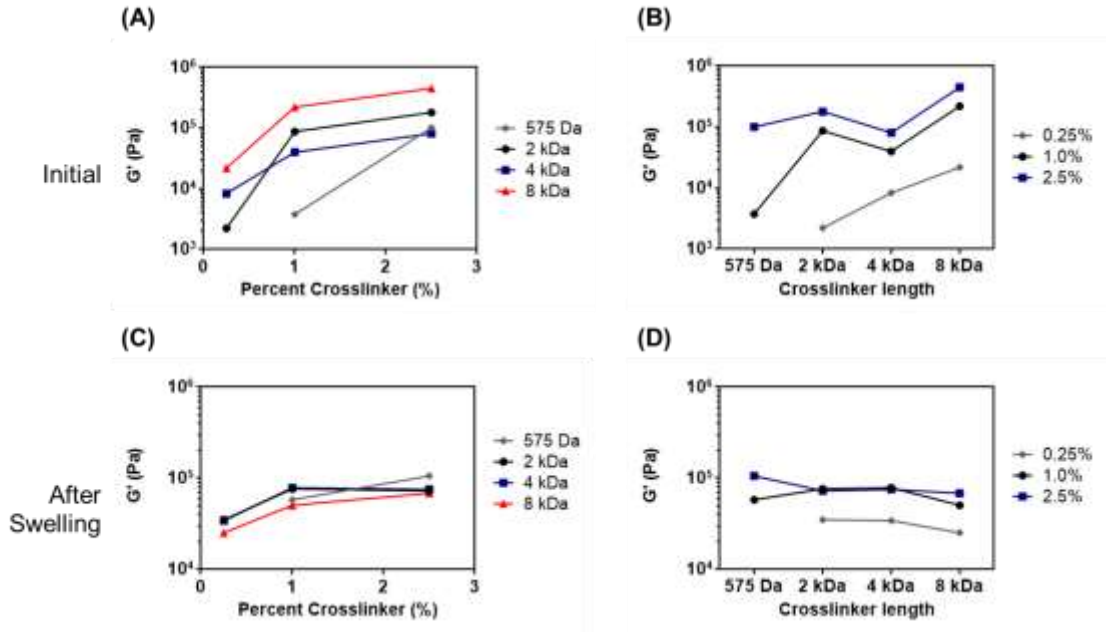

Figure 2.7: Effect of varying crosslinker length and percent on elastic modulus (G') of MTC gels/hydrogels before and after swelling at a fixed frequency. (A) Initial G' (dry) with respect to percent of crosslinker, (B) Initial G' (dry) with respect to crosslinker length, (C) G' after swelling for 3 days with respect to percent of crosslinker, and (D) G' after swelling for 3 days with respect to crosslinker length.

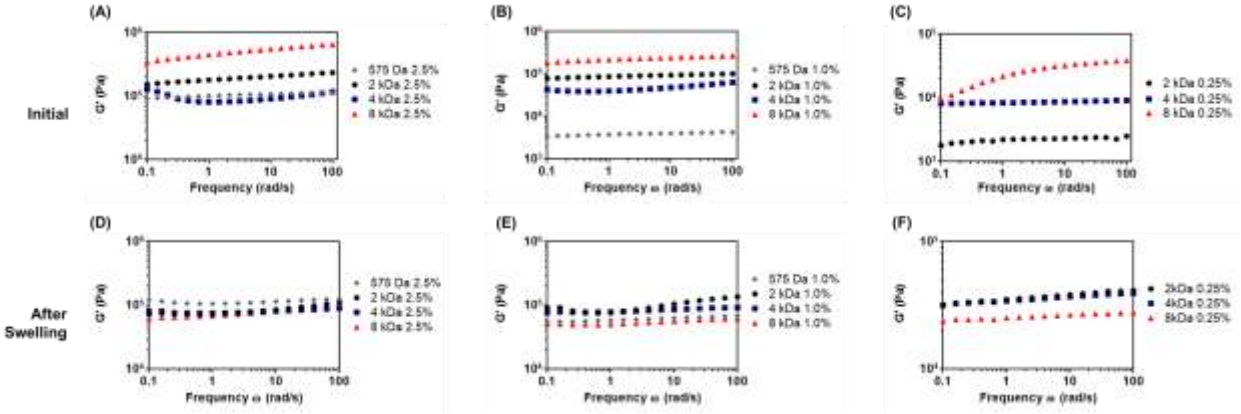

Figure 2.8: Effect of varying crosslink percent and length on elastic modulus (G') of MTC gels/hydrogels before and after swelling over a frequency sweep. G' elastic modulus values were measured for the samples immediately after fabrication for (A) 2.5 mole percent crosslinker, (B) 1.0 mole percent crosslinker, and (C) 0.25 mole percent crosslinker. G' elastic modulus values after swelling for 3 days for (D) 2.5 mole percent crosslinker, (E) 1.0 mole percent crosslinker, and (F) 0.25 mole percent crosslinker. The modulus values are generally consistent across the measured frequencies of 0.1 to 100 rad/s.

2.2.5. In vitro testing of ADSCs and DPSCs on gels/hydrogels to determine cell survival, proliferation, and infiltration into hydrogel scaffolds

Following all of the materials characterization, biocompatibility testing was done to assess the suitability of MTC gels/hydrogels as a biomaterial for tissue engineering use. The first assessment was done through a cell proliferation assay of all the gels/hydrogels. Using the samples with good cell proliferation, SEM imaging and a Live/Dead cell assay and imaging were performed next. While a porous mesh with 1-10 μm pores is produced after the gels/hydrogels are submerged in water, this network itself does not produce an adequately sized, interconnected network for cells to thrive long-term. To improve these conditions and taking advantage of the anomalous lack of solvent needed for MTC gel/hydrogel crosslinking, an interconnected, porous network was introduced into the material using a sugar bead template method previously described. This is the first time this facile sugar porogen method was used to form porous hydrogels. Using this method is only possible due to the absence of water or another solvent in the gel/hydrogel crosslinking process. These porous MTC gels/hydrogels were used for the remaining tissue engineering testing. *In vitro* testing was done by seeding adipose-derived stem cells (ADSCs) and dental pulp stem cells (DPSCs) onto the scaffolds to evaluate the utility for more than one stem cell source. Proliferation assays were performed over one week to determine which MTC-PEGDA compositions promoted cell growth for both cell types and, therefore, be more suitable for future *in vivo* application. From the proliferation results, the 1.0% PEGDA crosslinker gels showed continued cell proliferation for both ADSCs and DPSCs over seven days **(Figure 2.9)**. These results stem from the differences in local gel/hydrogel modulus, which plays a critical role in cell attachment, survival, and proliferation[29,30]. SEM and Live/Dead images of the gels/hydrogels fabricated with 1.0% PEGDA crosslinker were also taken and show cell

attachment and spreading for the 1.0% gels overall and especially for 575 Da and 2 kDa porous gels with ADSCs and 2 kDa porous gels with DPSCs **(Figure 2.10, 2.11,** and **Figure A.6)**. Taken together, along with the swelling behavior presented earlier that shows over 200% swelling for hydrogels prepared with 4 kDa and 8 kDa molecular weight crosslinker, it was concluded that 4 kDa and 8 kDa do not help promote cell spreading and survival and are not candidates for use as tissue engineering scaffolds. Significant swelling of 4 kDa and 8 kDa crosslinked hydrogels leads to poor cell morphology and communication, and overall cell death, as the pores continue to grow in size and cells become more isolated within the hydrogels. From this work, it can be concluded that 575 Da and 2 kDa 1.0% porous MTC gels are suitable for tissue engineering applications and can be utilized in future *in vivo* work for the regeneration of tissue in the 100 kPa modulus range such as skin, cardiac muscle, and tissues in close range like intestinal tissue[132–134].

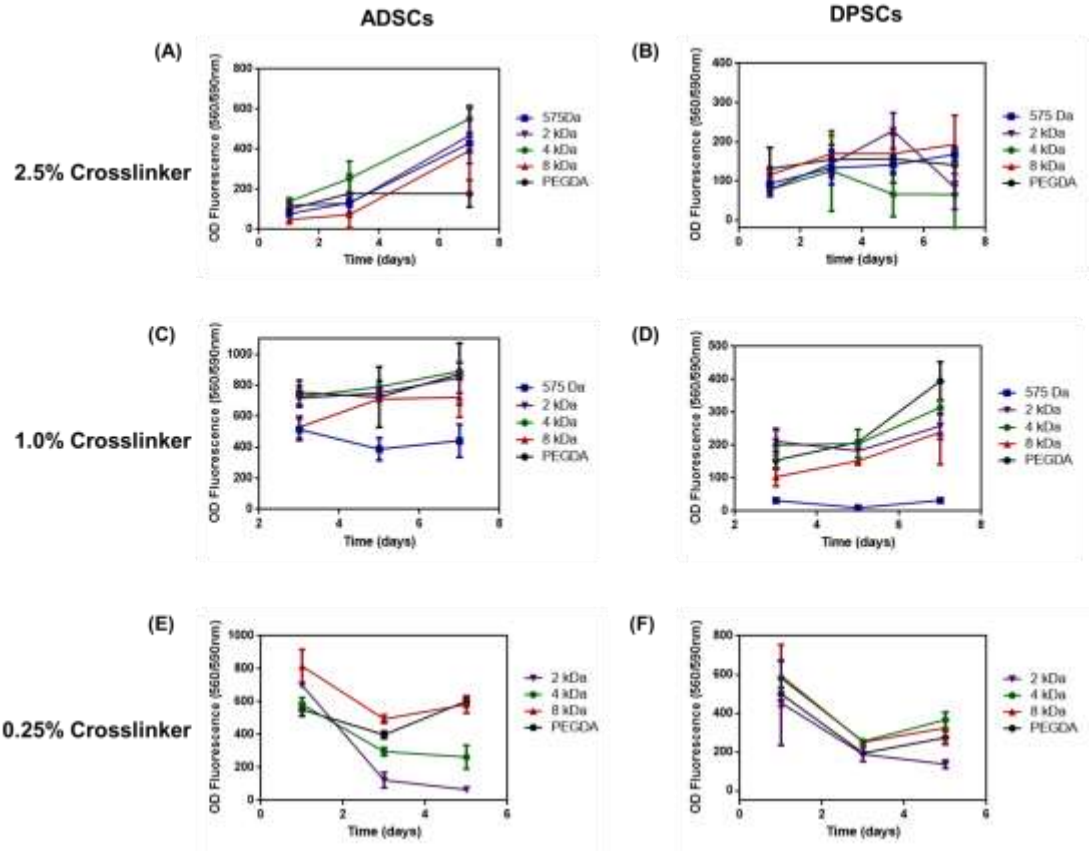

Figure 2.9: Cell proliferation trends of MTC gels/hydrogels with varying percents and length of crosslinker over 7 days. (A) ADSCs on samples 2.5% crosslinker, (B) DPSCs on samples with 2.5% crosslinker, (C) ADSCs on samples with 1.0% crosslinker, (D) DPSCs on samples with 1.0% crosslinker, (E) ADSCs on samples with 0.25% crosslinker, and (F) DPSCs on samples with 0.25% crosslinker. All values reported as mean ± SD (n=3).

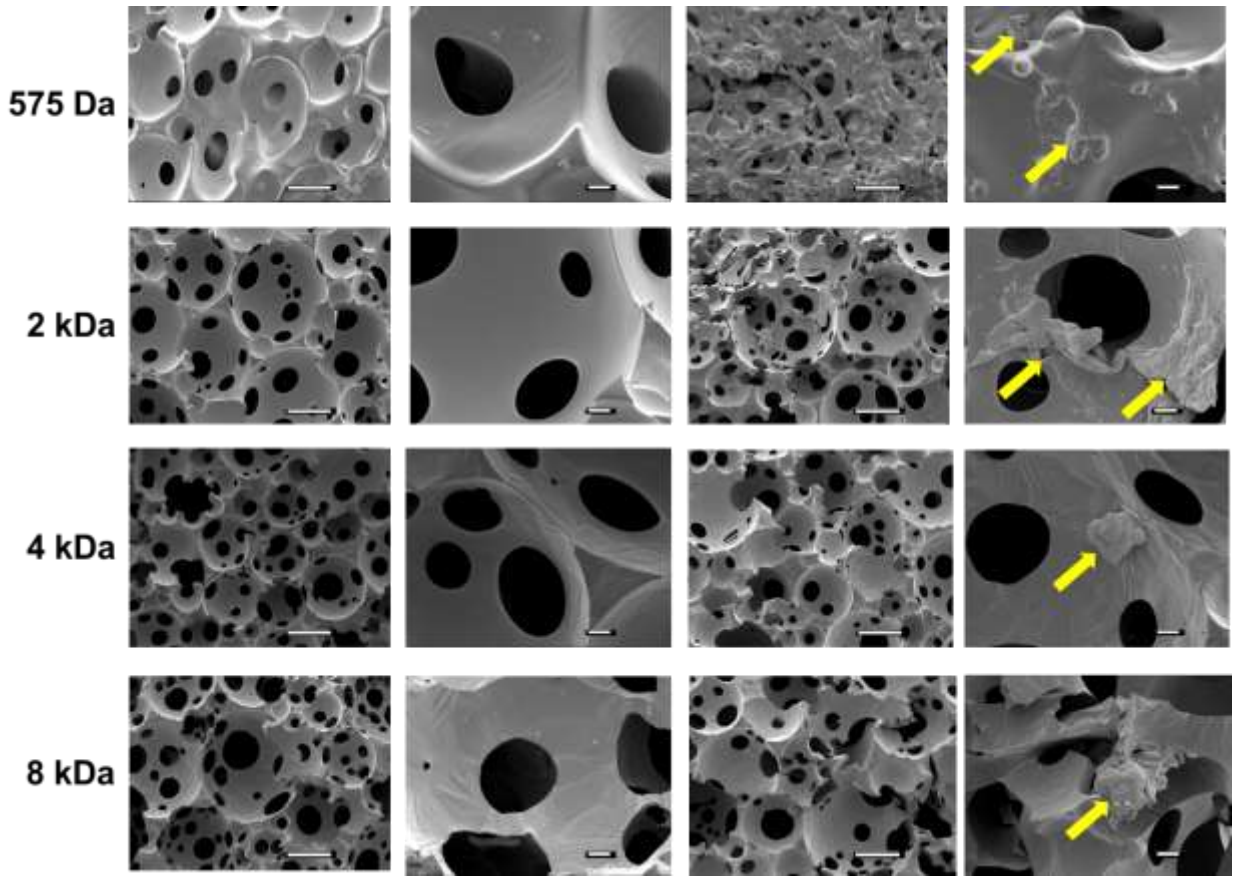

Figure 2.10: SEM imaging of 1.0% gels seeded without and with ADSCs after 3 days of incubation. Columns 1 and 2 show porous gels with no cells seeded. Columns 3 and 4 show gels with ADSCs seeded after 3 days. (Columns I and III images at 200x magnification, scale bar= 100 µm; Columns II and IV images at 1000x magnification, scale bar=10 µm).

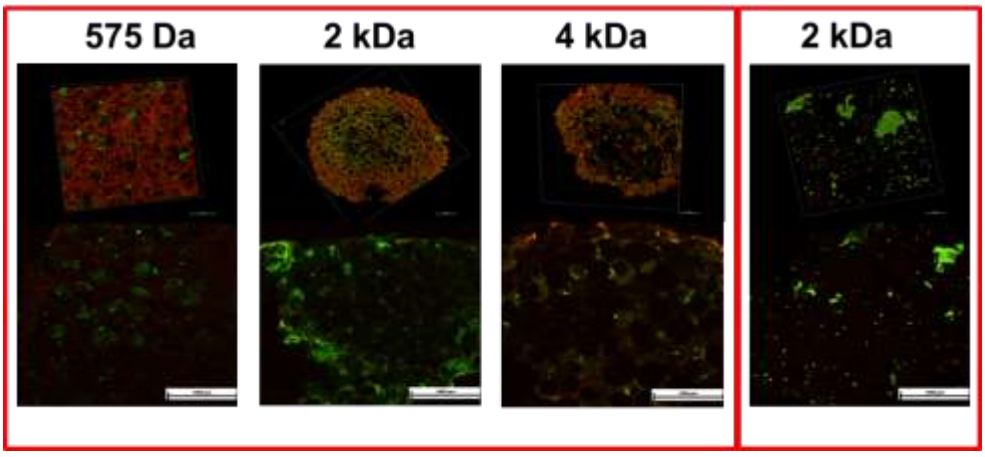

Figure 2.11: Live/Dead cell viability imaging of 1.0% porous gels with ADSCs and 2 kDa 1.0% porous gels with DPSCs (far right). Cells were seeded on scaffolds for 7 days, stained, and imaged. Top row shows 3D rendering of cell seeded gels/hydrogels and the bottom row shows 2D captured images.

2.3. Conclusion

In this work, a novel and extraordinary gel/hydrogel material was fabricated using the cyclic ketene acetal monomer, 2-methylene-1,3,6-trioxocane (MTC). With the unique features of this monomer, a degradable hydrogel was fashioned by crosslinking with poly(ethylene glycol) diacrylate (PEGDA). A porous, interconnected network using a sugar bead template as a mold was used to create samples for cell testing, taking advantage of the atypical properties of the monomer (liquid state) and its processability (solvent-free). As expected, the swelling, mass loss behavior, and mechanical properties of the MTC gels/hydrogels can be controlled by regulating the crosslinker concentration and the crosslinker length, which changes the hydrophilic-hydrophobic balance within the construct. Overall through characterization of these novel MTC gels/hydrogels, tailorable scaffolds with superior interplay between the hydrophilicity and hydrophobicity demonstrated enhanced biocompatibility and can be used for tissue engineering application. These scaffolds have adequate mechanical properties and multiple advantages due to advanced degradability and ability to form porous crosslinked substrates.

2.4. Experimental Section

2.4.1. Materials

Chloroacetaldehyde dimethyl acetal, Dowex® 50 WX-2, Tetrahydrofuran (THF), Aliquat® 336, diethylene glycol, Cumene hydroperoxide, and 2,2-Dimethoxy-2-phenylacetophenone, 99% were all purchased from Sigma Aldrich (St. Louis, MO). Potassium tert-butoxide and aluminum oxide were purchased from Oakwood Chemical (Estill, SC). Acrylate-PEG-Acrylate (PEG diacrylate) MW 2,000 was purchased from Laysan Bio, Inc. (Arab, Alabama). PEGDA 4000 and PEGDA 8000 were purchased from Polysciences, Inc. (Warrington, PA)

2.4.2. Synthesis of 2-methylene-1,3,6-trioxocane (MTC)

The synthesis of methylene trioxocane followed the work described by Hiraguri[112] *et. al.* and later Undin[51] *et. al.* based on the method developed by Bailey[47,48] *et al.* Briefly, Chloroacetaldehyde dimethyl acetal and diethylene glycol were mixed in a 1:1 ratio in the presence of Dowex® 50 (H^+) in a round bottom equipped with a fractioning column. The mixture was heated to 120 °C until the calculated theoretical amount of methanol was collected. The reaction was vacuum filtrated to remove the Dowex® and purified by vacuum distillation yielding white crystals of 2-chloromethyl-1,3,6-trioxocane **(1)**. The monomer **(1)** was placed in a round bottom flask and dissolved at a ratio of 1:2 g/mL of anhydrous THF and placed in an ice bath. To this, 2 mol % of Aliquat® 336 was added and stirred for an additional 30 min in an ice bath. To this, 2 mol equivalents of potassium tert-butoxide were added slowly to the mixture and then allowed to stir overnight. The product was concentrated to remove the THF and dissolved in ethyl ether and purified using aluminum oxide. The filtrate was concentrated and dissolved in fresh ethyl ether and purified in aluminum oxide twice more to remove traces of tert-butoxide. Finally, the filtrate was purified by vacuum distillation using a 10 cm fractioning column to produce MTC **(2)** as a transparent liquid. The MTC steps were evaluated for NMR and FTIR to confirm synthesis as previously reported. Chloromethyl trioxocane IR (neat): 2950, 2880, 1470, 1390, 1140, 1080 cm^{-1}. ^1H NMR ($CDC1_3$, 500 MHz):δ 3.49 (d, 2H, ClCH2), 3.60-4.14 (m, 8H, $OCH_2CH_2OCH_2CH_2O$), 4.83 (t, 1H, CH). Methylene trioxocane IR (neat): 2960, 2870, 1660, 1450, 1370, 1150, 1080 cm^{-1}. ^1H-NMR ($CDC1_3$, 500 MHz): δ 3.69 (s, 2H, CH_2=), 3.75-3.85, 4.16-4.26 (m, 8H, $OCH_2CH_2OCH_2CH_2O$).

2.4.3. Bulk polymerization of MTC

Polymerization of MTC was carried out by adding 0.5 g of MTC into a reaction vessel and adding 1.0% of Cumin before conducting a standard freeze-pump-thaw 3 times. The reaction was then allowed to polymerize at 70 °C for 1 day.

2.4.4. Scanning electron microscopy (SEM) image analysis of unswollen and swollen PEGDA-crosslinked MTC disks

Disks of crosslinked MTC polymer were prepared with 3 different crosslinker (poly(ethylene glycol) diacrylate) contents utilizing four different molecular weights for material characterization (575 Da, 2 kDa, 4 kDa, and 8 kDa). Crosslinked MTC samples with 2.5, 1.0, and 0.25 mole percents of PEGDA, relative to the MTC monomer, were prepared with 0.1% 2,2-Dimethoxy-2-phenylacetophenone (DMPA) UV initiator. 150 µl of prepared solutions were pipette into circular Teflon molds with dimensions of 8 mm in diameter and mm in depth. Following a gelation time of approximately 3 minutes, samples were removed from Teflon mold and cut in half. One half of the circular sample was immediately lyophilized and the other half was submerged in deionized water for 3 days to swell. Following 3 days in water, semicircle samples were removed and lyophilized. Unswollen and swollen samples were prepared for SEM by attaching to SEM stage holders affixed through copper tape. Samples were coated with gold for 120 seconds using a coating machine (Denton Vacuum Desk II) prior to SEM imaging (JEOL JSM-7800FLV).

2.4.5. Preparation of MTC gels for swelling and degradation studies

Disks of crosslinked MTC monomer were prepared as described under the sample preparation for SEM. Prior to beginning the study, MTC disks were removed from the mold, washed to remove unreacted monomer and crosslinker, and air dried for 1 day and lyophilized. For both swelling and degradation studies, gel disks were submerged in phosphate buffer solution (PBS) pH 7.4 and kept at 37 °C. At predetermined timepoints, the samples for swelling experiments were completely blotted to remove excess surface water, and the mass of the samples was quickly weighed. For the mass loss studies, PBS was removed from the sample vial and samples were dried through lyophilization for about 6 hours at each time point. The dry mass of the sample at each timepoint was determined. The degree of swelling was determined using the formula:

$$Swelling\ (\%) = \left(\frac{W_s - W_d}{W_d}\right) * 100$$

where W_d is the initial polymer mass and W_s is the weight of the swollen polymer measured at each time point. The percent of polymer remaining was calculated according to the formula:

$$Remaining\ polymer\ (\%) = \frac{W_{deg}}{W_d} * 100$$

Where W_d again is the initial polymer mass at the start of the experiment and W_{deg} is the dried mass of the polymer measured at each specific time point.

2.4.6. Rheological testing of gels

The rheological properties of the produced gels were measured using a TA Instruments ARES rheometer. Parallel plates with 8 mm diameter with sandpaper modified surfaces were used for

all tests. The gap distance between the plates was 2.5-3 mm. A constant stress of ~50 Pa was applied for frequency spectrum measurements between 1-100 rad/s.

2.4.7. Fourier Transform Infrared Spectroscopy (FTIR) degree of crosslinking characterization

Fourier Transform Infrared Spectroscopy (FTIR) was used to characterize the gels/hydrogels and determine the degree of crosslinking as crosslinker mole percent and length were changed (and MTC amount stayed constant). Gels/hydrogels were crosslinked as previously described. Samples were then analyzed by FTIR on a Thermo Scientific Nicolet iS50 instrument with attenuated total reflection (ATR) attachment. The spectra were accumulated from 50 scans at resolutions of 1 cm^{-1}. The FTIR spectra were normalized and spectra band positions and area were analyzed using the OMNIC software program.

2.4.8. Differential scanning calorimetry (DSC) to glass transition temperature (Tg)

Differential scanning calorimetry was carried out on a Perkin-Elmer DSC 7 differential scanning calorimeter. Roughly 10 mg of gel/hydrogel, PEGDA, and liquid MTC monomer sample were loaded into either standard aluminum sample pans or hermetic aluminum sample pans (liquid samples). Each sample was run separately against a reference empty aluminum sample pan. Samples were run according to the following program: (1) hold for 1.0 min at -80.00 °C, (2) heat from -80.00 °C to 150.00 °C at 10.00 °C/min, (3) Hold for 3.0 min at 150.00 °C, (4) cool from 150.00 °C to -50.00 °C at 10.00 °C/min, (5) hold for 5.0 min at -50.00 °C, (6) heat from -80.00 °C to 150.00 °C at 10.00 °C/min, (7) hold for 3.0 min at 150.00 °C, and (8) cool from 150.00 °C to -80.00 °C at 10.00 °C/min. Using Pyris software, the glass transition temperature (T_g) was extrapolated from the heating and cooling runs using the second heating curve (step 6). The

inflection point of the left and right limits were used to determine the T_g for each sample and compared.

2.4.9. Fabrication of porous MTC gels and sterilization for in vitro cell testing

To make a more suitable microenvironment for cell attachment, migration, and proliferation, porous gels were formed according to a previously established sugar porogen/leaching technique[37,135]. Sugar spheres of 250-425 μm of sieved sugar spheres where collected and packed into a Teflon vial with hexane and heat treated for 10 minutes at 37 °C. Following this, hexane was removed and the sugar template was dried under vacuum. Approximately 1.0 mL of the combined solutions of MTC, PEGDA, and 0.25% UV initiator was cast into the assembled sugar template. A mild vacuum was applied during casting to help pull the solution throughout the sugar template. A UV light of 365nm wavelength was again shone on the top of the Teflon vial until complete gelation. The sugar loaded gels were then removed from the vials, and the sugar template was leached away in distilled water. Gels disks were cut into 2 mm thick slices and subsequently punched into 5 mm diameter disks. To sterilize, samples were placed in 48-well suspension plates (Greiner Bio-One) and submerged in 70% ethanol. A vacuum was applied for 10 min to remove air throughout the sample. After 30 min in ethanol on a shaker, samples were washed thoroughly 3 times in sterile PBS. After washing, gel samples were then soaked in cell medium with 15% FBS for 2 hours. Adipose-derived stem cells (ADSCs) and dental pulp stem cells (DPSCs) (200,000 cells/ gel scaffold) were seeded directly onto the gel scaffold in a minimum volume (~12 μL) for the first two hours before cell medium was added to the whole well. This was done to avoid having cells falling to the bottom of the plate rather than directly

onto the scaffold. Cell proliferation measured over the course of a week using CellTiter-Blue® Reagent (Promega Corporation) according to the manufacturer's instruction.

2.4.10. Live/dead histological staining of in vitro cell testing samples

Following 7 days of *in vitro* testing, cell-seeded hydrogel samples were washed in PBS 3 times, left unfixed, and immediately stained with Live/Dead Viability/Cytotoxicity Kit for Mammalian Cell (ThermoFisher Scientific) according to manufacturer's protocol. Samples were then imaged and visualized using confocal fluorescence microscopy (Nikon Eclipse C1).

Chapter 3. Delivery of Hydrophobic Small Molecule, Hydrophilic Small Molecule, and Protein Drugs from Novel 2-methylene-1,3,6-trioxocane (MTC) Hydrogels

Prepared for publication in *Journal of Controlled Release* with co-authors: Navarro R*, Awada M, Adler N, Henry W, Tamas T, and Ma PX., "Delivery of hydrophobic small molecule, hydrophilic small molecule, and protein drugs from novel 2-methylene-1,3,6-trioxocane (MTC) hydrogels." *Both authors contributed equally to this work.

3.1. Introduction

Developing suitable and controlled drug delivery systems with tunable release kinetics for therapeutic agents with different properties has been a challenge within the field of nanomedicine. Due to the physicochemical and biological challenges posed by many drugs such as poor stability, low permeability, short half-life, enzymatic and proteolytic susceptibility, and systemic toxicity, drug delivery systems have been developed to encapsulate and deliver drugs using various delivery vehicles, overcoming many of the issues listed[55,57,136]. Through the drug delivery strategies created, controlled-release systems evolved as a means of tuning the pharmacokinetic and pharmacodynamic profiles of loaded drugs[137]. Overall, this control in drug release and encapsulation formulations leads to sustained release from a drug reservoir, improved drug efficacy, and better safety for the patient. Advantages in drug encapsulation are compared to liquid formulations that are administered through injections or intravenously, which

readily lead to large fluctuations in drug concentration overtime, systemic issues, and patient compliance.

Hydrogels are a class of polymeric materials that have been used to satisfy the goals of controlled release drug delivery systems[75]. Hydrogels are generally defined as three-dimensional, crosslinked networks of polymers that are able to uptake up to thousands of times their dry weight in aqueous solution and keep their shape when placed in solution[78,81]. Hydrogels offer a number of benefits as they relate to drug delivery. The first benefit is that they are largely composed of water and mimic native tissue and extracellular matrix. In this way, they are highly biocompatible, biomimetic, and are appropriate for biomaterials use[81]. The next advantage is that controlled drug release can be tailored and classified as diffusion-controlled, swelling-controlled, chemically-controlled (release dictated by reactions occurring in the polymer matrix), or a combination of these mechanisms. Nevertheless, it is possible to understand how a hydrogel performs in solution and manipulate and adjust parameters to develop a repeatable and reliable controlled drug delivery system. Two great disadvantages exist in hydrogel drug delivery systems despite their tunability. One of the disadvantages is that hydrogel drug release systems lack versatility in drug loading. As hydrogels are normally fashioned from hydrophilic polymers, they are mostly used to deliver hydrophilic drugs. Hydrophobic drugs, which make up about 40% of drugs already on the market and 60% of drugs at the research stage, are immiscible in many of the drug systems developed, which leads to poor drug loading[81,138]. Release of a variety of hydrophilic and hydrophobic molecules from the same system would help advance the field of drug delivery. The next disadvantage is that traditional hydrogels fabricated from polymers such as poly(ethylene glycol) and poly(vinyl alcohol) (PVA) are not inherently degradable based on their chemistry and must be made degradable through the

addition of enzymatically, photolytically, or hydrolytically degradable or cleavable linkages[54,116,139]. This complicates their chemistry and adds synthesis steps. Depending on the type of drug delivery system being fabricated and the desired properties and/or kinetics, degradation at a specific rate may be necessary and beneficial during the controlled release of therapeutics.

The cyclic ketene acetal monomer 2-methylene-1,3,6-trioxocane (MTC) was previously presented as a material for tissue engineering application. This monomer is unique and advantageous in that it undergoes radical ring-opening polymerization (RROP) and a structure switching mechanism that leads to the formation of a polyester during polymerization[49,51,112]. An ester linkage in the polymer backbone allows the polymer to undergo hydrolysis and break down when tested in an aqueous medium *in vitro* or *in vivo*. When used in a drug delivery system, the ability to degrade allows for materials to be implanted or injected *in vivo* and subsequently resorb over time following release of the encapsulated drug. The presence of a radical during the ring-opening process of MTC allows the monomer to react with molecules containing alkene structures that induce crosslinking between the MTC chains. This ability to crosslink and form a gel/ hydrogel material lends the MTC crosslinked material produced to be used as a novel drug delivery system. Unlike traditional aliphatic polyesters which have high crystallinity and greater hardness, polymerized cyclic ketene acetals like MTC tend to have lower crystallinity and produce materials that are more flexible and have high elasticity, similar to the properties of previously developed hydrogels[51]. Hydrogels, just as those being fabricated in this work, form highly porous structures when placed in water[77]. This porosity supports the loading and release of drugs from the gel/hydrogel matrix at a rate that is dependent on the material-drug interaction, diffusion coefficient of the loaded drug throughout the MTC network,

and the physical properties of the gels/ hydrogels that can be tuned such as the mesh size. Along with the capacity to degrade and the ability to form robust gel/ hydrogel constructs, MTC is advantageous in that it exists in a liquid state and is miscible with crosslinking agents like poly(ethyelene diacrylate). This miscibility and liquid state allows for a one-pot synthesis reaction to take place as well as the ability to inject the solution to allow crosslinking *in vivo*. Finally, MTC is a more hydrophobic in its physical properties, which allows for loading of different drugs from the traditional hydrophilic hydrogel systems developed.

To evaluate the utility of MTC gels/ hydrogels in drug delivery, MTC is crosslinked with varying concentrations and lengths of PEGDA crosslinker in a one-pot reaction as previously mentioned. Prior to crosslinking, small molecule drugs with different miscibilities or a macromolecule (protein) are also dissolved in solution or physically mixed to assess how the release of these distinct model therapeutics takes place from the hydrogel matrices. Long term release is evaluated in environments of different pHs, pH 7.4 and pH 4.0. With the information gathered from these studies, we show that a wider range of drugs can be delivered in a controlled manner from hydrogel materials and that this release behavior can be moderately tuned for different drugs. The injectability and possibility of crosslinking this novel hydrogel *in situ* is also demonstrated in this work for future drug delivery applications.

3.2. Results and Discussion

3.2.1. Loading and release behavior of Rhodamine-B dye from crosslinked MTC samples

It was examined in this work whether drug loading and controlled drug release from MTC samples crosslinked with PEGDA can occur and how varying the crosslinker concentration, molecular weight, and physical properties of the drug influence this behavior. To adequately

characterize MTC for use as a drug delivery system, a range of crosslinker concentrations and molecular weights that change the hydrogel from a weaker material to a more rigid material were selected, building on the concentrations tested in the previous MTC tissue engineering work. The crosslinker concentrations tested include 1.0, 2.5, 5.0, 7.5, and 10 mole percents, with respect to moles of MTC monomer, and crosslinker lengths of 575 Da and 2, 4, and 8 kDa; a reasonably broad spectrum of parameters were selected to characterize release from the MTC hydrogels and determine the tunability of this drug release system. For the sake of visually observing the loading and release capability of MTC hydrogels, the pink-red dye Rhodamine was conjugated to 2000 g/mol poly(ethylene glycol)- amine (HO-PEG-Amine), in order to prevent rapid leaching and aid in solubility, and incorporated into the crosslinked MTC hydrogel matrix **(Figure 3.1)**. Using 1.0% crosslinked samples, PEG-Rhodamine was successfully incorporated into the hydrogel matrices as seen in the color change and even distribution within the clear samples. Samples were placed in vials of phosphate buffer saline (PBS) at pH 7.4. Within an hour, differences in the release behavior can be seen among the samples with respect to the crosslinker length. Visually, a change in the buffer solution is seen as the Rhodamine dye is released from the hydrogel samples. There is seemingly more rapid release of the loaded PEG-Rhodamine as the crosslinker length is increased; this effect is evaluated and quantified using models drugs in the remainder of this work. 8 kDa crosslinked samples seem to show a delayed release, however. It is presumed that water takes longer to penetrate these samples and fully saturate the disks from their initial glassy and more rigid states, which could also observed previously in Chapter 2. Because of this, the loaded PEG-Rhodamine B is well entrapped within the PEGDA-MTC matrix and released slowly at early timepoints. The apparent release trend among the 575 Da, 2 kDa, and 4 kDa samples is supported from the discussion in the MTC tissue engineering work

that changes in the hydrophilicity-hydrophobicity balance dictate the behavior within these crosslinked structures. In this analysis, a greater molecular weight (length) in the crosslinker increases the hydrophilicity and leads to more rapid release early on. Knowing that MTC hydrogel matrices can adequately load and release through PEG-Rhodamine, the tailorability, through changes in the crosslinker concentration and length, and control of this drug delivery system was further characterized.

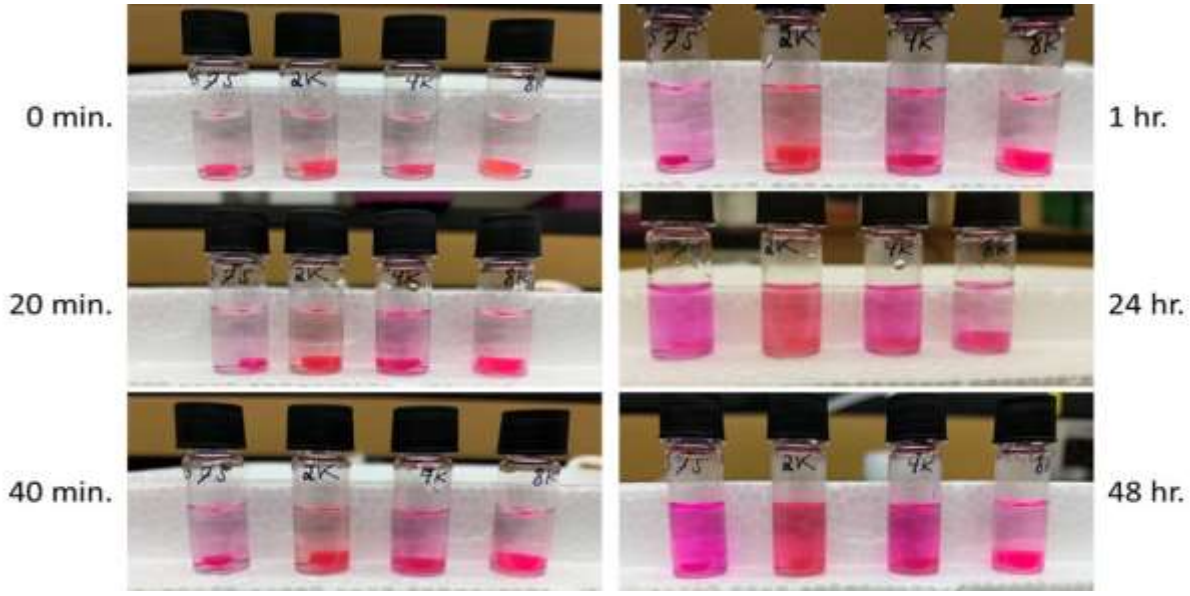

Figure 3.1: Demonstration of drug release from 1% crosslinker MTC-PEGDA hydrogels loaded with Rhodamine-B dye.

3.2.2. Drug release behavior based on the crosslinker molecular weight and concentration of the small molecule hydrophobic drug from crosslinked MTC samples

Following confirmation of the ability to load and release molecules through testing of the PEG-dye from the 1.0% gels, a comprehensive release test was carried out, determining the release behavior at the selected crosslinker concentrations and molecular weights. Two different small molecule drugs were used to determine how the release kinetics can vary from this hydrophobic crosslinked monomer and if this crosslinked MTC hydrogel drug delivery system is suitable for

different drug types. Simvastatin was selected as the small molecule model hydrophobic drug (logP = 4.68) and Aspirin was selected as the small molecule model hydrophilic drug (logP = 1.19)[140,141]. Drug release was also evaluated at two different pHs to assess any changes that occur as pH is varied. The differences seen in release trends due to all of the different parameters mentioned are discussed only in terms of quantitative kinetic models (R^2 and K values) and their curve fitting.

From Simvastatin release tests, differences in release behavior are seen with respect to crosslinker molecular weight (length) and pH. The first notable trend is that at pH 7.4, Simvastatin shows minimal burst release and seemingly consistent linear release over an extended 10 week release period. The release kinetics are evaluated for zero-order (linear) and first order behavior, with all of the curve fitting included in **Appendix B** with and without the early "burst" release timepoints during the first week of release. Developing drug delivery systems with zero order release kinetics has been a challenge among scientists and engineers, which makes it intriguing to see trends leaning towards this behavior in this MTC delivery system. A zero-order release system is one that does not show an extended burst release, delayed release, or an inconsistency in drug release over time[142,143]. Zero-order release kinetics indicates that the release of drug is only a function of time and release takes place at a constant rate that is not dependent on factors such as the drug concentration. This behavior can be modeled by the equation:

$$C_t = C_0 + K_0 t,$$

where C_t is the amount of loaded drug released by time t, C_0 is the initial concentration of drug release, which in an ideal system would be 0, and K_0 is a release rate constant. This type of kinetics is desired because of the consistency it provides in terms of the amount of drug

measured in the blood or in tissue at a specific time and the ability to keep more patients in the therapeutic window. These systems and precisely predicting drug concentrations are difficult to achieve largely because of diffusion and other factors such as dissolution, partitioning, swelling, and erosion[144]. Evaluating zero-order release is done using graphs of cumulative amount of drug released versus time and finding the R^2 values for a linear regression. Even with variations in the crosslinker concentration and molecular weight, the majority of drug release curves of Simvastatin from the MTC hydrogels remains linear and zero-order **(Table 3.1)**. Although first order can be considered in the 575 Da pH 7.4 release test based on the R^2 values, the curve fitting does not follow the first order graphs as closely, with nonlinear curve behavior appearing in the graphs at later timepoints. First order release is represented by the equation:

$$\log C = \log C_0 - \frac{Kt}{2.303},$$

where C_0 is the initial concentration of drug, K is the first order rate constant, and t is the time. By graphing the log cumulative percent drug remaining versus time, first order behavior can be evaluated and quantified with the R^2 value of the linear regression, with the slope being equal to -K/2.303[145]. From the curves of cumulative drug release versus time, comparing the crosslinker molecular weight extremes of 575 Da and 8 kDa, the zero-order linear regression R^2 values are at 0.9529 or greater when including all of the timepoints **(Figure 3.2 and Table 3.2)**. Based on the amount of drug released over time amongst the 575 Da and 8 kDa samples (K_0 constant), an average of 23 µg/day is released from 575 Da samples and an average of 33 µg/day is released from 8 kDa samples. This daily drug amount can be scaled up for the *in vivo* release of similar small molecule hydrophobic drugs.

Table 3.1: Kinetics data of Simvastatin drug release from 575 Da crosslinked samples at pH 7.4.

	575 Da pH 7.4							
CL Conc.	Zero-order r^2	K_0	Zero-order r^2 (Minus burst)	K_0	First order r^2	K_1	First order r^2 (Minus burst)	K_1
1%	0.9725	0.0175	0.9885	0.0158	0.9909	0.0112	0.9922	0.0105
2.5%	0.9861	0.0253	0.9919	0.0232	0.9764	0.0249	0.9642	0.0259
5%	0.9745	0.0255	0.9877	0.0226	0.9399	0.0373	0.9162	0.0399
7.5%	0.9593	0.0229	0.9840	0.0204	0.9678	0.0348	09496	0.0359
10%	0.9529	0.0227	0.9899	0.0199	0.7914	0.0582	0.7395	0.0652

Table 3.2: Kinetics data of Simvastatin drug release from 8 kDa crosslinked at pH 7.4.

	8 kDa pH 7.4							
CL Conc.	Zero-order r^2	K_0	Zero-order r^2 (Minus burst)	K_0	First order r^2	K_1	First order r^2 (Minus burst)	K_1
1%	0.9778	0.0311	0.9736	0.0336	0.8884	0.0259	0.9079	0.0331
2.5%	0.9692	0.0387	0.9721	0.0429	0.8183	0.0412	0.8659	0.0567
5%	0.9819	0.0313	0.9748	0.0338	0.9241	0.0238	0.9417	0.0295
7.5%	0.9827	0.0311	0.9723	0.0328	0.9338	0.0232	0.9480	0.0284
10%	0.9861	0.0323	0.9778	0.0340	0.9427	0.0238	0.9592	0.0288

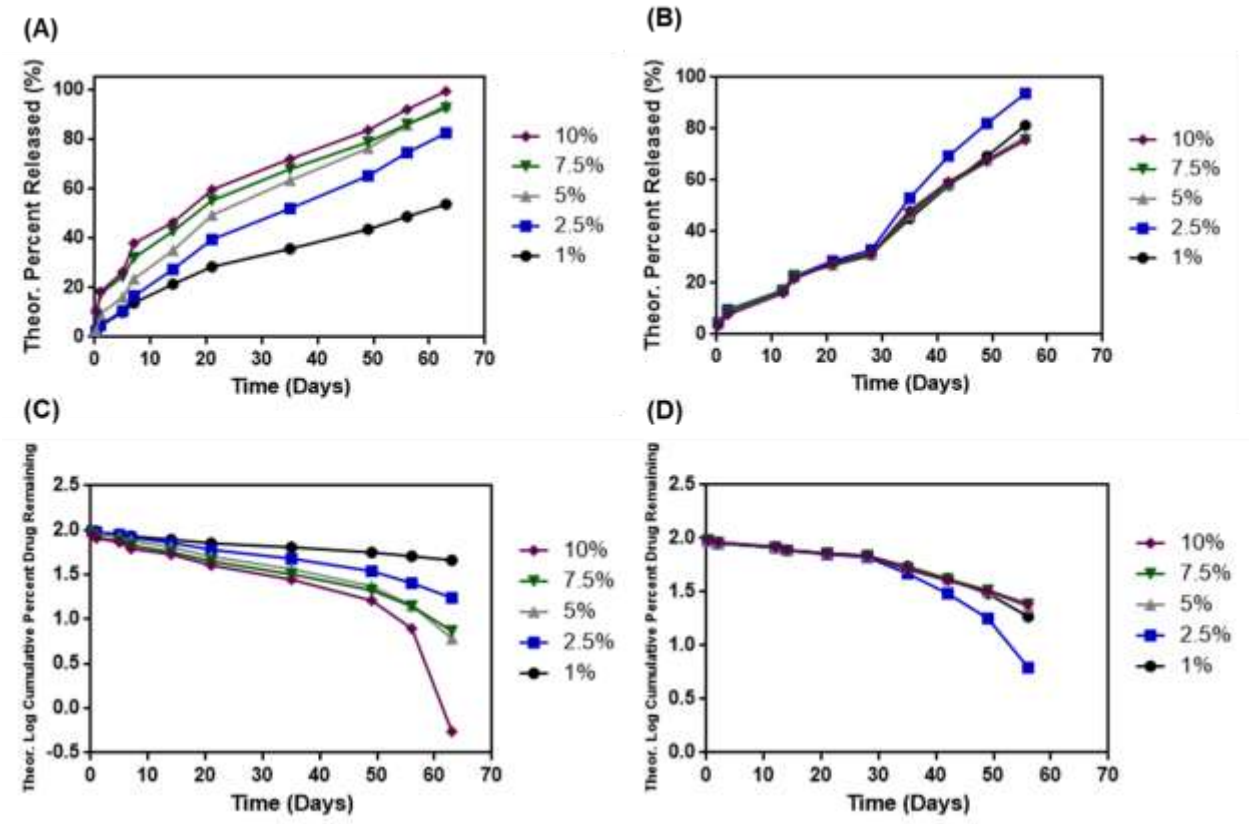

Figure 3.2: Release kinetics graphs of Simvastatin from 575 Da and 8kDa MTC hydrogels. Graphs (A) and (C) show zero-order and first order release kinetics, respectively, of 575 Da samples. Graphs (B) and (D) show zero-order and first order release kinetics, respectively, of 8 kDa samples.

A unique trend is also seen consistently in the drug release experiments performed where, as crosslinker concentration is increased in the samples crosslinked with 575 Da PEGDA, there is an increase in the amount of drug release over time. This trend is seen clearly in the theoretical cumulative percent release graph for Simvastatin **(Figure 3.3)**. This reverse release behavior, exclusive to samples crosslinked with 575 Da PEGDA, is in line with the hydrophobicity and hydrophilicity argument presented in the MTC tissue engineering work in Chapter 2. Generally, as the percent of crosslinker is increased, mesh size decreases, which should inhibit or the slow the rate of drug release[119]. Instead, as the concentration of 575 Da crosslinker is increased from 1% to 10%, a greater release rate is seen as the amount of crosslinker increases. This suggests

that at this lower molecular weight, as the 575 Da MTC samples become more hydrophilic, this leads to an increase in the hydrophilicity of the hydrogel which increases the rate of drug release from the MTC matrix. The change in hydrophilicity for this hydrophobic crosslinked MTC material is significant enough to drive drug release. A greater difference in the release rate as the percent of crosslinker is changed is also seen between the release curves of Simvastatin from MTC samples crosslinked with 575 Da PEGDA in pH 7.4 buffer.

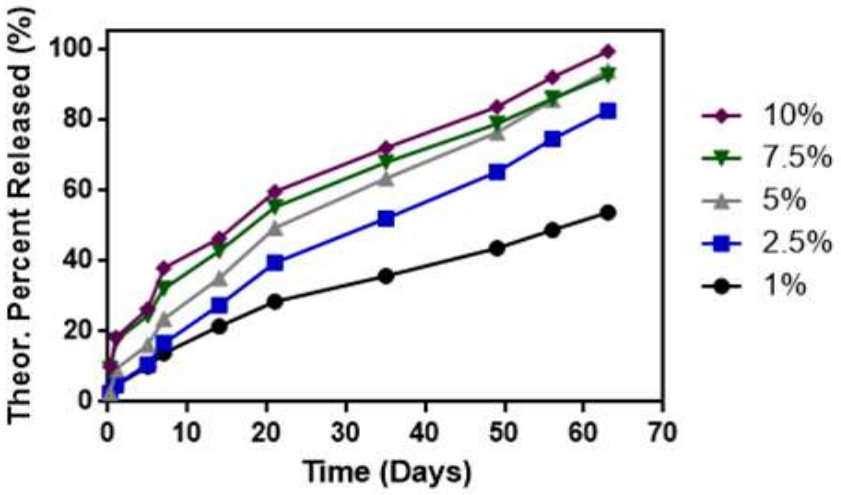

Figure 3.3: Unique release trend in 575 Da crosslinked MTC hydrogels. Theoretical percent released drug over time shows an increase in drug release as crosslinker concentration increases.

The cumulative percent release graphs of Simvastatin in pH 7.4 PBS show a more classical release trend in the 2 kDa, 4 kDa, and 8 kDa crosslinked samples where the trend is the greater the crosslinker concentration, the less drug release over time. This suggests that a longer crosslinker causes the drug release behavior of MTC hydrogels to mimic that of typical hydrogels fabricated from hydrophilic monomers or polymers. The hydrophilic effect of changing the crosslinker length, however, can still be evaluated by noticing the change in the slope of cumulative percent release graphs, which is related to K_0 of the cumulative amount of drug released graphs, as the crosslinker molecular weight is increased from 2 kDa, 4 kDa, and 8

kDa. When crosslinked with 2 kDa PEGDA crosslinker, the average slope of the theoretical percent released curves is 0.6924 ± 0.1437 (%/day). As the crosslinker length increases to 4 kDa, the average slope of the curves increases to 0.9377 ± 0.1209, and for 8 kDa, the average slope is 1.3572 ± 0.1350. This means that as molecular weight of the crosslinker increases and the samples become more hydrophilic, there is an overall effect on how quickly the drug is released. A longer crosslinker in turn leads to a faster release rate of Simvastatin from the MTC hydrogels. The difference in release rate, however, as crosslinker concentration is increased becomes less pronounced as crosslinker length is increased. This can be seen in comparing the concentration extremes (1% and 10%) of Simvastatin released from 2 kDa and 8 kDa MTC samples **(Figure 3.4)**. In general, at the crosslinker concentrations tested in this drug delivery strategy, the variation in crosslinker mole percent with respect to moles of MTC from 1%, 2.5%, 5%, 7%, and 10% appears to not influence drug release as greatly as changing the crosslinker molecular weight.

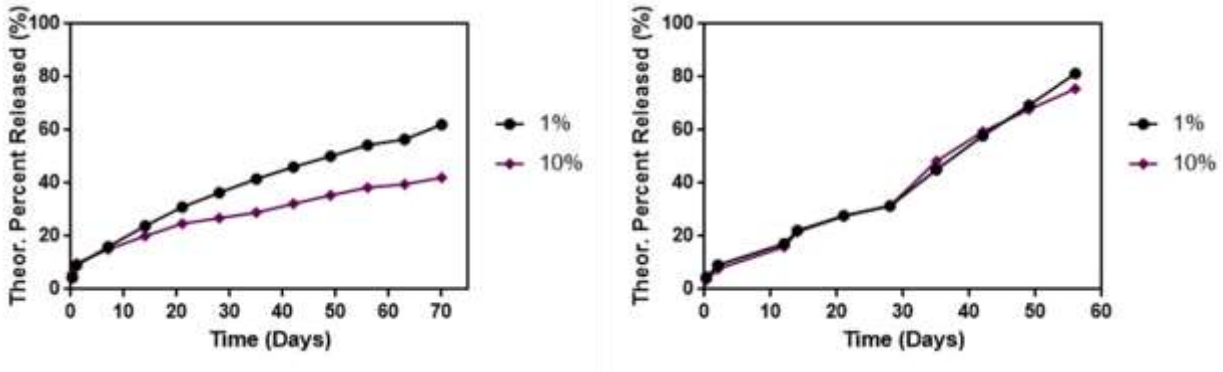

Figure 3.4: Change in release rate differences as crosslinker length is increased. 1% and 10% curves for 2 kDa (left) and 8 kDa (right) crosslinked samples shown.

While the release tests were performed at physiological pH (pH 7.4), samples cut from the same initial disk prepared for each crosslinked MTC combination were also tested at an acidic pH of 4.0. Evaluating drug release at this pH is important when characterizing the utility

of drug delivery systems as different areas of the body and different disease states have more acidic pHs, such as the stomach or tumor microenvironment [146,147]. Upon testing at pH 4.0, differences in the release trends were observed for the model hydrophobic drug Simvastatin compared to the release behavior that takes place at pH 7.4 **(Figure 3.5)**. Looking at the 1%, 5%, and 10% crosslinker concentration curves for 2 kDa PEGDA crosslinker samples, notable changes in the slopes or release rates for each percent at pH 4.0 can be seen when compared to the release rate achieved at pH 7.4 **(Table 3.3)**. The drug release is severely dampened in the acidic PBS buffer. The remaining crosslinker lengths (575 Da, 4 kDa, and 8 kDa) also follow this trend when comparing release at pH 7.4 and pH 4.0, with shallower slopes and slower release occurring in an acidic environment. This change is slope is also reflected in a drop in the K_0 values when comparing the zero-order release kinetics at the two pHs tested **(Table 3.4 and Table 3.5)**. With both zero-order and first order behavior at play following a more pronounced burst order than at pH 7.4, the curves for cumulative percent of drug released over time at pH 4.0 tends towards behavior that suggests that both the time-independent release kinetics characteristic of swelling-controlled drug release and kinetics of the diffusion process are driving drug release; this situation is known as anomalous transport[148]. Detailed modeling, however, should be used to verify the type of release mechanism by finding the value of the diffusion coefficients, which falls into specific ranges depending on the diffusion mechanism. The change in release kinetics and potentially release mechanism and why this occurs in acidic pH for this MTC hydrogel system crosslinked with PEGDA is not completely understood at this time. Where generally an acidic pH enhances degradation and swelling of most polymers and should, therefore, lead to a greater amount of drug released at each timepoint compared to the release at pH 7.4, the opposite effect is seen consistently in this work. It is hypothesized based on the

shallow release that there is a shrinking or deswelling effect on the MTC hydrogels, causing a shrinking in the pores of the hydrogel mesh and retardation in the release of the loaded small molecule drug. This hypothesis can be verified through future swelling tests of the MTC samples at the crosslinker concentration used in this drug delivery work in acidic PBS buffer. The change in mesh size can also be evaluated visually using SEM, as previously shown in the MTC tissue engineering work, and more robustly using fluorescent dextran beads[149,150].

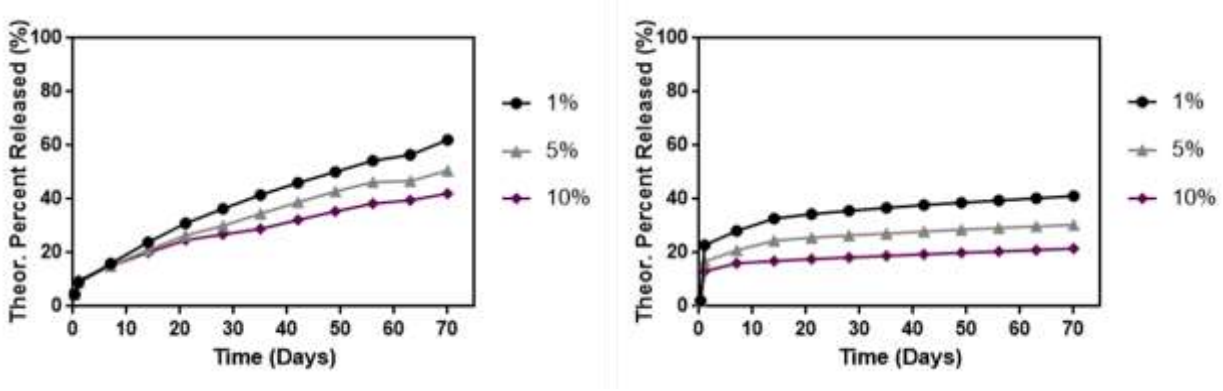

Figure 3.5: Simvastatin release at physiological pH versus at acidic pH from 2 kDa crosslinked MTC samples. Drug release is shown at pH 7.4 (left) and pH 4.0 (right) at varying crosslinker concentrations.

Table 3.3: Change in slope/drug release rate of Simvastatin at pH 7.4 versus pH 4.0 at different crosslinker concentrations.

2 kDa pH 7.4	Slope	2 kDa pH 4.0	Slope
1%	0.7828 ± 0.04438	1%	0.3486 ± 0.09112
5%	0.6291 ± 0.03775	5%	0.2549 ± 0.06659
10%	0.4806 ± 0.03239	10%	0.1671 ± 0.04530

Table 3.4: Kinetics data of Simvastatin release from 2 kDa crosslinked MTC samples at pH 7.4.

	2 kDa pH 7.4							
CL Conc.	Zero-order r^2	K_0	Zero-order r^2 (Minus burst)	K_0	First order r^2	K_1	First order r^2 (Minus burst)	K_1
1%	0.9689	0.0185	0.9871	0.0154	0.9951	0.0125	0.9959	0.0119
5%	0.9652	0.0157	0.9809	0.0131	0.9883	0.0091	0.9905	0.0084
10%	0.9565	0.0124	0.9903	0.0010	0.9787	0.0065	0.9939	0.0057

Table 3.5: Kinetics data of Simvastatin release from 2 kDa crosslinked MTC samples at pH 4.0.

	2 kDa pH 4.0							
CL Conc.	Zero-order r^2	K_0	Zero-order r^2 (Minus burst)	K_0	First order r^2	K_1	First order r^2 (Minus burst)	K_1
1%	0.5941	0.0082	0.9845	0.0034	0.6645	0.0049	0.9889	0.0023
5%	0.5943	0.5943	0.9897	0.0026	0.6407	0.0032	0.9919	0.0014
10%	0.5763	0.0043	0.9973	0.0021	0.6088	0.0020	0.9980	0.0010

While Simvastatin was able to show long-term release from the hydrophobic crosslinked MTC, Aspirin did not perform well in this drug delivery system. Although Aspirin appeared soluble and dissolved directly into the solutions of MTC, PEGDA, and initiator prior to crosslinking, close to 100% of drug was released within 24 hours (the first two measured timepoints) at both pH 7.4 and pH 4.0. This effect is similar to how hydrophobic drugs fail to show sustained release in traditional hydrogel drug delivery systems fabricated from hydrophilic monomers or polymers[(77)]. Aspirin acts as a negative control for this drug delivery system, further showing the benefit of this hydrogel matrix for loading and delivery of the numerous hydrophobic drugs.

3.2.3. Drug release behavior based on the crosslinker molecular weight and concentration of BSA loaded protein

The release behavior of Bovine Serum Albumin (BSA), a globular protein, was also evaluated from this MTC drug delivery system. BSA was loaded at the same concentration as Simvastatin and Aspirin and evaluated at physiological pH and at an acidic pH as the crosslinker concentration and molecular weight were varied. It is important when characterizing this novel drug delivery system to compare the release behavior of the small molecule drugs previously discussed to that of a protein such as BSA not only because of the physical hydrophilic properties of proteins, but also because of the great difference in the size of the molecules. Simvastatin and Aspirin, with molecular weights of 418.6 Da and 180.16 Da, respectively, are classified as small molecule drugs as they are organic compounds that are less than 900 Da[(151)]. BSA, on the other hand, is much larger with a molecular weight of 66.5 kDa and is expected to behave differently when eluting from a hydrogel system. Representative of the release kinetics of BSA from all of the MTC combinations tested, the graphs of BSA release at pH 7.4 and pH 4.0 from samples crosslinked with 575 Da PEGDA indicate the release behavior of this protein **(Figure 3.6)**. Unlike the steady and linear release Simvastatin shows at pH 7.4 and the complete dumping of Aspirin under all conditions that takes place within 6-24 hours, BSA consistently shows burst release behavior over the first 3-7 days of release followed by slower steady release. The greater the crosslinker concentration the faster the drug or protein is completely released. Following the first week of drug release, at all of the crosslinker lengths tested, release at pH 7.4 continues at more first order kinetics for samples with a lower crosslinker concentration, while release at pH 4.0 shows evidence of zero-order release at these same crosslinker concentrations in the upward linear slope of the curves. The kinetics at pH 7.4 **(Table 3.6)** and at pH 4.0 **(Table**

3.7) (minus the 10% curves) were evaluated through the zero-order and first order R^2 values with and without the burst release values up to day 3. BSA release at pH 7.4 displays consistent first order release behavior, whereas BSA release at pH 4.0 shows first order release within the first 7 days followed by an apparent change in release that can be classified as zero-order release for the remaining time of the experiment. As previously mentioned when discussing Simvastatin, modeling should be used in the future to find the value of the diffusion coefficients and determine the release mechanism of BSA from MTC hydrogels.

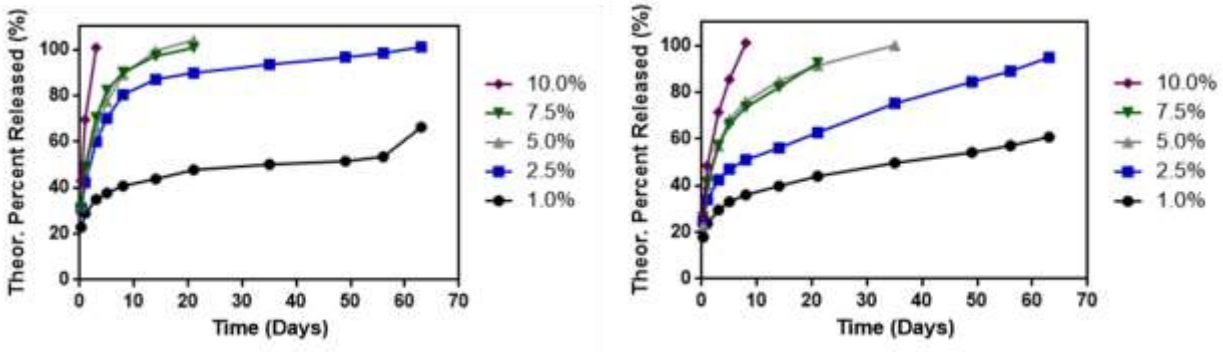

Figure 3.6: BSA release at physiological pH versus at acidic pH from 575 Da crosslinked MTC samples. Drug release is shown at pH 7.4 (left) and pH 4.0 (right) at varying crosslinker concentrations.

Table 3.6: Kinetics data of BSA release from 575 Da crosslinked MTC samples at pH 7.4 with and without 3 day burst release timepoints.

575 Da pH 7.4 BSA Release				
CL Conc.	Zero-order r^2	Zero-order r^2 Minus burst	First order r^2	First order r^2 Minus burst
1%	0.7490	0.8942	0.8055	0.9145
2.5%	0.6443	0.8306	0.9443	0.9665
5%	0.7853	0.8901	0.9523	0.9759
7.5%	0.6977	0.9060	0.9926	0.9997
10%	--	--	--	--

Table 3.7: Kinetics data of BSA release from 575 Da crosslinked MTC samples at pH 4.0 with and without 3 day burst release timepoints.

575 Da pH 4.0 BSA Release				
CL Conc.	Zero-order r^2	Zero-order r^2 Minus burst	First order r^2	First order r^2 Minus burst
1%	0.9004	0.9861	0.9501	0.9933
2.5%	0.9382	0.9957	0.9574	0.9403
5%	0.7216	0.9316	0.9631	0.9988
7.5%	0.8191	0.9913	0.9975	0.9753
10%	--	--	--	--

Just as in the case of release of Simvastatin from 575 Da crosslinked samples at pH 7.4, the release of BSA at both pHs and all four molecular weights show a reverse trend in release. As the crosslinker percent is increased within the hydrophobic MTC samples, instead of a traditional inhibition in release as the mesh size decreases with increasing crosslinker concentration, the release rate of BSA increases. This behavior is illustrated again looking at the graphs for the crosslinker molecular weight extremes (575 Da and 8 kDa) for 1%, 5%, and 10% crosslinker concentrations **(Figure 3.7)**. For a hydrophilic protein encapsulated in a hydrophobic material this can be expected as the protein would rather move into a more hydrophilic environment. Therefore, as the samples become more hydrophilic with the increase in crosslinker concentration, BSA release rate is enhanced. It is postulated that BSA shows this same "reverse" release pattern at both pH 7.4 and pH 4.0 despite any physical changes to the MTC hydrogels at different pHs because the release of the proteins from highly crosslinked hydrogels is generally independent of pore or mesh size[152,153]. As BSA is a much larger molecule than the small

molecule drugs discussed earlier, BSA does not travel as extensively through or get trapped and interact with pores within the gel matrix as closely as a small molecule like Simvastatin. Instead, proteins may diffuse through hydrogels based on theories such as the free volume theory, which describes how high molecular weight molecules (proteins/drugs) diffuse by jumping into previously occupied voids in a polymer (solvent) system[154,155]. Changes in the hydrogel morphology or pore size and any related changes in material surface charge and charge interactions, however, can be evaluated to rationalize the consistent differences in kinetics between the more flat release curves seen at pH 7.4 and the upward sloping linear release seen at pH 4.0.

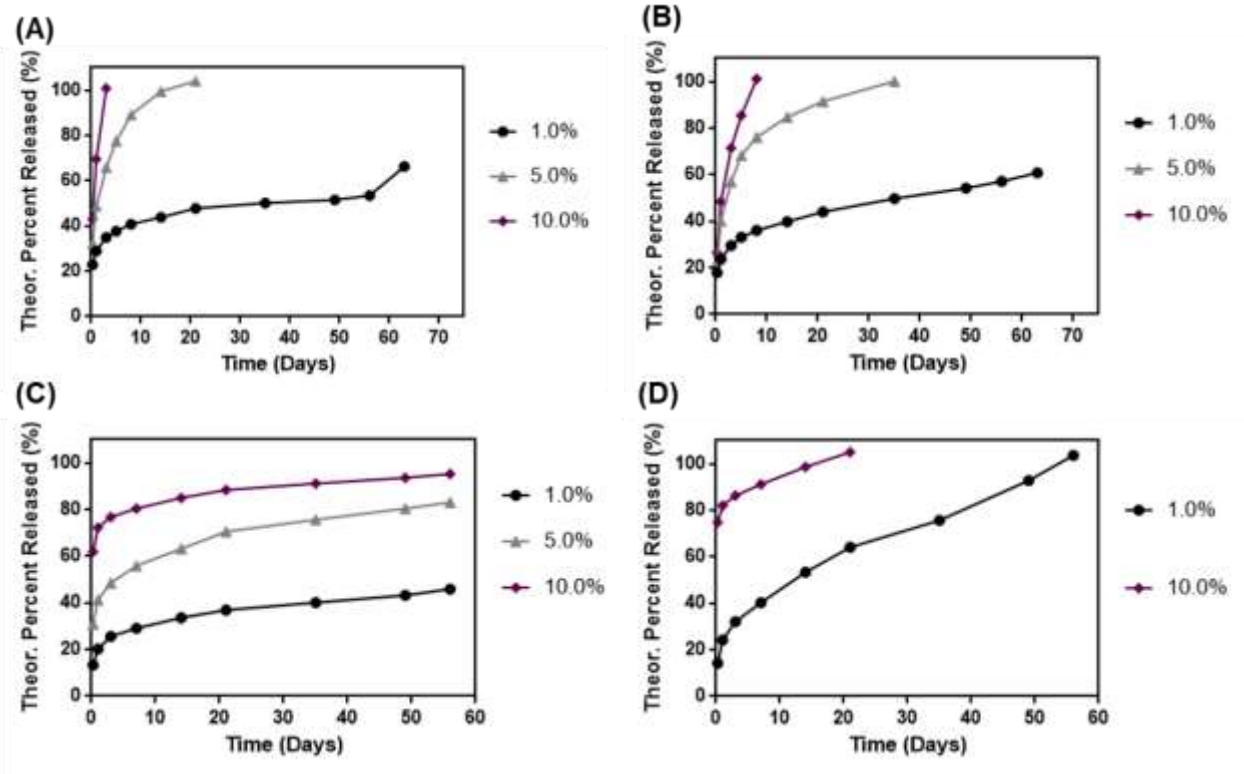

Figure 3.7: Reverse trend in drug release: increase in BSA release as crosslinker concentration is increased. (A) BSA release from 575 Da samples at pH 7.4, (B) BSA release from 575 Da samples at pH 4.0, (C) BSA release from 8 kDa samples at pH 7.4, and (D) BSA release from 8 kDa samples at pH 4.0 at 1%, 2.5%, and 10% crosslinker concentrations.

Finally, the BSA release experiments did not show any substantial trends with respect to crosslinker molecular weight. This can be due to how BSA interacts with the MTC hydrogel matrix as well as how changes in crosslinker molecular weight versus changes in the crosslinker concentration tested influence changes in sample hydrophilicity.

3.2.4. Testing in situ injectability of MTC hydrogels

The ability to inject the MTC-PEGDA solution subcutaneously into a mouse prior to forming the robust hydrogel biomaterial was tested. To assess the injectability, the 2 kDa 1.0% PEGDA crosslinker MTC hydrogel formulation was injected at volumes of 100 µL to 250 µL subcutaneously into a euthanized mouse using a standard 18G needle, assisted by a colleague Zhen Zhang. The minimum amount of time needed for gelation under the 365 nm wavelength UV light was also tested. The goal was to show that the MTC solution could successfully pass through a needle, collect in a subcutaneous pocket, and gel through the mouse skin *in situ* to potentially deliver a drug. From the trials done, injecting 100 µL and administering the UV light for 1 minute help form a complete and contained gel reservoir **(Figure 3.8)**. A larger volume or less time (30 seconds) for gelling leads to spreading of the material under the skin of the mouse, which could cause the material to be washed away and drug being released away from the intended site of action. Injectability is desirable for hydrogels, whether used for drug delivery or tissue engineering, because it allows for minimally invasive *in situ* delivery of therapeutic agents or a tissue engineering scaffold[156]. Traditionally, hydrogels have been formed at the bench, sterilized, and implanted using an invasive surgical process. With the advent of injectable hydrogels, novel hydrogels developed should meet this criterion of injectability as they help reduce procedure costs, diminish pain to the patient, and protect the drug payload being delivered

in vivo. Improving the gelation in future experiments to possibly reduce the time of UV light exposure and help prevent the gel from flowing away could be achieved using a probe or point source light rather than a larger UV light available for these experiments. Formulations with higher molecular weights that have a slightly higher viscosity may also better form intact drug depots *in situ*.

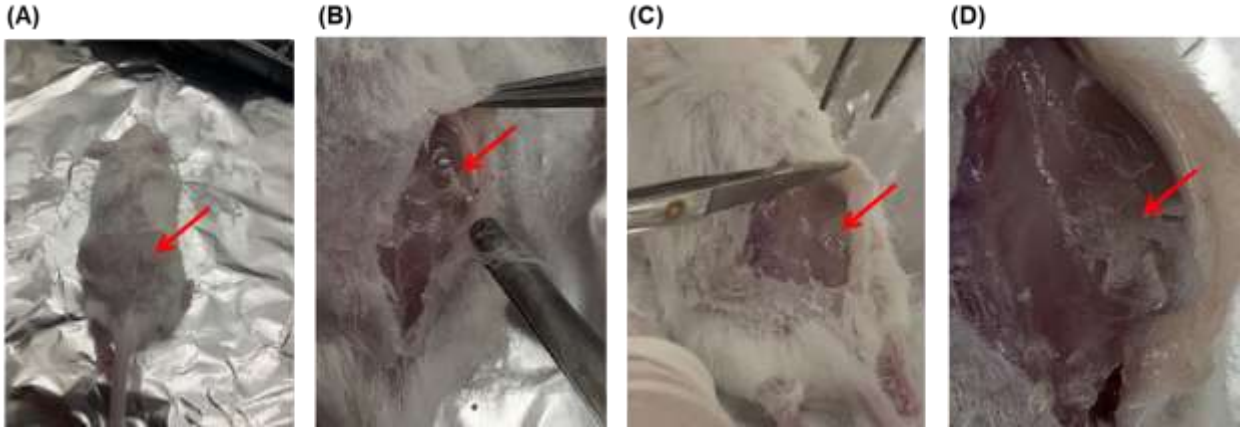

Figure 3.8: Testing injectability of MTC hydrogel through subcutaneous injection and gelling *in situ* into mouse. (A) Subcutaneous pocket of gel formed, (B) 100 µL MTC solution and 30 seconds gelling, (C) 100 µL MTC solution and 1 minute gelling, and (D) 250 µL and 1 minute gelling.

3.3. Conclusion

The utility and biocompatibility of MTC gels/ hydrogels have been previously shown for tissue engineering purposes. Here, MTC was adapted and characterized for use as a drug delivery system for the release of small molecule hydrophobic drugs, small molecule hydrophilic drugs, and proteins. Based on different parameters including the crosslinker molecular weight, crosslinker concentration, physical properties of the molecule being delivered, and the delivery environment (pH), different trends were found. Overall, this drug delivery system appears highly suitable for the long-term delivery of small molecule hydrophobic drugs, such as the model drug Simvastatin, and is also suitable for the release of proteins, such as BSA, tested in this work.

This system was not ideal for the release of Aspirin, a small molecule hydrophilic drug, which showed rapid, uncontrolled release. Simvastatin release curves showed zero-order release behavior at physiological pH, while at an acidic pH of 4.0 this release was stifled. Hydrophilic effects were seen in crosslinked concentration and molecular weight and reflected in the drug release rate as discussed. Similarly, the release of BSA showed a dependence on crosslinker concentration especially, with a consistent increase in the amount of drug released over time as crosslinker concentration was increased. The greatest challenge in future protein release, as in many drug delivery projects, is reducing the initial burst release. An understanding of how different molecules interact with this novel drug delivery system was attained through these experiments. By tailoring the transport and physical characteristics of the components of this drug delivery system, it shows great potential for injectable, controlled release applications of hydrophobic drugs and proteins.

3.4. Experimental Section

3.4.1. Materials

Chloroacetaldehyde dimethyl acetal, Dowex® 502W, Tetrahydrofuran (THF), Aliquat® 336, diethylene glycol, Rhodamine-B, MES, and 2,2-Dimethoxy-2-phenylacetophenone, 99% were all purchased from Sigma Aldrich (St. Louis, MO). Potassium tert-butoxide and aluminum oxide were purchased from Oakwood Chemical (Estill, SC). N-(3-Dimethyaminopropyl)-N'-Ethylcarbodiimide (EDC) Hydrochloride was purchased from Advanced Chemtech. Acrylate-PEG-Acrylate (PEG diacrylate) MW 2,000 and HO-PEG-Amine 2000 were purchased from Laysan Bio, Inc. (Arab, Alabama). PEGDA 4000 and PEGDA 8000 were purchased from Polysciences, Inc. (Warrington, PA). The drug Simvastatin was purchased through Acros

Organics, Aspirin was purchased through Sigma Aldrich, and Bovine Serum Albumin Standard Grade was purchased through Alkali Scientific Inc.

3.4.2. Synthesis of 2-methylene-1,3,6-triococane (MTC)

The synthesis of methylene trioxocane followed the work described by Hiraguri[112] et. al. and later Undin[51] et. al. based on the method developed by Bailey[47,48] et al. Synthesis is identical to the process used in the tissue engineering MTC gel/ hydrogel work. Briefly, Chloroacetaldehyde dimethyl acetal and diethylene glycol were mixed in a 1:1 ratio in the presence of Dowex® 50 (H^+) in a round bottom equipped with a fractioning column. The mixture was heated to 120 °C until the theoretical amount of methanol was collected. The reaction was vacuum filtrated to remove the Dowex® and purified by vacuum distillation yielding white crystals of 2-chloromethyl-1,3,6-trioxocane **(1)**. The monomer **(1)** was placed in a round bottom and dissolved at a ratio of 1:2 g/mL of anhydrous THF and placed in an ice bath. To this, 2 mol % of Aliquat® 336 was added and stirred for an additional 30 min in an ice bath. To this, 2 mol equivalents of potassium tert-butoxide were added slowly to the mixture and then allowed to stir overnight. The product was concentrated to remove the THF and dissolved in ethyl ether and purified using aluminum oxide. The filtrate was concentrated and dissolved in fresh ethyl ether and purified in aluminum oxide twice more to remove traces of tert-butoxide. Finally, the filtrate was purified by vacuum distillation using a 10 cm fractioning column to produce MTC **(2)** as a transparent liquid.

3.4.3. Fabrication of MTC drug loaded samples

Disks of crosslinked MTC polymer with loaded drug were prepared with five different crosslinking percents of poly(ethylene glycol) diacrylate and utilizing four different molecular weights (575Da, 2kDa, 4kDa, and 8kDa). 1.0%, 2.5%, 5.0%, 7.5%, and 10.0% mole percent of crosslinked MTC samples were prepared with 0.1% 2,2-Dimethoxy-2-phenylacetophenone (DMPA) UV initiator. Crosslinker was dissolved within MTC solution with added heat at 55°C, if necessary. Small molecule hydrophobic drug (Simvastatin), small molecule hydrophilic drug (Aspirin), and a model protein (Bovine Serum Albumin- BSA) were loaded at 3 weight/volume percent to determine changes in release behavior of different types of drugs. Simvastatin and Aspirin were dissolved directly into the MTC monomer, while BSA was dissolved at 2 µg/µl in distilled water and added to MTC. MTC monomer, dissolved crosslinker, added drug, and DMPA initiator solutions were vortexed for 10 seconds for even mixing, and 1mL of solution was added into an 18mm Teflon vial. Samples were left for 5 minutes under 365nm wavelength light for complete gelation. Disks were removed from Teflon vials and left in DI water for 5 minutes to remove unreacted solution on disk surfaces. 5 mm samples were cut from this larger disk for drug release testing.

3.4.4. Fabrication of Rhodamine-B drug loaded samples and evaluation of release

The dye Rhodamine-B was loaded into crosslinked MTC samples to observe how loading and release takes place from the hydrogel matrices. Prior to loading, Rhodamine-B was conjugated to HO-PEG-Amine 2000 through EDC chemistry. To do this, PEG-amine and Rhodamine-B were both dissolved in MES buffer pH 4.7. PEG-Amine and Rhodamine-B were reacted in a 1:3 molar ratio to ensure conjugation. EDC was dissolved in MES buffer and added to the reaction and left

to react for 24 hours. The reaction was then dialysed to remove the unreacted Rhodamine-B and subsequently lyophilized. Using a mold, 8 mm diameter and 2 mm thickness disks were fabricated utilizing four different molecular weights (575Da, 2kDa, 4kDa, and 8kDa) at 1.0% crosslinker concentration with 1.0% weight/volume PEG-Rhodamine-B loaded according to the crosslinking protocol mentioned in the previous section. Samples were then placed into 1 mL of DI water to observed release over time visually.

3.4.5. Performing drug release test of drug loaded MTC samples

5 mm gel/hydrogel samples were punched from 18 mm drug loaded MTC disks and placed into an eppendorf tube with 1 mL of phosphate-buffered saline (PBS) at either pH 7.4 or pH 4.0. At the desired timepoints, PBS solution was collected and gel sample was resuspended in 1 mL of fresh PBS until the next timepoint. To form a curve of cumulative drug released over time, Simvastatin and Aspirin timepoints were measured using ultraviolet-visible (UV-Vis) spectroscopy, measuring the drugs at their characteristics wavelengths of 247nm and 230nm, respectively. BSA was measured using a MicroBCA Protein Assay kit according to the manufacturer's protocol. N=3 was for all samples at both pH values tested. Theoretical drug loading was calculated based on the volume of the MTC disks after washing and prior to punching out samples, and scaled based on the amount of drug loaded into 1 mL of solution used for crosslinking and the volume of the 5 mm diameter samples.

3.4.6. *Testing injectability and gelling of MTC gel/ hydrogel*

Injectability of the MTC gel was tested using the 2 kDa 1.0% PEGDA crosslinker formulation. To do this, mice were euthanized via CO_2 asphyxiation followed by cervical dislocation and

experiments were performed on dead mice. 100-250 µL of solution without drug was subcutaneously injected using an 18 gauge (G) needle and gelled with 365 nm wavelength UV light in NOD-scid mice. Various gelling times were tested to find the minimum time needed for complete gelation. Skin of mice was subsequently cut open and pulled back for imaging of gel material.

Chapter 4. Targeting of HER2+ SKBR3 cells with Novel Conjugated Targeting Peptides on "Single" versus "Palm-tree" PEG-PLGA Nanoparticles (NPs)

Prepared for publication in *Nanomedicine* with co-authors: Chen J, Wang J, Cao Z, Wang SH, and Ma PX., "Efficacy of linear PEGMA-PLGA versus branched PEGPET-PLGA nanoparticles with conjugated novel targeting peptides against HER2+ SKBR3 Breast Cancer Cells."

4.1. Introduction

With over 268,600 new cases diagnosed in 2019 and over 41,760 deaths annually in the same year, breast cancer is the most common cancer diagnosed and second most common cause of cancer-related deaths in women in the United States [97,157]. Among the types of breast cancer diagnosed, human epidermal growth factor receptor 2 (HER2) positive breast cancer currently accounts for 15-20% of all diagnosed breast cancer cases[96,99]. HER2+ breast cancer patients generally have expression of HER2 that is 50-100 fold higher in tumor cells than normal cells (HER2+). It is one of the most aggressive types of breast cancer, and patients faced with this type of breast cancer often become resistant to treatment regimens. Treatment options for HER2+ breast cancer includes different systemic therapy options including chemotherapy for highly proliferative tumors, hormonal therapy, radiation therapy, and/or HER2-targeted therapy, including the use of the popular anti-HER2 monoclonal antibody trastuzumab[98]. Significant disadvantages exist in the use of these systemic treatments. In particular, the use of trastuzumab

is limited in the number patients' prognoses it improves and presents challenges with determining the most appropriate adjuvant sequence for patients as well as the necessary treatment duration. Trastuzumab also poses serious cardiac toxicity effects, especially when used in combination with frequently used anthracycline chemotherapeutics[158]. Issues with these systemic treatments, especially chemotherapy, stem from the fact that they not only kill cancer cells, but also fast-growing healthy cells. Because of this many short-term and long-term side effects result from the systemic nature of treatments including nausea, vomiting, loss of appetite, fever, and fatigue along with heart, kidney, lung, and nerve dysfunction in the months to years following treatment. The demonstrated low-efficacy of anthracycline based treatment regimens and resistance of HER2+ breast cancers to these treatments contribute to an overall high mortality rate in HER2+ breast cancers.

Nano drug delivery systems have been developed to address these systemic effects and other challenges that exist with delivering drugs into the body to treat diseases such as HER2+ breast cancer. These additional challenges include poor drug solubility, especially when delivering hydrophobic drugs like the chemotherapeutics, poor absorption by the body, lack of *in vivo* stability, and poor bioavailability/distribution[55]. Different nanoparticle types have helped to address some of these issues, such as the liposomal anthracycline formulation known as Doxil[83]. Although this liposomal doxorubicin treatment is FDA approved and decreases toxicity effects compared freely floating doxorubicin, the delivery of liposomal doxorubicin has failed to significantly improve patient treatment and prognosis compared to conventional doxorubicin treatment[158]. As with early nanoparticle systems for cancer treatment that rely solely on size and the enhanced permeation and retention (EPR) effect to enter tumors, Doxil and other non-ligand conjugated nanoparticle systems are passive targeting[159]. The majority of administered

nanoparticles in these systems fail to reach their intended site of action and are largely ineffective in reaching and treating tumors and any metastatic breast cancer cells.

Instead, active targeting approaches are useful in helping nanoparticles delivered into the body more precisely reach HER2+ breast cancer cells and deliver drugs to the cells they are intended to kill. By modifying nanoparticles' chemistry and attaching targeting ligands such as with antibodies or peptides on their surface, nanoparticles can selectively interact with HER2+ cancer cell receptors to bind to these cells[82,160,161]. A number of polymeric nanoparticle systems designed to treat HER2+ breast cancer cells have used targeting peptides, specifically folic acid-derived peptides, cyclic RGD, and peptide mimics of the trastuzumab antibody[68,83,162,163]. While peptides are a superior choice in targeting moiety due to their size, selectivity, risk of immunogenicity, ease of conjugation, and low cost of fabrication, these nanoparticle-peptide systems are not very effective or ideal[160]. Folic acid and RGD are more nonspecific peptides as healthy cells also express the folate receptor targeted by the folic acid peptides and the RGD peptide is a general cell binding sequence[92,164]. As with the trastuzumab antibody, targeting using a trastuzumab peptide-mimic shows selectivity, but limited ability to effectively treat HER2+ cancer. More selective and effective HER2+ targeting peptides in combination with drug-loaded nanoparticles must be employed to meet this treatment goal and improve nanoparticle delivery to and into HER2+ breast cancer cells.

A number of targeting peptides specific to HER2+ breast cancer has have been identified through various screening processes over the past decade[165,166]. Among these, novel peptide sequences have been identified through phage display with high specificity for the HER2+ SKBR3 cell type[167,168]. In this work, the peptide with the greatest affinity, L1 (sequence: VSSTQDFP), was selected and assessed as a peptide strategy conjugated to polymeric

nanoparticles to target and ultimately kill HER2+ breast cancer cells. In addition to testing how this peptide performs as a component in a nanoparticle drug delivery system, additional strategies are employed to determine if they improve the efficacy of the nanoparticles to not only target HER2+ breast cancer cells, but also ensure internalization of the particles into cells to then release drug and cause cell death. The first strategy involves incorporating a cell-penetrating peptide (CPP) sequence to that of the L1 sequence. CPPs are short sequences, up to 30 amino acids, that help arrange extracellular components and overcome intracellular barriers of entry to facilitate the movement of cargo across the cell membrane and into the cell cytoplasm[169–171]. One of the first identified, most effective at intracellular routing, and commonly used CPPs is the transactivator of transcription (TAT) protein isolated from the human immunodeficiency virus (HIV) (sequence: GRKKRRQRRRPQ). The ability of these novel peptide combinations to improve nanoparticle targeting and entry into HER2+ cells and how varying position of this added TAT sequence (preceding or following the L1 sequence) is evaluated. The second strategy manipulates the nanoparticle chemistry, by (1) preliminarily determining the appropriate spacer length for the peptides used and (2) using this spacer length, testing mono- (poly(ethylene glycol methacrylate)-poly(lactic-co-glycolic acid): PEGMA-PLGA) versus multi-functionalized (poly(ethylene glycol) pentaerythritol triacylate -poly(lactic-co-glycolic acid): PEGPET-PLGA) copolymer chemistries to increase peptide presentation on the nanoparticle surface. Spacers are necessary to allow for peptide flexibility and interaction with the cell membrane, but cannot be too long as this can inhibit cell attachment[92]. By using this information and applying it to the two different chemistries, it can be determined whether more peptide presence leads to increased cell binding.

A number of nanotechnology approaches, namely the use of chemistries, nanoparticles, targeting ligands, and their individual modifications, are used in this work to improve and test this HER2+ targeted drug delivery strategy. The hypothesis is that nanoparticles fabricated from the novel multi-functionalized "palm-tree" structured PEGPET-PLGA copolymer conjugated with a combined targeting and internalization peptide sequence will show increased nanoparticle uptake and subsequent cell death compared to the "single" nanoparticles fabricated from PEGMA-PLGA. A series of peptides (L1, L1-TAT, and TAT-L1) are conjugated through a click chemistry reaction to the surfaces of the two different nanoparticle types produced. From the *in vitro* targeting affinity and cell viability/cell death experiments completed and outlined in this work, a platform is established to improve treatment of invasive HER2+ breast cancer.

4.2. Results and Discussion

4.2.1. Fabrication of Poly(ethylene glycol) methacrylate – Poly(lactic-co-glycolic acid) (PEGMA-PLGA) nanoparticles and testing of appropriate PEGMA peptide spacer length

Initially in this work, PEGMA-PLGA nanoparticles were fabricated to test the efficacy of the newly identified L1 peptide in targeting and treating HER2+ SKBR3 cells. The PEGMA-PLGA copolymer, where the PEG segment serves as the peptide spacer, was synthesized as outlined in the methods section. Using this copolymer, nanoparticles identified as "single" nanoparticles (SNPs) or PEGMA-PLGA nanoparticles were developed using a standard water/oil/water (w/o/w) double emulsion process. Following fabrication, the peptide was conjugated to the nanoparticle by reacting with the surface PEGMA polymer component. While synthesizing the PEGMA-PLGA copolymer is not unique to this work, conjugation of this specific peptide

through a thiol-ene “click” chemistry reaction had not been previously explored. To facilitate this reaction, peptides were purchased with a modification adding a Cysteine amino acid to the C-terminus to take advantage of the thiol (-SH) functional group available with this amino acid. It was then important within this fabrication to determine the ideal PEGMA spacer length for peptides within this range of molecular weight/# of amino acids (983 Da, 9 amino acids). PEG and its derivatives have been previously used for the purpose of serving as a peptide spacer which helps improve peptide stability in solution, but is also beneficial in nanoparticle work to impart a stealth layer to particles and reduce uptake by immune cells[82,172–174]. 1 kDa, 2 kDa, and 10 kDa PEGMA spacers were selected and tested based on guidance from the literature[172,175,176]. Using confocal microscopy imaging and Rhodamine-B loaded particles, 1 kDa and 2 kDa spacer particles both showed similar L1 conjugated nanoparticle uptake **(Figure 4.1)**. As 2 kDa PEGMA-PLGA nanoparticles showed a consistent slight increase in uptake as analyzed using ImageJ (3-5%) compared to 1 kDa spacer particles, 2 kDa PEGMA was selected to proceed with all of the particle formulations and remaining experiments. Particles with 10 kDa spacer showed poor uptake overall as expected based on the literature.

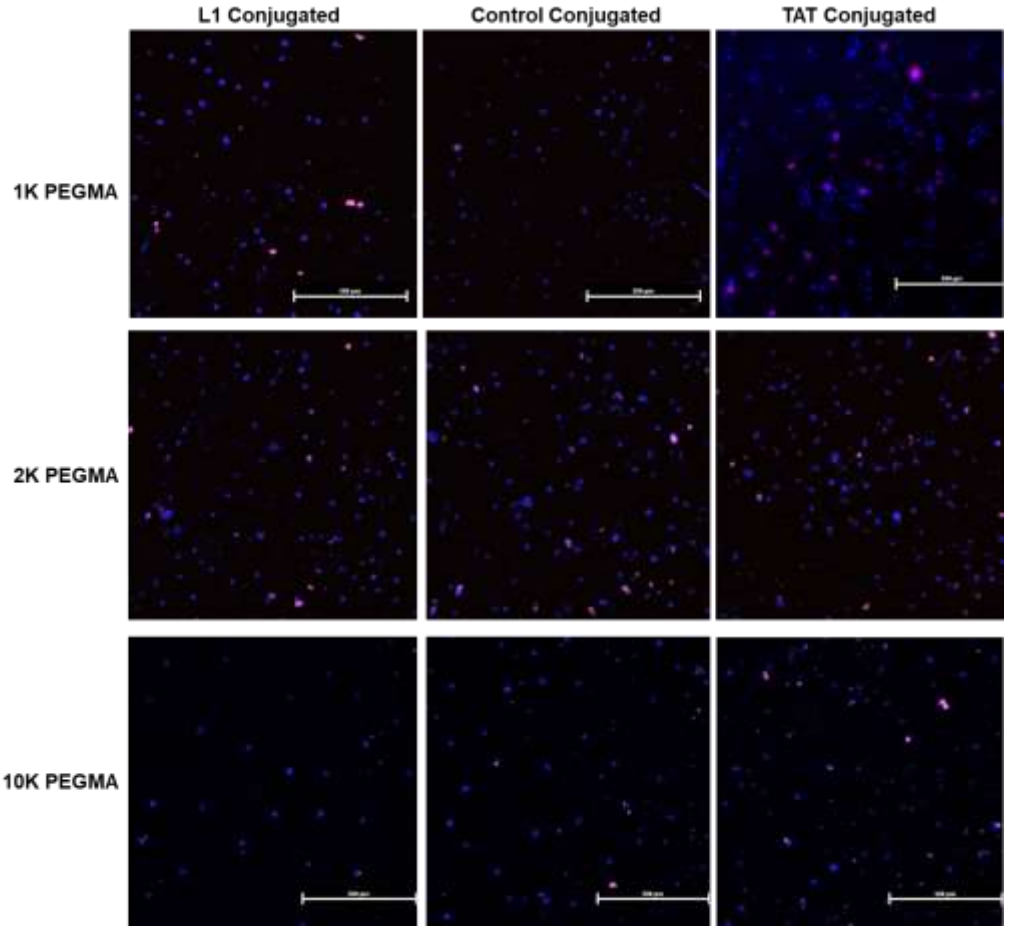

Figure 4.1: Nanoparticle PEG spacer length testing. 1 kDa, 2 kDa, and 10 kDa PEGMA spacers (rows) tested on L1, scrambled peptide (negative control), and TAT (positive control) conjugated nanoparticles.

Through SEM, the PEGMA-PLGA particles were then visualized, and using dynamic light scattering (DLS), the average diameter of the particles was also measured and found to be 645.4 nm **(Figure 4.2)**. Through FITC-labeling of the peptide and confocal imaging, there was confirmation of peptide conjugation onto to the PEGMA-PLGA nanoparticles as seen on the perimeter of the individual particle **(Figure 4.3a)**. Using this same nanoparticle formulation with FITC-labeled L1 peptide, preliminary testing of the L1 peptide on the PEGMA-PLGA nanoparticles for their cell binding was done against SKBR3 cells, which are HER2+ breast cancer cells, and MCF7 cells, which are HER2- breast cancer cells used as a negative control. Greater uptake is seen in the target SKBR3 cells, where more minimal uptake is seen in the

MCF7 cells **(Figure 4.3b)**. The L1 peptide was screened in the literature against MCF10A cells, which are HER2- breast cancer cells as a negative control[167]. Testing these conjugated particles against MCF7 cells here further shows good peptide specificity to continue this nanoparticle work.

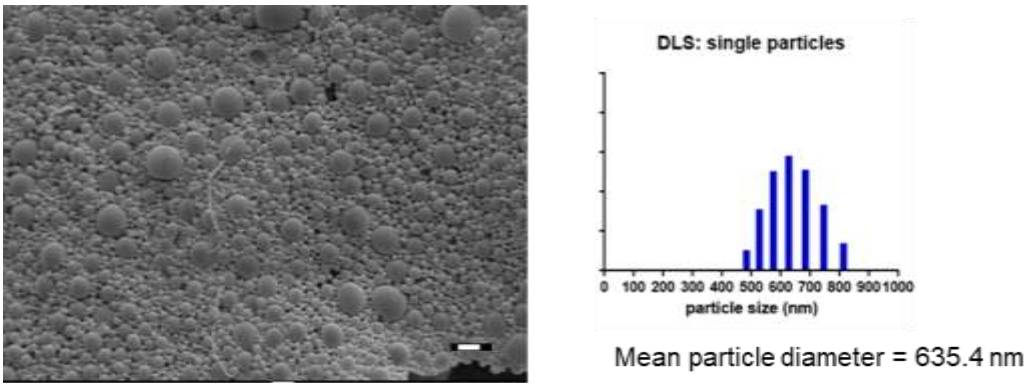

Figure 4.2: Imaging and size evaluation of PEGMA-PLGA nanoparticles. SEM was used to visualize PEGMA-PLGA nanoparticles (left) and dynamic light scattering (DLS) was used to determine the mean particle diameter. Scale bar= 1μm.

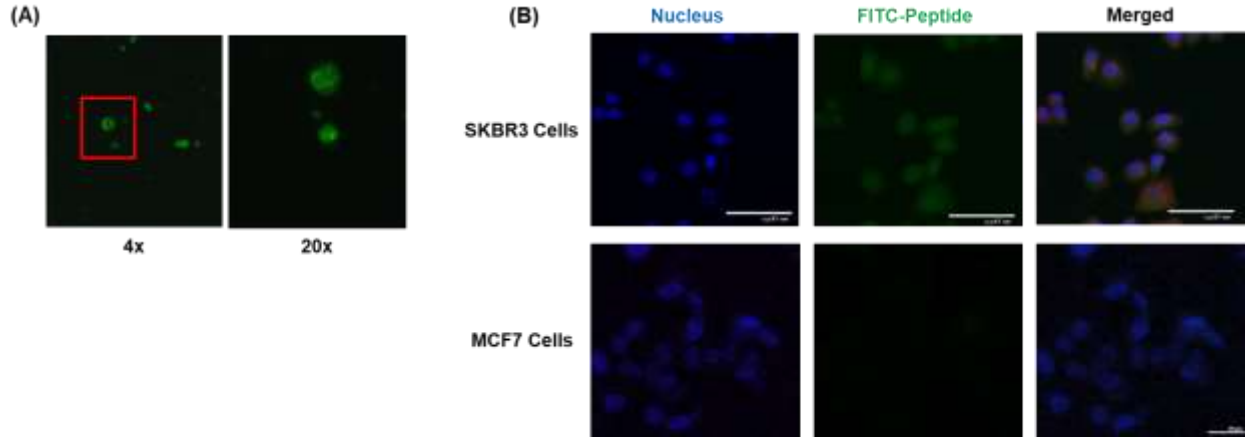

Figure 4.3: Confocal imaging of peptide conjugated PEGMA-PLGA "single" nanoparticles (SNPs). (A) Confocal image of individual FITC-labeled L1 conjugated SNPs at 4x (left) and 20x (right) magnifications, and (B) Testing of peptide L1 conjugated SNPs against HER2+ SKBR3 cells and HER2- MCF7 cells. Cell nuclei labeled with DAPI.

4.2.2. Peptide affinity and dosage testing of "single" PEGMA-PLGA nanoparticles

Peptide affinity was more robustly tested using flow cytometry to quantify the degree of cell targeting or binding by the peptide conjugated SNPs. This experiment was also used to discover

any dose dependency on cell binding and to test the material toxicity as these nanoparticles do not contain a therapeutic and should not inherently cause cell death or significantly affect cell viability. The goal of this experiment was settling on an optimal dose for further *in vitro* testing. Peptide affinity was assessed by measuring the increase in fluorescence intensity as particle binding occurs, which is measured along the x-axis of histogram plots produced from flow cytometry runs. This is always compared to untreated control cells, and the percentage recorded represents the percent of particle-bounce cells with increased fluorescence as measured in in a specific fluorescent channel (i.e. FITC, Rhodamine/PE).The corresponding scatter plots allow for gating or selecting by the user for a specific population in the sample, which are generally the live cells. Although FITC-labeled peptide was used for confocal microscopy, this was not found to be a reliable detection method because, as previously noted in the literature, there was great batch-to-batch differences in peptide conjugation[177]; some batches of L1 peptide displayed less than 10% FITC conjugation as confirmed through high-performance liquid chromatography (HPLC) performed by Lydia Atangcho in the Thurber Laboratory (UMich). With a low amount of dye conjugation, cell binding could be taking place that is not being measured due to a lack of fluorescence signal. FITC is also documented as having poor photostability in buffer[178]. Instead Rhodamine-B loaded PEGMA-PLGA nanoparticles were used as the dye is loaded homogenously through a double emulsion. This loading with Rhodamine-B led to fewer issues with batch-to-batch variability compared to the conjugation of FITC to the peptide, as a loading efficiency of ~70% is steadily achieved for this small molecule. A single batch of Rhodamine-loaded nanoparticles could also be used for multiple experiments. From the flow cytometry results, run and compiled by collaborator Jesse Chen in Prof. SuHe Wang's laboratory (UMich), a dose dependent shift is in fact seen **(Figure 4.4)**. At a concentration of 0.5 mg/mL of peptide

conjugated PEGMA-PLGA nanoparticles, there was a 4 times increase in Rhodamine-B fluorescence (22.10%) when incubated with L1 particles compared to untreated cells (4.97%), which leads to the assumption that L1 is binding to the SKBR3 cells. When this concentration was increased to rule out higher concentrations, a clear decrease in cell viability was seen through the scatterplots produced **(Figure C.1)**. Based on this dosage and toxicity testing, the 0.5 mg/mL particle concentration was established as the concentration to be used moving forward. A scrambled negative control peptide, designated as $L1_c$ (sequence: SDPQVFSTC) was evaluated at the same particle concentration of 0.5 mg/mL and showed no specific binding, essentially with similar fluorescence readouts to the untreated cells at 5.69% and 4.33%, respectively **(Figure 4.5)**. As a negative control, this means there are not any non-specific effects for L1 conjugated nanoparticle binding and it is due to peptide sequence specificity.

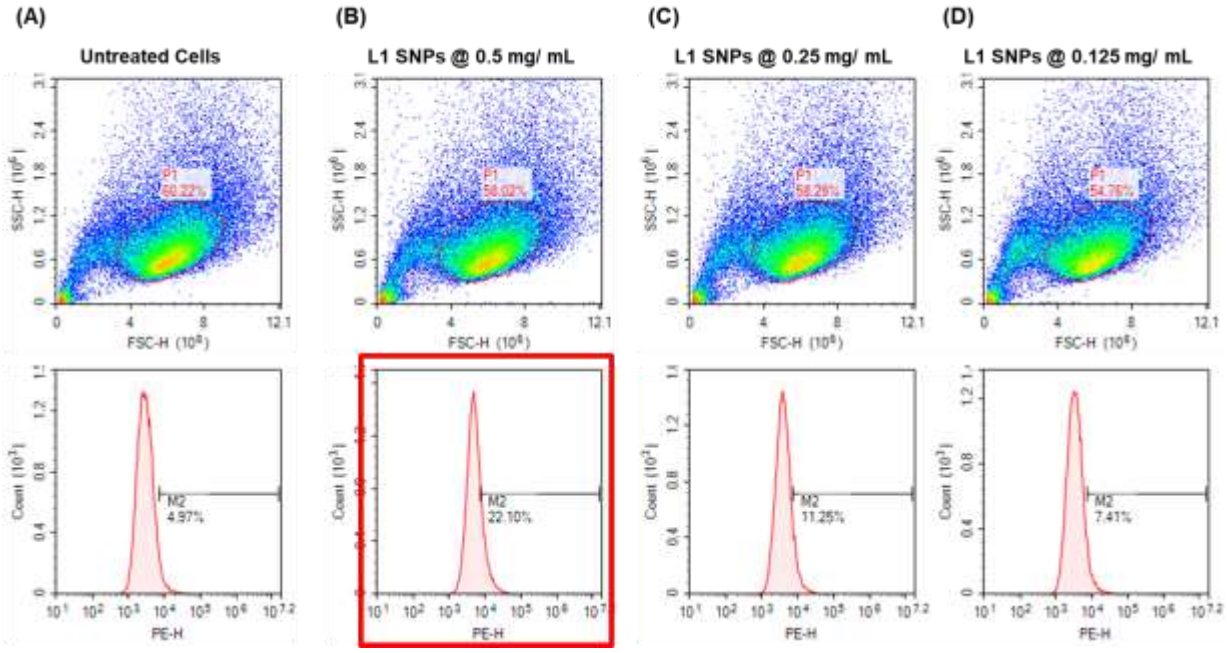

Figure 4.4: Flow cytometry affinity and dose testing of L1 conjugated PEGMA-PLGA "single" nanoparticles (SNPs) against HER2+ SKBR3 cells. (A) Untreated cells, (B) Cells tested at a particle concentration of 0.5 mg/mL, (C) Cells tested at a particle concentration of 0.25 mg/mL, and (D) Cells treated at a particle concentration of 0.125 mg/mL.

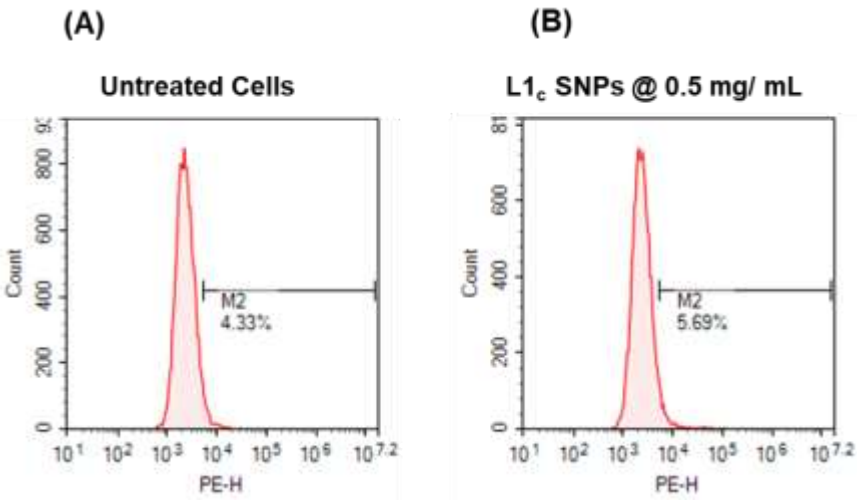

Figure 4.5: Flow cytometry affinity dose testing of L1c conjugated PEGMA-PLGA nanoparticles (SNPs) against HER2+ SKBR3 cells. (A) Untreated cells and (B) Cells tested at a particle concentration of 0.5 mg/mL.

4.2.3. Ligand strategy to improve nanoparticle targeting and uptake through combination peptide sequences

While targeting was achieved with L1 conjugated PEGMA-PLGA nanoparticles, strategies were applied to test whether the targeting and internalization can be amplified. The first way in which this was done was by creating combination peptide sequences that incorporated a cell-penetrating peptide (CPP) sequence. In this way, a small library of peptides was created for testing **(Table 4.1)**. The TAT sequence, described in the introduction, has been extensively used as a CPP due to its high solubility and ability to penetrate a multitude of cells[(179)]. This sequence was used in conjunction with the L1 sequence either following or preceding the TAT sequence to test whether HER2+ targeting specificity can be maintained and increased nanoparticle internalization can be achieved using these specific combination peptide sequences. Conjugating L1 and TAT separately onto the same nanoparticle surface would be futile in achieving this goal as TAT is a non-specific CPP.

Table 4.1: Peptide sequences tested to improve HER2+ cell targeting and internalization of peptide conjugated nanoparticles.

Peptide	Sequence
L1	VSSTQDFP(C)
$L1_C$	SDPQVFSTC
L1-TAT	VSSTQDFPGRKKRRQRRRPQ(C)
TAT-L1	GRKKRRQRRRPQVSSTQDFP(C)
TAT	GRKKRRQRRRPQ(C)
C1 (control)	GRRRVSDFPQRRKKSTDQ(C)

4.2.4. Peptide affinity testing of combination peptides conjugated to "single" PEGMA-PLGA nanoparticles

At the determined concentration for PEGMA-PLGA nanoparticles thus far, the targeting affinity of L1 and the combination peptides and their scrambled combination sequence, C1, were assessed against both SKBR3 and MCF7 cells. From this first flow cytometry run tested against SKBR3 cells, L1 again shows about 20% FITC positive cells when incubated with L1 particles. Preliminarily, the increase in relative fluorescence of FITC, which was conjugated to the peptide N-terminus, was measured before switching to more reliable method of loading Rhodamine-B in the particle core. Comparatively, the TAT-L1 conjugated nanoparticles showed 43.9% FITC positive SKBR3 cells **(Figure 4.6)**. This means that 23.7% more SKBR3 cells are able to bind with the added nanoparticles when the TAT-L1 sequence is conjugated to their surface and that there is greater affinity of SKBR3 cells to the TAT-L1 conjugated particles than those conjugated with the L1 sequence alone. As a positive control, TAT showed strong cell binding as

expected; this targeting is nonspecific across numerous cell types and would not specifically help target HER2+ as desired in this drug delivery system. The fluorescence measured from the control C1 conjugated nanoparticles was in line with that measured for the untreated cells, which indicates peptide sequence specificity of the combination peptides. While lower fluorescence intensity values or decreased particle-cell affinity was seen for the peptide conjugated nanoparticles tested against MCF7 cells, specifically those conjugated with L1, L1-TAT, TAT-L1, and the positive control TAT, the specificity of the combination peptide TAT-L1 comes into question. Repeating these flow cytometry runs with the Rhodamine-B loaded nanoparticles and an additional non breast cancer cell source, such as fibroblasts or endothelial cells, will help to truly assess the peptide specificity.

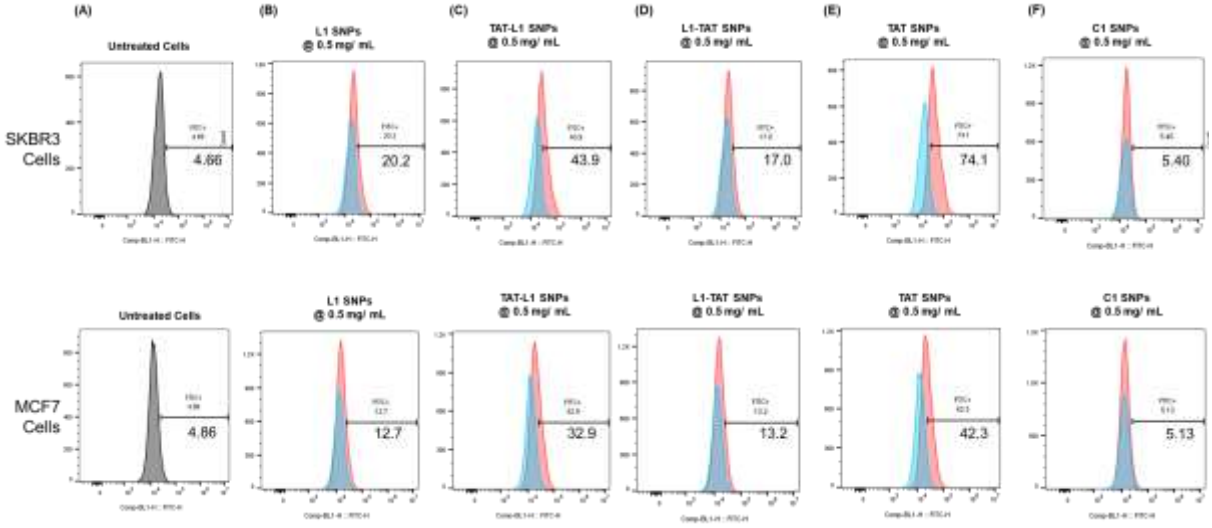

Figure 4.6: L1, combination peptides, and controls conjugated to PEGMA-PLGA "single" nanoparticles (SNPs) tested against SKBR3 and MCF7 cells. Flow cytometry affinity testing of peptides conjugated to PEGMA-PLGA nanoparticles against HER2+ SKBR3 cells (top) and MCF7 cells (bottom). (A) Untreated cells, (B) L1 conjugated NP, (C) TAT-L1 conjugated NP, (D) L1-TAT conjugated NP, (E) TAT conjugated NP, and (F) C1 conjugated NP.

4.2.5. Chemistry strategy to improve nanoparticle targeting and uptake through novel Poly(ethylene glycol) Pentaerythritol triacrylate- Poly(lactic-co-glycolic acid) (PEGPET-PLGA) nanoparticles

As mentioned in the introduction, the second strategy used to improve HER2+ breast cancer treatment involves modifying the initial PEGMA-PLGA chemistry. The PEGMA-PLGA copolymer used thus far allows for conjugation of one peptide at the end of each chain. A novel copolymer called PEGPET-PLGA was synthesized in this work. With three times the C=C bonds available per polymer chain through the reaction with pentaerythritol triacrylate, this significantly increases the possible peptide presentation on the nanoparticles' surface. The PEGPET-PLGA copolymer was synthesized first by modifying PEG to have a –COOH end group followed by two Steglich Esterification reactions **(Figure 4.7)**. The synthesis of this original polymer and the chemical structure that was expected was confirmed using ^{1}H NMR and FTIR analysis through assignment of the chemical groups of the polymer components **(Figure 4.8)**. Through gel permeation chromatography (GPC), the number average molecular weight (M_n) was found to be 31,463 g/mol. With this copolymer developed, PEGPET-PLGA was used to fabricate nanoparticles through the same double emulsification process as the PEGMA-PLGA particles. Based on the copolymer structure with multiple functional groups dangling at one chain end, these particles were called "palm-tree" nanoparticles (PNPs) or PEGPET-PLGA nanoparticles. PEGPET-PLGA nanoparticles showed good spherical morphology through SEM imaging and were found to be on the same scale size-wise as the SNPs, with an average diameter of 543.5 nm measured through DLS **(Figure 4.9)**.

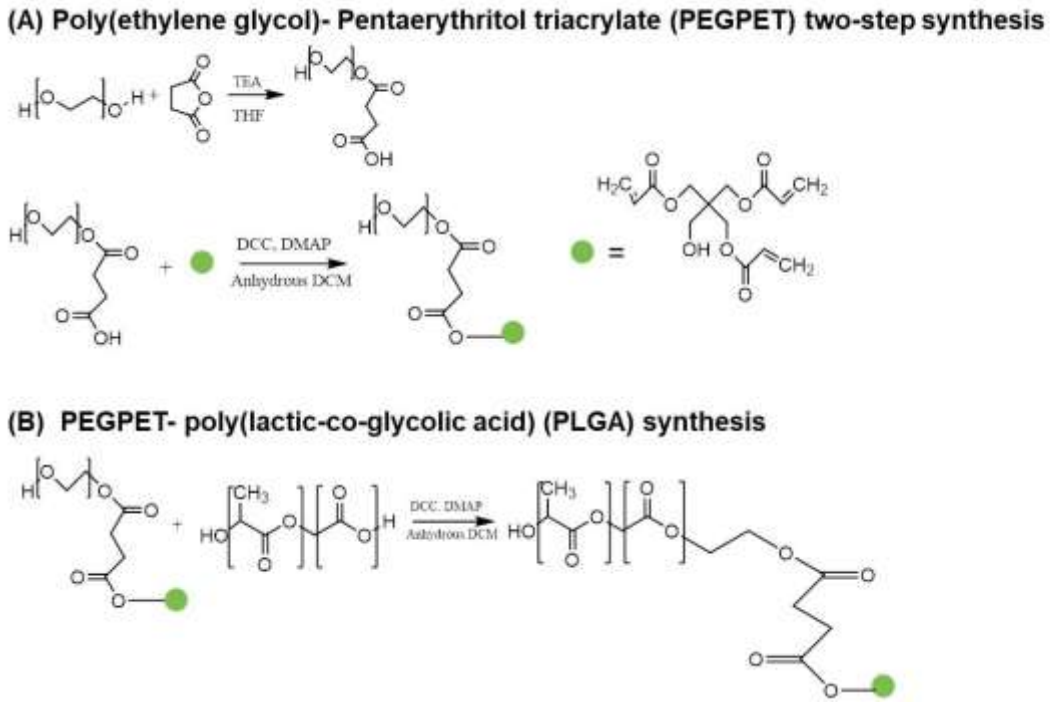

Figure 4.7: Reaction scheme for PEGPET-PLGA copolymer synthesis. (A) Two-step synthesis of PEGPET and (B) Complete copolymer synthesis of PEGPET-PLGA.

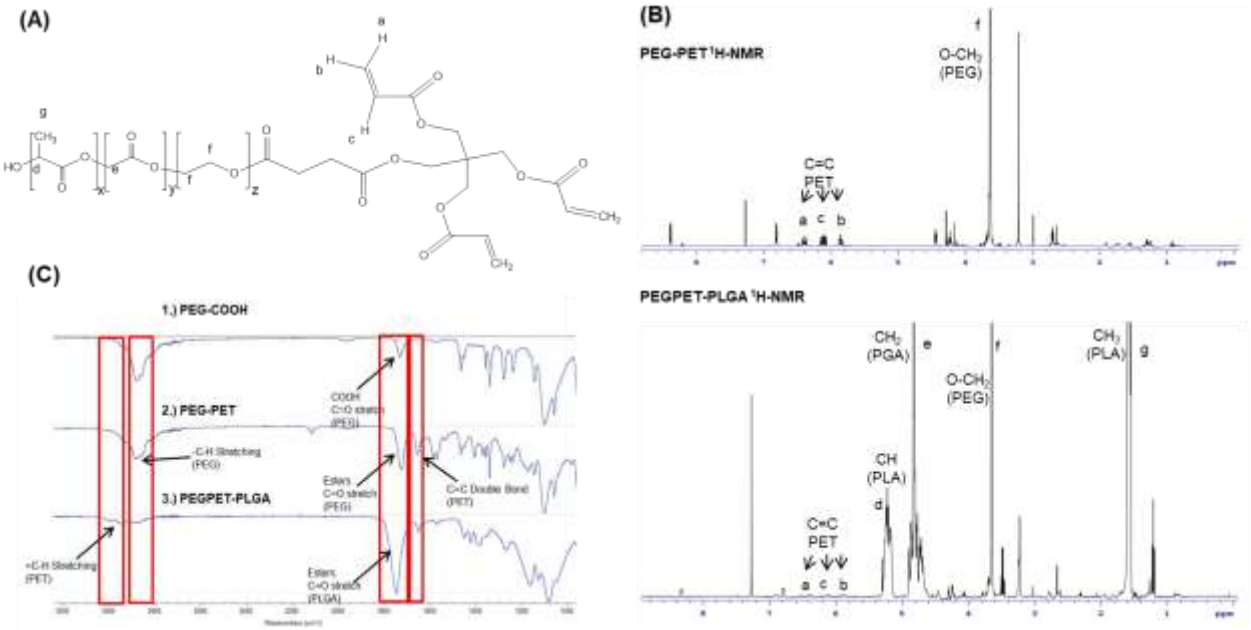

Figure 4.8: Confirmation of PEGPET-PLGA copolymer synthesis through chemical analysis. (A) Labeled structure of PEGPET-PLGA copolymer, (B) ^{1}H NMR of PEGPET and PEGPET-PLGA, and (C) FTIR of all synthesis components.

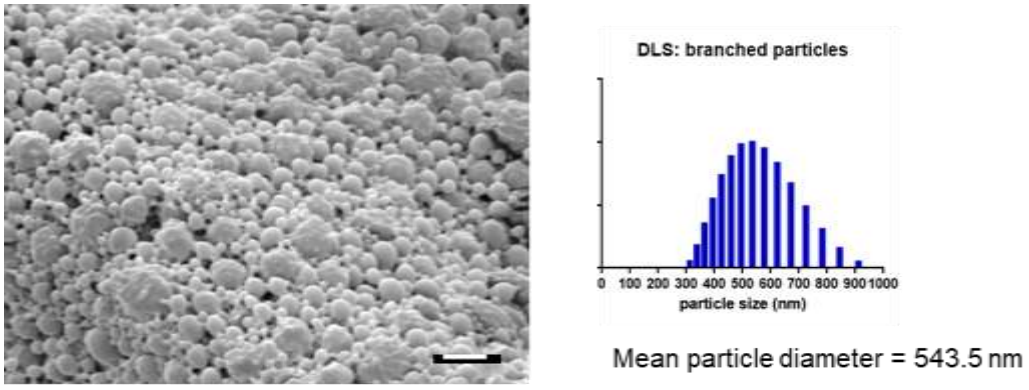

Figure 4.9: Imaging and size evaluation of PEGPET-PLGA nanoparticles (PNPs). SEM was used to visualize PEGPET-PLGA nanoparticles (left) and dynamic light scattering (DLS) was used to determine the mean particle diameter size. Scale bar=1µm.

4.2.6. Peptide affinity and dosage testing of "palm-tree" PEGPET-PLGA nanoparticles

Just as with the PEGMA-PLGA nanoparticles, flow cytometry was used to quantify the degree to which cell targeting takes place as well as settle on an optimal dose based on effect of increasing doses on cell viability. Using the PEGPET-PLGA polymer, nanoparticles were again fabricated from a w/o/w double emulsion process. L1 conjugated PEGPET-PLGA nanoparticle concentrations were assessed as the "first pass" prior to testing nanoparticles conjugated with the novel combination sequences described in the previous section. Peptide affinity was assessed by again measuring relative fluorescence as particle-cell binding occurs. From this early testing, nanoparticle concentrations ranging from 0.5 mg/mL down to 0.0625 mg/mL were assessed **(Figure 4.10)**. While this testing is being repeated with the Rhodamine-B dye, this experiment gave insight into an optimal PEGPET-PLGA nanoparticle concentration of 0.25 mg/mL. At the dose of 0.5 mg/mL cell viability began to decrease significantly for particles fabricated with the PEGPET-PLGA copolymer, where at 0.25 mg/mL, cell viability was in line with the cell viability of the untreated cells (currently cannot access figure). This increase in fluorescence intensity for the PNPs at their optimal concentration shows a 27.3% increase in particle-cell

binding over the SNPs at their optimal concentration (although based on a modified particle formulation with loaded Rhodamine-B). This is supportive of the hypothesis regarding increased peptide presentation on the nanoparticle surface because not only do the PEGPET-PLGA peptide conjugated nanoparticles bind more cells, but a lower concentration of the PNPs is necessary to achieve this compared to optimal concentration of the SNPs. This experiment is indicative of cell surface binding and possible internalization that will be confirmed through future cell viability testing with drug loaded nanoparticles, where increased cell death will be indicative of nanoparticle uptake. These repeated results are promising and show the intended benefit of introducing the novel PEGPET-PLGA copolymer chemistry. Peptide affinity testing remains with the Rhodamine-B loaded formulations at the optimal doses found for both the SNPs and PNPs. The remaining combination peptides and the appropriate control sequences will be tested against the target SKBR3 cells and MCF7 negative control cells. The aims are to determine whether (1) L1 specificity remains in the combination sequences, (2) the addition of the CPP TAT sequence leads to increased cell death in a cell viability test with loaded DOX HCl chemotherapeutic drug in the nanoparticles' core, and (3) increased peptide presentation on the PNPs contributes to increased cell death compared to the SNPs.

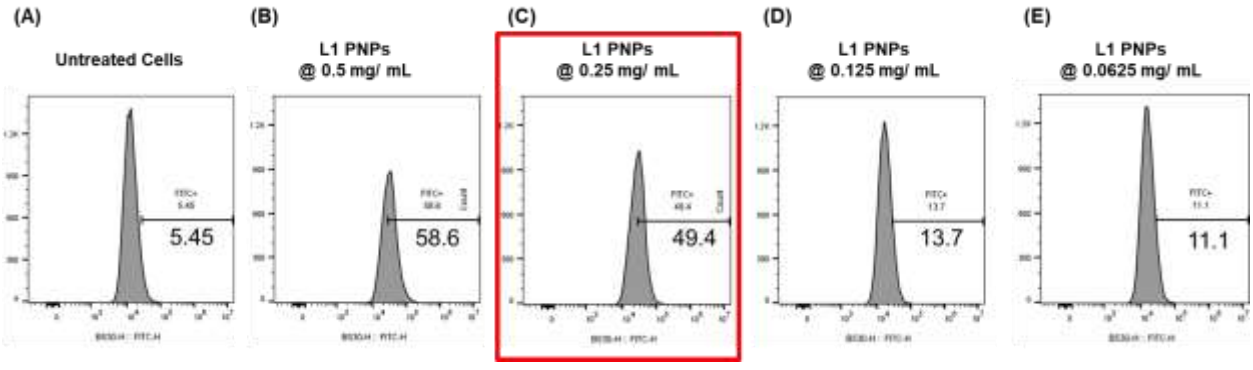

Figure 4.10: Flow cytometry affinity and dose testing of L1 conjugated PEGPET-PLGA "palm-tree" nanoparticles against HER2+ SKBR3 cells. (A) Untreated cells, (B) Cells tested at a particle concentration of 0.5 mg/mL, (C) Cells tested at a particle concentration of 0.25 mg/mL, (D) Cells tested at a particle concentration of 0.125 mg/mL, and (E) Cells tested at a particle concentration of 0.0625 mg/mL.

4.3. Conclusion

When used to treat diseases such as prevalent HER2+ breast cancer, drug loaded nanoparticles with targeted peptide ligands are beneficial for more closely treating this disease and reducing the systemic effects of the loaded drugs. The L1 peptide previously identified was used in this work to examine its utility in a drug delivery system with a suitable peptide spacer/linker of 2 kDa PEG. On top of this initial testing, nanomaterial strategies were developed to further evaluate how targeting and internalization could be improved. Preliminary testing with the added TAT CPP peptide shows promise through flow cytometry, although questions remain with regards to the specificity imparted by the L1 peptide. Most importantly, an innovative PEGPET-PLGA chemistry was synthesized, analyzed, and investigated to determine if increased cell targeting and uptake can be achieved. Comparing the results thus far, the effect of increased peptide presentation was shown as anticipated. With completed results from these two strategies, future *in vitro* remains to complete the conclusion of this work and truly analyze this nanoparticle drug delivery system.

To complete *in vitro* testing, quantification of the actual amount of peptide on the PNPs surface compared to the LNPs will be done using a Quantitative Colorimetric Peptide Assay kit. Next, the peptide affinity testing at the optimal doses for LNPs and PNPs will be completed for all of the peptide conjugated nanoparticles as begun in this dissertation. Finally, *in vitro* cell viability or Live/Dead testing will help determine the degree to which nanoparticles are internalized with the different peptide sequences conjugated to the nanoparticle surface, and whether the addition of the TAT sequence to the combination peptides helps with internalization and also allows for the maintenance for L1 specificity to HER2+ cells. To do this, DOX HCl will

be loaded into the nanoparticles and those that enter the cell will lead to increased cell death, as opposed to particles that only successfully attach onto the cell surface and are not able to release the loaded cytotoxic agent inside the cells. The flow cytometry and cell viability experiments against target HER2+ SKBR3 cells, control HER2- MCF7 cells, and an additional control cell source such as fibroblasts will complete this story and help confirm the hypotheses for this nanoparticle HER2+ targeting and internalization work.

4.4. Experimental Section

4.4.1. Materials

Succinic anhydride, 99%, pentaerythritol triacrylate, triethylamine, 99%, Rhodamine B, fluorescein isocyanate isomer I (FITC), Tris(2-carboxyethyl)phosphine hydrochloride, silica gel (60Å, 230-400 mesh particle size), sand (50-70 mesh particle size), anhydrous sodium carbonate, sodium bicarbonate, 2 mL clear glass GPC vials and caps, and acryloyl chloride were all purchased from Sigma Aldrich (St. Louis, MO). Solvents: methylene chloride, tetrahydrofuran, methanol, acetone, ethyl ether anhydrous, and dichloromethane, 99.8% extra dry over molecular sieve were purchased from Fisher Scientific/Acros Organics (Hampton, NH). Fetal Bovine Serum (FBS), phosphate buffer saline (PBS) pH 7.4, McCoy's 5A cell medium and Penicillin-Streptomycin (P/S) were purchased from ThermoFisher Scientific. Polyethylene glycol 1000 and 2000 were purchased from Millipore Sigma (Burlington, MA) and polyethylene glycol 10,000 was purchased from Fluka (currently Honeywell Morristown, NJ). Resomer RG 503 H Poly (D,L-lactide-co-glycolide) (PLGA) polymer was purchased from Boehringer Ingelheim, currently sold through Millipore Sigma. N'N-Dicyclohexylcarbodiimide, 99% (DCC) and 4-

(Dimethylamino)pyridine, 99% were purchased from Alfa Aesar (Haverhill, MA). 1M Tris-HCl pH 8.0 buffer was purchased through Invitrogen (Carlsbad, CA). Synthetic peptides used in this work were ordered at crude purity from GenicBio Limited (Shanghai, China). ProLong Gold Antifade Reagent with DAPI was purchased through Cell Signaling Technology. PTFE membrane syringe filters (13 mm diameter) with 0.45 µm pores were purchased from Thomas Scientific. SKBR3 and MFC7 cells were generously donated from Dr. SuHe Wang's laboratory in the Department of Medicine at the University of Michigan (originally purchased from ATCC). Doxorubicin hydrochloride for injection, USP was purchased from the University of Michigan Health System pharmacy (distributed from Mylan).

4.4.2. Synthesis of Poly(ethyelene glycol) methacrylate spacer polymer

Copolymers of PEGMA-PLGA were synthesized with three different lengths of poly(ethylene glycol) (PEG) to determine the appropriate spacer lengths for peptide conjugated nanoparticle experiments. To begin, PEGMA was first synthesized by reacting PEG with acryloyl chloride (AC) at a molar ratio of 1.1:1 PEG:AC in the presence of triethylamine under nitrogen gas in 10% weight/volume anhydrous dichloromethane (DCM) for 24 hours. AC was added slowly and left to react while spinning in an ice bath. Reaction was purified by completely removing DCM solvent using rotovap, resuspending the polymer in fresh methylene chloride solvent, and washing three times with 10% sodium bicarbonate solution to remove unreacted AC. PEGMA polymer was precipitated in cold ethyl ether, collected, and dried under vacuum for two days.

4.4.3. Synthesis of Poly(ethyelene glycol) methacrylate- Poly(lactic-co-glycolic acid) (PEGMA-PLGA) linear copolymer

The complete PEGMA-PLGA linear copolymer was synthesized through a standard Steglich Esterification reaction. To carry this out, the PEGMA polymers previously synthesized were reacted with commercially bought PLGA polymer in a 3:1 molar ratio of PEGMA:PLGA. The reaction was carried out under nitrogen gas in anhydrous DCM and DCC and DMAP were added while the reaction was spinning under ice. The reaction was left to proceed for 24 hours. Following this, the reaction was filtered to remove any salt byproducts, precipitated in cold ethyl ether, and washed with methanol to remove any unreacted PEGMA polymer. The copolymer was filtered once more, collected, and left to dry under vacuum for two days.

4.4.4. Synthesis of polyethylene glycol- pentaerythritol triacrylate (PEGPET) polymer

Synthesis of the PEGPET polymer takes place through a two-step procedure. To begin, PEG 2000 is reacted with succinic anhydride (SA) in a 1:1.3 ratio of PEG:SA to form PEG-COOH. This reaction takes placed under nitrogen in 10% weight/volume of tetrahydrofuran in the presence of triethylamine as a catalyst. This reaction is left to react for 24 hours after which the solvent is dried completely using a rotovap and the polymer is reconstituted in DCM. The reaction is filtered two times to remove any unreacted SA, precipitated in cold ethyl ether, collected, and dried under vacuum for two days. Once the PEG-COOH polymer is completely dried, it was reacted through a Steglich Esterification reaction with pentaerythritol triacrylate (PET) in a 1:3.3 ratio of PEG:PET. This reaction took place under nitrogen protection in 10% weight/volume anhydrous DCM with DCC and DMAP added slowly while spinning in ice. After reacting for 24 hours, the reaction was filtered to remove any salt byproduct that formed, put on

a rotovap to completely remove the DCM solvent, and resuspended in water to filter out the unreacted pentaerythritol triacrylate. After filtering, the polymer was lyophilized. The polymer was further purified through a gravity column packed with sand and silica gel with a running solvent of 15:85 of ethyl ether:DCM (500mL) followed by a running solvent of 15:85 methanol:DCM (1200mL) was used.

4.4.5. Synthesis of Poly(ethyelene glycol) pentaerythritol- Poly(lactic-co-glycolic acid) (PEGPET-PLGA) copolymer

The complete PEGPET-PLGA copolymer was synthesized through a second Steglich Esterification reaction. To complete this, the previously synthesized PEGPET polymer was reacted with commercially bought PLGA polymer in a 3:1 molar ratio of PEGPET:PLGA. The reaction was carried out under nitrogen gas in anhydrous DCM, adding the DCC and DMAP solution while the reaction was spinning under ice. The reaction was left to proceed for 24 hours. Following this, the solvent was dried completely using a rotovap and resuspended in fresh DCM (100mL). Water (20mL) was added and using a separatory funnel, the reaction was washed three times. After washing, the polymer was precipitated in cold ethyl ether, collected, and dried under vacuum for two days.

4.4.6. NMR Observation

^{1}H spectra of the polymers developed in this work were recorded with a Varian Inova 500 NMR instruments operating at 500 MHz at room temperature using deuterated dimethyl sulfoxide $(CD_3)SO$ for the PEGMA polymer and deuterated chloroform ($CDCl_3$) for the PEGPET and PLGA block copolymers.

4.4.7. Measuring molecular weight using gel permeation chromatography (GPC)

Molecular weights of the copolymers were measured using gel permeation chromatography on a Shimadzu GPC system. Samples were prepared at a concentration of ~20 mg/mL in tetrahydrofuran and filtered using a 0.45 µm PTFE syringe filter into 2 mL GPC vials. Samples were run at a flow rate of 1 mL/min and were run through a refractive index detector. Analysis was done using Shimadzu GPC postrun software to determine the number average molecular weight (M_n) and/ or the weight average molecular weight (M_w).

4.4.8. Fabrication of PEGMA-PLGA and PEGPET-PLGA nanoparticles

PEGMA-PLGA and PEGPET-PLGA nanoparticles were fabricated through standard water/oil/water (w/o/w) double emulsion processes. Preliminarily, ratios of commercial PLGA and the synthesized polymers were tested to determine the ideal ratio for peptide conjugation, drug loading/ drug release, and to prevent particle agglomeration. From this, the ratio of 0.4g of commercial PLGA and 0.1g synthesized copolymer was determined. 5 weight percent of polymer was dissolved into DCM. The small water phase, depending on the testing being performed, can be DI water (for flow cytometry), Rhodamine B at a concentration of 1mg/mL (confocal microscopy), or varying concentrations of doxorubicin hydrochloride (DOX HCl) (for cell viability testing). The first emulsion was carried out by combining 100uL of the small water phase and 1mL of the polymer (oil) phase and mixed with a probe sonicator for 10 seconds on power 10. Following this, the first emulsification was slowly dripped into 20mL of a larger water phase of 1.0% poly(vinyl alcohol) (PVA) and mixed using the probe sonicator for 15 seconds following the complete addition of the first emulsion. The particles were then left to spin on a hot

plate for 3 hours to allow sufficient time for the DCM solvent to evaporate. Particles were then centrifuged for 6 minutes at 12,000 RPM and washed 2-3 times, collected, and lyophilized.

4.4.9. Fluorescein isocyanate (FITC) labeling of N-terminus peptides

Peptides were labeled by combining 3 mg FITC to a solution of 50 mg peptide/mL into carbonate-bicarbonate buffer (CBB) pH. 9.2. CBB stock was prepared by preparing 0.2 M solution of anhydrous sodium carbonate (1) and 0.2 M solution of sodium bicarbonate (2). 4 mL of the carbonate solution (1) is combined with 46 mL of bicarbonate solution (2), and the solution is brought up to 200 mL through the addition of deionized water. FITC is dissolved in the minimum volume (~0.5 mL) of acetone prior to adding to the buffered peptide solution. Reaction is left to stir for 24 hours under ice. Following this, peptides are dialyzed until excess FITC is removed and subsequently lyophilized to use.

4.4.10. Conjugating peptides to PEGMA-PLGA and PEGPET-PLGA nanoparticles

After particles were fabricated, peptides were then conjugated to the nanoparticle surfaces. Through a thiol-ene based Michael addition reaction, possible through cysteine-terminated synthetic peptides (C-terminus), facile reactions were carried out. To do this, nanoparticles, peptide, and Tris(2-carboxyethyl)phosphine hydrochloride (TCEP) catalyst are reacted in a [1]:[5]:[2.5] ratio for 2 hours in 1M Tris-HCl pH 8.0 buffer (25 mg nanoparticles in 3mL of buffer). After 2 hours, particles were centrifuged, washed twice, and lyophilized. Prior to *in vitro* experiments, nanoparticles are sterilized using ethylene oxide (EtO) gas for 12 hours and aired out.

4.4.11. Fourier-transform infrared spectroscopy (FTIR) analysis

FTIR was performed for the components of the new copolymer, PEG-COOH and PEG-PET, and complete PEGPET-PLGA copolymer after they were all dried under vacuum. Polymers were run on a Thermo-Nicolet IS-50 bench-top FTIR instrument. Background and sample scans were run at the following conditions: resolution of 1.0 cm^{-1}, 32 scans each, and run at a spectral range of 4000 cm^{-1} to 1000 cm^{-1} recording the % Reflectance.

4.4.12. Scanning Electron Microscopy Observation

Nanoparticles were imaged using a scanning electron microscope. To do this, the particles were sputter-coated with gold for 90 seconds in a Denton Desk II sputter coater. Imaging was done at 5 kV with a JEOL-7800FLV SEM at various magnifications. Size and particle architecture was assessed using this technique.

4.4.13. Measuring size distribution through Dynamic Light Scattering (DLS)

The particle size of the PEGMA-PLGA and PEGPET-PLGA nanoparticles were measured by dynamic light scattering using a DelsaNano C, Beckman Coulter particle size analyzer. The mean diameter and size distribution of the minimum amount of particles necessary in suspension were measured at 25°C in PBS pH 7.4. 70 scans were performed during each run of the instrument.

4.4.14. *Confocal imaging and testing of PEGMA spacer on PEGMA-PLGA peptide conjugated nanoparticles*

Nanoparticle confocal imaging and *in vitro* cell uptake experiments were performed to test the effect of different PEGMA spacer lengths by visualizing particle uptake using confocal microscopy. To do this, Rhodamine B loaded nanoparticles were fabricated as previously described with 1 kDa, 2 kDa, and 10 kDa molecular weight PEG. Peptides were also conjugated to the nanoparticle surfaces as previously mentioned. SKBR3 cells were seeded in a 24-well plate on a glass cover slip (14 mm diameter) with a seeding density of 10,000 cells/ well with McCoy's 5A medium modified with 15% FBS and 1% P/S. After seeding the cells for 24 hours, 300 µL of sterilized particles with and without peptide were added at a concentration of 2 mg/mL to each well. Cells and particles were incubated for 4 hours and subsequently washed twice with PBS pH 7.4, stained with ProLong Gold Antifade Reagent with 4'6-diamidino-2-phenylindole (DAPI) to stain the cell nuclei, and imaged. Overlap with the cell nuclei (blue DAPI) and nanoparticle (red Rhodamine) appear as a purple color in confocal microscopy, indicative of nanoparticle attachment and/or uptake into the cell after extensive washing. The laser parameters, intensity and gain, were adjusted using control cells with no particles and kept constant to image particle-treated cells without changing the laser parameters. Quantification analysis was done using the colocalization and cell counting functions found in ImageJ.

4.4.15. Peptide-conjugated particle affinity testing to target HER2+ SKBR3 cells

Targeting affinity was tested using flow cytometry. To do this, cells were grown to 80% confluency in a T-75 flask, digested with 0.25% Trypsin-EDTA, and then washed with fresh DMEM complete medium for cell recovery. Cells were then blocked with 1% bovine serum

albumin (BSA) in PBS at 4°C. Samples (0.5×10^{-6} cells) were incubated with peptide conjugated nanoparticles loaded with Rhodamine-B dye for 1h at room temperature in the dark. Samples were then washed three times and suspended in 0.1% BSA/PBS and analyzed with an Accuri C6 Flow Cytometer (BD Biosciences, San Jose, CA).

Chapter 5. Conclusions and Future Directions

5.1. Summary

This dissertation focused on manipulating and evaluating novel materials and components for tissue engineering and drug delivery applications. These biomaterials, which are made to interact with cells on the nanoscale, were specifically modified to change the materials' functionalization, surface area/processability, nanofeatures, and mechanical properties. Materials, whether hydrogels or polymeric nanoparticles, can be made to better perform if characteristics of the material are in line with the nanoscale components they are mimicking or helping to support. By tailoring these nanotechnology-derived biomaterials and modifying physical and chemical components such as the crosslinking density, crosslinker length, porous architecture, and ligand presentations, the two novel materials presented in this work were made suitable for their respective aims.

To this end, the hydrophobic monomer 2-methylene-1,3,6-trixococane (MTC) was crosslinked with Poly(ethylene glycol) diacrylate at various molecular weights and at varying concentrations to characterize its materials' properties and ultimately evaluate its biocompatibility as a hydrogel for future use in tissue engineering applications **(Chapter 2)** and evaluate its performance as a hydrogel material for drug delivery use **(Chapter 3)**. With its chemical structure nearly identical to that of the FDA-approved polymer PCL, it was presumed that it would be non-toxic and show good biocompatibility, especially when crosslinked as part of a water-absorbing hydrogel. The chemical structure and nature of MTC made it interesting to

explore for these biomaterials applications because it was hypothesized based on its chemistry that it could function as the main component in a degradable, tunable, and processable hydrogel system. Degradability was considered the greatest advantage and one of the driving factors for pursuing the use of this monomer due to the ester linkage formed upon radical ring-opening polymerization, allowing the material to undergo hydrolysis. Overall in Chapter 2, it was observed that the swelling and degradation properties of the MTC gels/hydrogels were dictated by the hydrophilic-hydrophobic balance of the samples. The hydrophilic-hydrophobic balance was varied by changing the crosslinker length and changing the crosslinker mole concentration with respect to moles of MTC monomer. Uniquely, the increase in hydrophilicity as crosslinker length and concentration were increased in the samples contributed to an uncharacteristic hydrogel trend which was that the degree of swelling increased as crosslinker concentration was increased. Additional advantages included the: (1) one-pot synthesis that was possible through the monomer existing in a liquid state at room temperature and being miscible with the PEGDA crosslinker upon heating, and (2) processability due to the absence of water or organic solvent during processing that allowed for a larger interconnected, porous network to be fabricated through the sugar sphere porogen process. In Chapter 3, the tunability of this gel/hydrogel system was again shown, specifically with respect to the different drug release kinetics that can be achieved as crosslinker concentration, crosslinker length, solution pH, and drug type are changed. Taken together, these properties and advantages produced low and high swelling and degradable scaffolds and drug delivery vehicles. For tissue engineering, compositions with low to moderate swelling showed good biocompatibility as cells were not as isolated within the MTC scaffold and showed greater numbers in cell viability assays presumably due to better cell attachment, an advantage of hydrophobic scaffolds. As mentioned in the introductory chapter,

hydrophilic scaffolds/hydrogels like PEG are inherently bioinert and often used to prevent cell and protein adhesion, which is due to their hydrophilicity. The drug delivery testing showed the MTC samples to be a suitable drug delivery system for hydrophobic drugs with controlled, even release showed over a long-term study. Drug delivery systems for hydrophobic drugs are in increased demand in the biomaterials field as over 40% of drugs on the market and many in the research phase are hydrophobic[138]. The model protein tested showed more sustained release compared to the rapid release model small molecule hydrophobic drug tested, although the protein release curves were characterized by a greater burst release and drug concentration dependent behavior compared to the small molecule hydrophobic drug tested. The tunability of this MTC gel/hydrogel material as far as varying the crosslinker and selecting for a degree of swelling, degradation rate, specific modulus, and/or drug release kinetic, sets the stage for its future utility in numerous nanobiomaterial applications. Some of these specific early applications are highlighted in the future works section.

Similarly, in Chapter 4, polymeric nanoparticles were tailored for their particular application, namely improved breast cancer cell targeting and internalization. A copolymer of PEGMA-PLGA was first synthesized to fabricate nanoparticles that were used to assess peptide conjugation and HER2+ SKBR3 cell targeting and binding, specifically for the HER2+ targeting L1 peptide identified, when attached onto a nanoparticle surface. SKBR3 cell targeting was achieved with 20% of tested cells achieving nanoparticle-peptide binding. This confirmed that the L1 peptide could perform when conjugated to a polymeric nanoparticle surface. Following this, combination peptides were developed with the added CPP TAT sequence to determine how the L1-TAT and TAT-L1 conjugated particles perform compared to particles with only the L1 peptide sequence. Through work done with a collaborator, early flow cytometry experiments

show increased binding of LNPs conjugated with the TAT-L1 peptide compared to LNPs conjugated with L1 alone. The L1-TAT conjugated LNPs showed similar binding affinity to SKBR3 cells as L1 conjugated LNPs and may not enhance HER2+ targeting. The remaining *in vitro* cell viability assays help determine the extent of peptide affinity, selectivity, and internalization. The hypothesis regarding an increase in peptide density on the nanoparticle surface was then evaluated. A novel copolymer chemistry using pentaerythritol was developed to theoretically triple the amount of peptide that could be conjugated to the nanoparticle surface. Through peptide affinity testing again using flow cytometry, the nanoparticles fabricated from this PEGPET-PLGA copolymer conjugated with the L1 peptide show an increase in cell binding, which is displayed by an increase in fluorescence intensity compared to the PEGMA-PLGA nanoparticles conjugated with the L1 peptide. Not only was increased cell binding of the PNPs to HER2+ SKBR3 cells shown, but a lower PNP concentration was utilized to achieve this compared to the optimal LNP concentration found and tested. Through these manipulations, the promise of enhanced HER2+ cell targeting is supported by this work thus far and the remaining *in vitro* experiments and future *in vivo* work will help analyze the internalization ability and selectivity of this nanoparticle drug delivery system.

5.2. Future Directions

5.2.1. 2-methylene-1,3,6-trioxocane (MTC) for specific tissue engineering and drug delivery applications

Throughout this work, the MTC gels/ hydrogels were characterized and evaluated for potential tissue engineering and drug delivery applications. On the tissue engineering front, the different formulations were evaluated with regards to biocompatibility to show that after multiple days of

cell seeding, cells continued to be viable, especially on more gel-like substrates that do not swell significantly and have elastic moduli in the range of 100 kPa. The gel/hydrogels that showed the best biocompatibility include the 575 Da and 2 kDa 1% PEGDA crosslinked MTC formulations. Keeping with the one-pot reactions used for gelation, one of the first goals to set the pace for future tissue engineering use is to determine if adhesion factors such as the RGD adhesion peptide motif and others could be incorporated into the reaction, taking advantage of the atypical properties of the monomer (liquid state) and gelation process (solvent-free). This has been preliminarily evaluated. 1% RGD peptide was added into the 2 kDa 1% MTC-PEGDA formulation and fabricated into 3D interconnected, porous scaffolds as discussed in the dissertation. By implanting these gel scaffolds subcutaneously into 4 pockets on the back of C57BL/6 mice, performed by Ma Lab colleague Zhen Zhang, native cells were left to infiltrate the substrates over two weeks. Through histological sectioning and Haemotoxylin and Eosin (H&E) staining performed at the histology core at the University of Michigan School of Dentistry, 2 kDa 1% gels with RGD incorporated showed cell infiltration throughout the gel and within the scaffold pores while the other groups tested showed cells only on the scaffold perimeter and empty pores within the gel **(Figure 5.1)**. This gel with RGD also showed evidence of blood vessel formation just as in the 575 Da PEGDA control, which is a very rigid, nondegradable scaffold. Future projects within the lab hope to build on this experimentation and system, specifically to regenerate adipose and other soft tissues within the laboratory. Based on the measured modulus values for the MTC gels, soft tissue regeneration as opposed to hard tissue regeneration seems to be a suitable application for the material over overall; and this novel scaffolding material can benefit future soft tissue regeneration projects in the lab. Previously, our laboratory has been well versed in scaffolds made from more crystalline polymers such as

poly(L-lactic acid) (PLLA), which has shown better utility for stiffer tissues such as bone and cartilage. Using these PLLA scaffolds, I have previously explored adipose-derived stem cells (ADSCs) growth and development into adipose tissue with and without added factors such as insulin conjugated to the scaffold surface as a supplemental project. Exploring how adipose tissue growth responds on the MTC gels with a modulus closer to native adipose tissue than the PLLA scaffold previously used for this work is expected to show enhanced results upon testing.

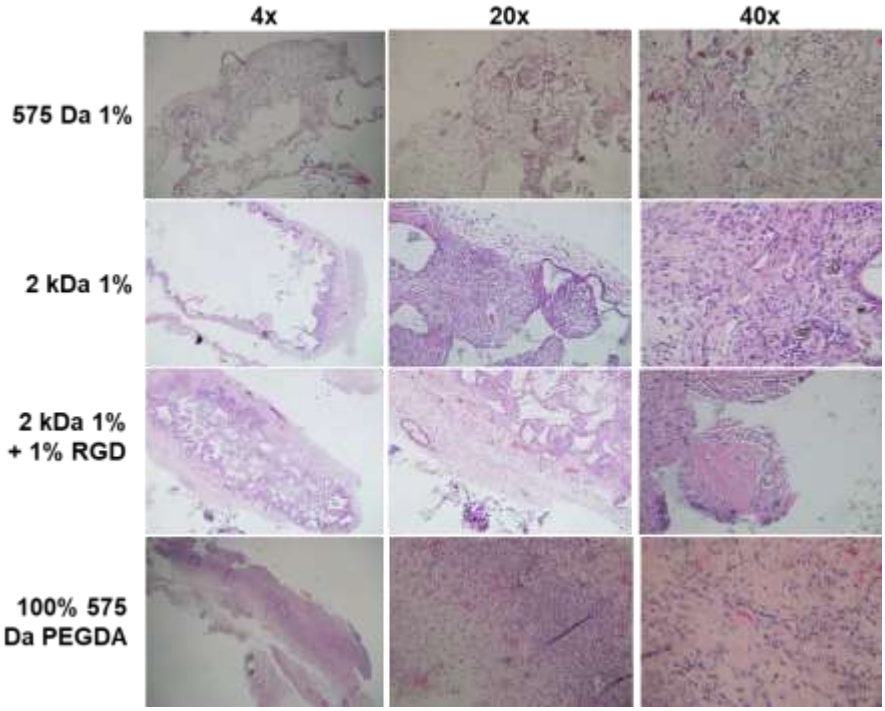

Figure 5.1: H&E staining of in vivo gels following subcutaneous implantation in mice for 2 weeks.

A major way in which this MTC tissue engineering work can be expanded is to test this material as a driving component of a specific tissue engineering system. A project currently being explored as a collaboration between myself (materials preparation and sterilization), Renato Navarro (monomer synthesis), and Dr. Younghun Jung (cell seeding and biological experiments) seeks to determine how MTC scaffolds can be used to improve the development of characteristic gland-like structures in both mammary and prostate cells grown from CXCL12γ-

overexpressing epithelial cells. Collagen gel has been used previously to attempt to grow these cells in an *in vivo* xenotransplantation animal with limited success and ability to recover the gland-like structures of these two cell types. In this work, Heparin is incorporated as an adhesion molecule and to support differentiation of the two cell types used into the fabricated 3D interconnected, porous substrates. Thus far, proliferation was evaluated for MCF10A breast epithelial cells and PNT2 prostate epithelial cells. The 2 kDa 0.25% and 1% MTC samples with Heparin show great promise with regards to cell proliferation, especially when compared to the MTC gels without heparin (vehicle) and collagen gels used as the gold standard in these studies **(Figure 5.2)**. Future experiments will continue using Heparin-MTC gels to evaluate the differentiation and gene expression of these two cell types with the goal of evaluating *in vivo* gland structure.

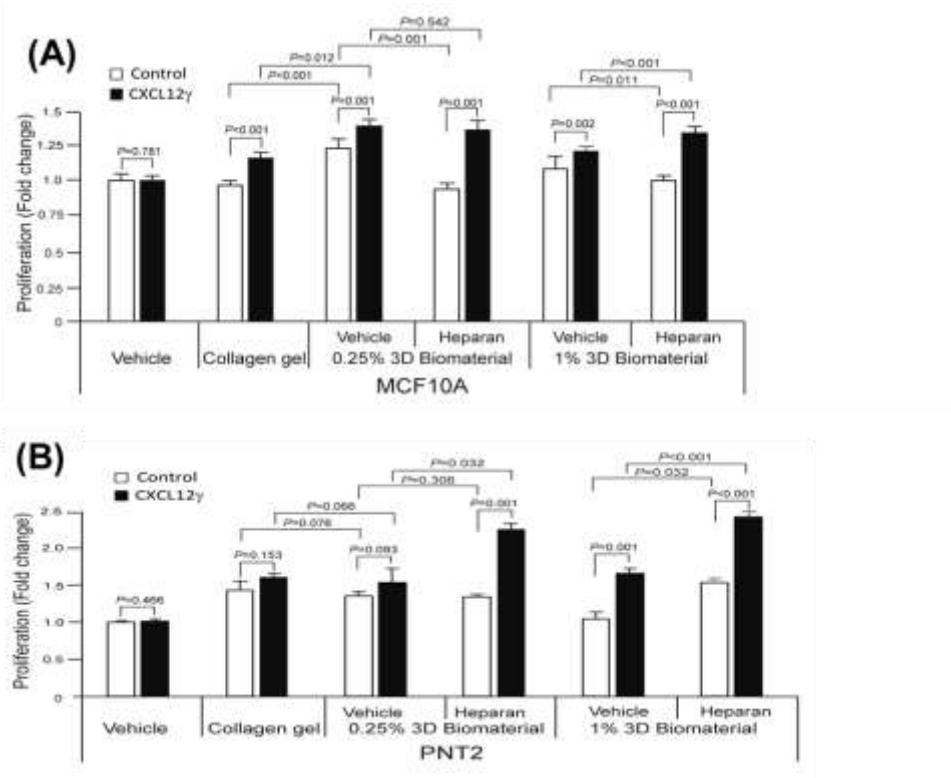

Figure 5.2: Proliferation results for CXCL12γ- mediated MCF10A and PNT2 epithelial cells after 3 days on various substrates including 3D porous MTC gels with and without heparin. Data is presented as mean ± SD (Student's *t*-test). (Data collected and prepared by Dr. Younghun Jung).

On the drug delivery application side of this MTC hydrogel material, as mentioned in Chapter 3, modeling can be used to determine the drug release mechanism. By solving for the diffusion coefficients and meshing this with the release kinetics found, more can be understood about this drug delivery system and the factors at play. Additional kinetic models can also be looked into such as the Higuchi, Hixon-Crowell, and Korsmeyer-Peppas models to help clarify the drug delivery kinetics found in this MTC drug delivery system. Nevertheless, much information was garnered from the work presented about drug release from the MTC hydrogels with respect to changes in crosslinker concentration, crosslinker molecular weight, and drug type. MTC hydrogels for drug release are currently being applied to projects within the Ma Lab, including as a delivery system for exosomes. This work is a collaboration between myself (materials fabrication) and labmates Renato Navarro (monomer synthesis) and Ming Guan (biological experiments). Exosomes are vesicles, composed of lipid bilayers, that are secreted by cells and range in size from 30-100 nm, slightly larger than the BSA model protein loaded[180,181]. These vesicles are important in cell-cell communication and have been found to contain genetic information and factors that help promote cell growth and function, and they are particularly being applied to the field of tissue engineering. Exosomes isolated from bone marrow stromal cells (BMSCs) have been concentrated and loaded into 2 kDa 1.0% gels, as a novel release system to aid in the growth of nucleus pulposus cells. Preliminarily, the release of exosomes from MTC hydrogel samples has been explored for 30 days thus far, and found to mimic the release behavior of BSA protein **(Figure 5.3)**. This system will be evaluated compared to traditional polymeric nanoparticles to determine a suitable drug release system for this regeneration goal.

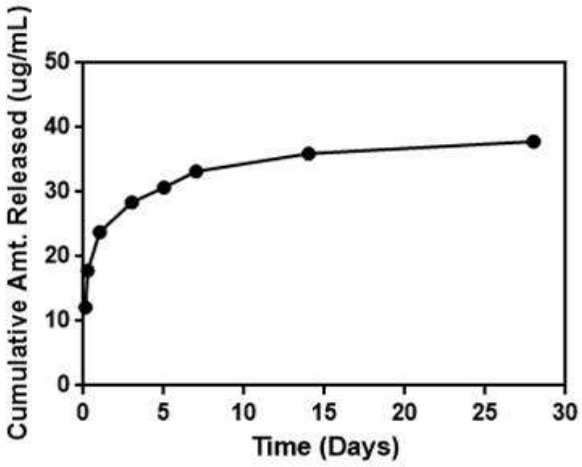

Figure 5.3: Cumulative exosome release from 2 kDa 1% MTC gels over 30 days. All values reported as mean ± SD (n=3). Error bars are smaller than size of markers on graph. (Data collected by Ming Guan).

The tissue engineering and drug delivery applications presented in this dissertation and being pursued as future works with this material apply the MTC gels/hydrogels for separate applications. An ideal material within the larger field of biomaterials would be one that can be used as a simultaneous tissue engineering and drug delivery platform. From the analysis presented here, this is where the future utility of this material lies and would help satisfy two components of the tissue engineering triad presented in the introduction chapter: as a scaffolding material to support the growth of cells into tissues and organs and as a controlled delivery vehicle for the necessary biological factors to support tissue growth. Balancing how best to achieve this will need to be done by selecting an appropriate crosslinker concentration, selecting an appropriate crosslinker length, considering the growth factors or drugs that must be loaded, and considering the rate at which these agents should be released. Some give and take may be necessary to support both functions; however, from that data presented and the larger plan for this material, this is what is envisioned and how the material can be applied. The injectability will also need to be assessed for this simultaneous tissue engineering and drug delivery

application due to the addition of cells, which may be disrupted by the UV light used for gelation.

Outside of the biomaterials scope of this dissertation, two additional future goals have been developed with respect to the MTC monomer. As previously mentioned, MTC is difficult to polymerize to high molecular weights using standard radical polymerization methods. Renato Navarro, a collaborator in the Ma Lab and the MTC work presented, has begun the chemistry work to make this process feasible. This is a great aim for this monomer and will open up more avenues for polymerized MTC use, including potential fabrication into tissue engineering scaffolds without the need for UV crosslinking. Another future work is creating the "next generation" of the MTC ring monomer and characterizing this original monomer and its properties when crosslinked (i.e. swelling, degradation, and rheological properties). This monomer, which we have named 'MQC' for the four oxygens in the ring structure, is expected to show good elastic properties and be more hydrophilic to MTC leading to an increase in its swelling and degradation properties. MQC synthesis, confirmation of structure and molecular weight, and analysis of crosslinked properties is currently underway for future publication at the time of this dissertation between myself and Renato Navarro.

5.2.2. Future testing of "single" PEGMA-PLGA and "palm-tree" PEGPET-PLGA nanoparticles

The best testing of a drug delivery system is *in vivo* in a clinically translatable animal model. A clinically translated model would be one that not only has the necessary disease presentation, but also has its own immune system intact rather than a knock-down of the immune system (nude model). This type of clinically relatable testing remains a future goal of this project through a collaboration with Prof. SuHe Wang's laboratory. Previous work in the Wang lab has developed

a transgenic mouse tumor model for HER2+ testing by inoculating mouse mammary cells engineered with human wild-type HER2 into C57BL/6 HER2 transgenic mouse[182]. This is the perfect model based on the HER2+ targeting of the initial L1 peptide sequence. Testing would be done through mouse tail-vein injection of the nanoparticles to observe (1) shrinkage of the tumor from initial size through successful delivery of the loaded drug into tumor cells and (2) specificity of the peptide conjugated nanoparticles by imagining the organs of the mouse and checking for red fluorescence, which is characteristic of the drug DOX HCl. This is an exciting future direction of this PEGMA-PLGA versus PEGPET-PLGA peptide conjugated nanoparticle testing.

5.3. Thesis Conclusion

The continued success and translation of tissue engineering and drug delivery research into the clinic depends on advances being continuously being made in the field of biomaterials. When considering the material-cell interaction and how cells respond to their environment, it is important to tailor materials' temporal and spatial properties and consider the influence of components on the nanoscale. This dissertation focuses on all of these factors and specifically applies them to meet the challenges found in two different areas, (1) hydrogel systems and (2) nanoparticle targeting and internalization. Advancements were made to the field of biomaterials by providing two novel materials, MTC gel/hydrogel and nanoparticles made from PEGPET-PLGA chemistry, and a platform for their future applications.

Appendix A. Supplemental images to Hydrogels with Unique Swelling Properties as a Biomaterial for Tissue Engineering Application

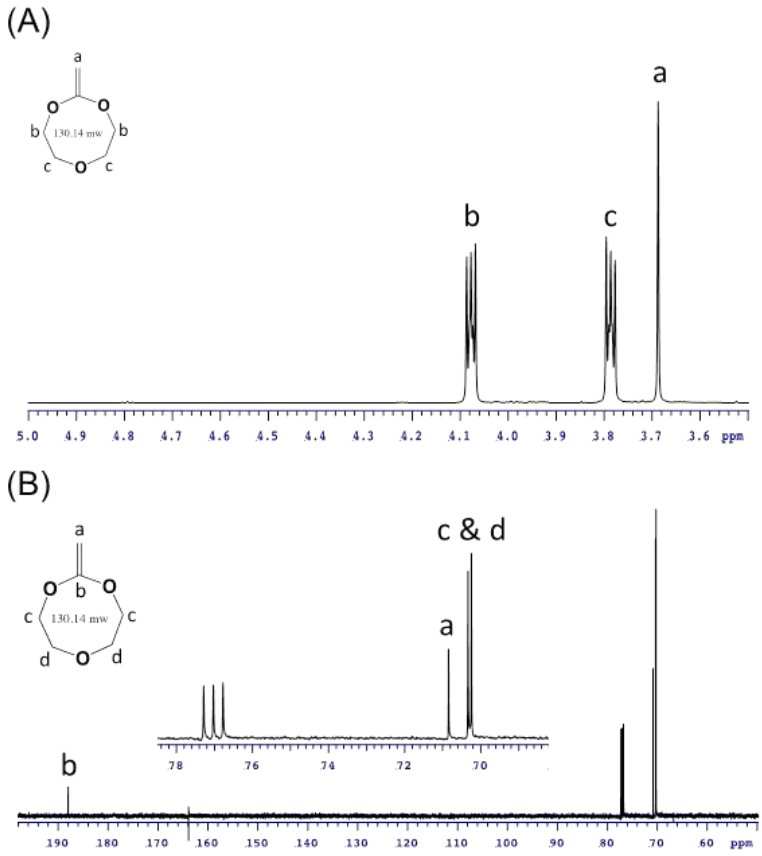

Figure A.1: NMR analysis of MTC monomer synthesis. 500 MHz NMR spectrum of 2-methylene-1,3,6-trioxocane (A) ^{1}H spectrum and (B) ^{13}C spectrum.

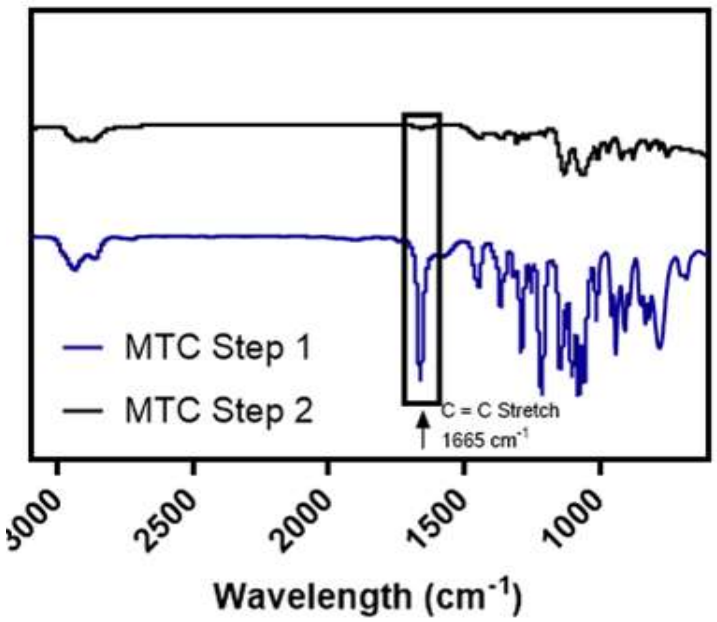

Figure A.2: FTIR analysis of MTC monomer synthesis. Fourier-transform infrared spectroscopy (FTIR) spectrum for MTC synthesis step 1 reaction and step 2 reaction.

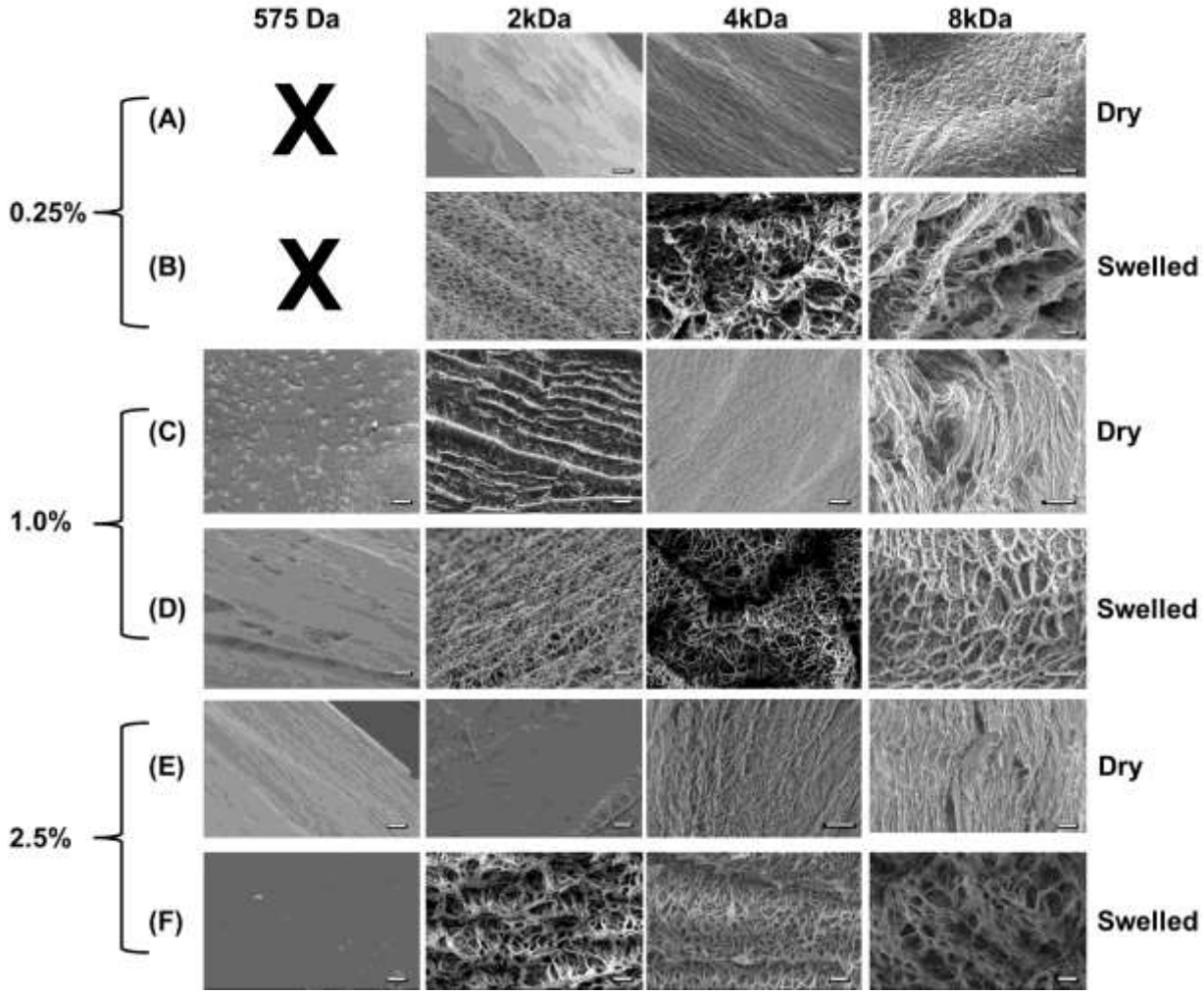

Figure A.3: Complete panel of SEM images of gels/ hydrogels. Scanning electron microscopy of initial dry and swelled gel/hydrogels with varying crosslinker percent and length.

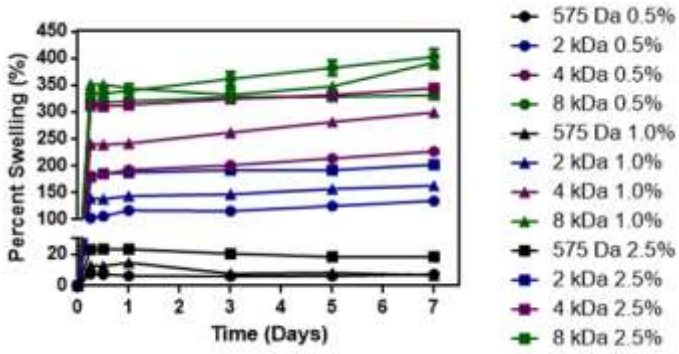

Figure A.4: Complete swelling test to decouple crosslinker molecular weight. Swelling tests further showing the effect of crosslinker concentration at varying crosslinker molecular weights. Concentrations tested are 2x (0.5% to 1.0%) and 5x (0.5% to 2.5%).

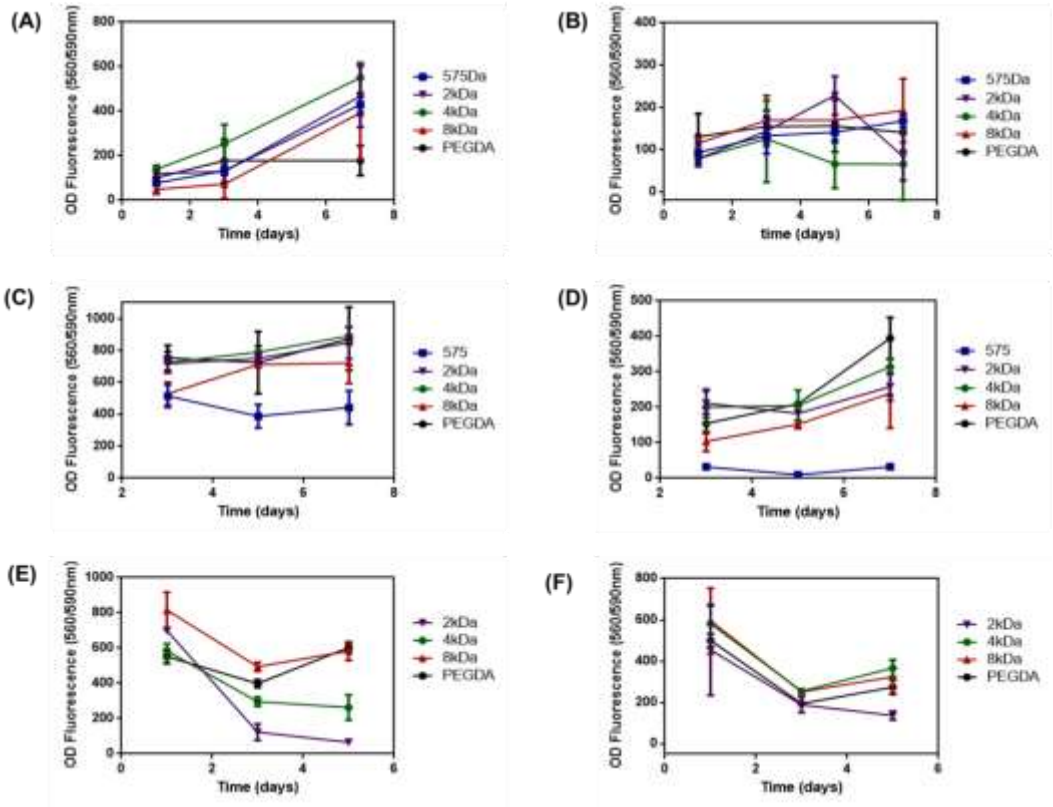

Figure A.5: *In vitro* biocompatibility testing through proliferation assay trends for porous gels/hydrogels seeded with ADSCs and DPSCs. (A) 2.5% scaffolds with ADSCs, (B) 2.5% scaffolds with DPSCs, (C) 1.0% scaffolds with ADSCs, (D) 1.0% scaffolds with DPSCs, (E) 0.25% scaffolds with ADSCs, and (F) 0.25% scaffolds with DPSCs.

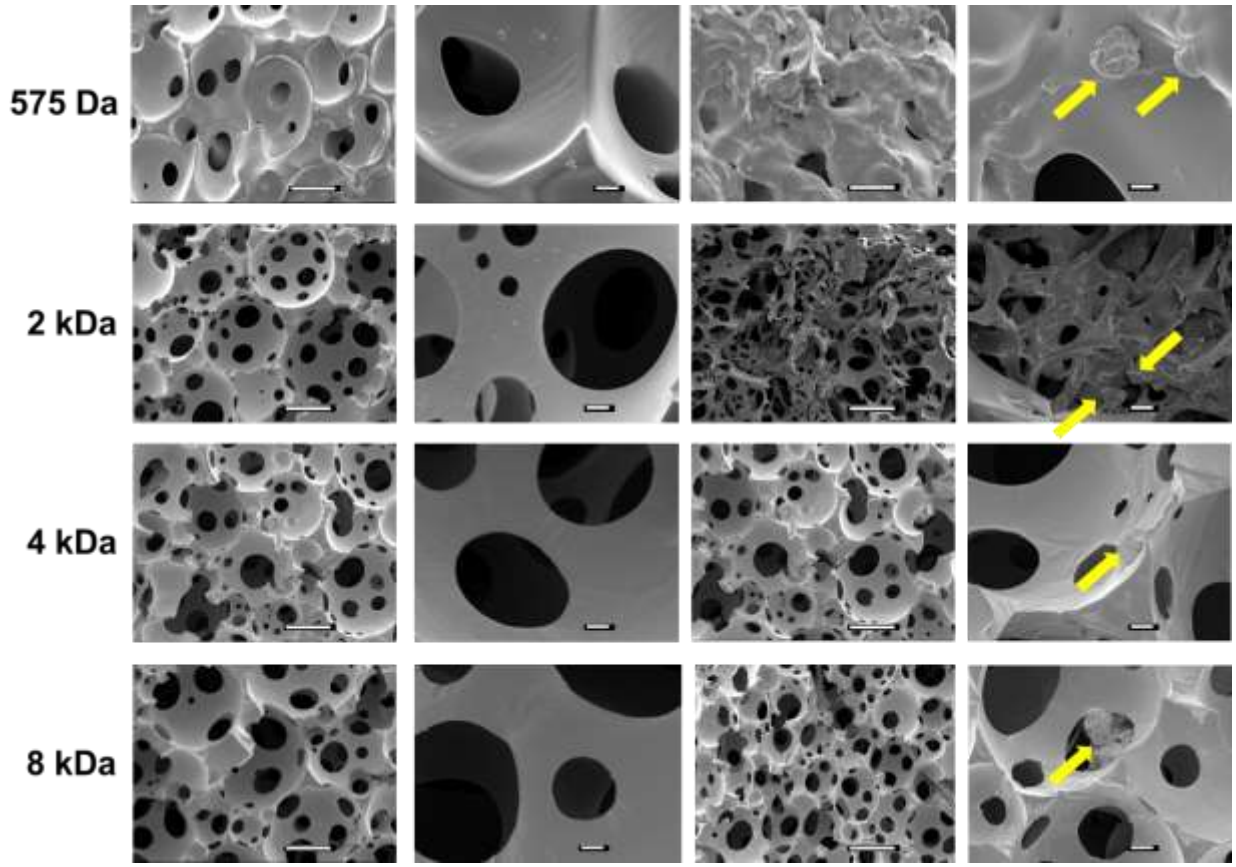

Figure A.6: *In vitro* through SEM images of 1.0% porous gels/ hydrogels seeded with DPSCs.

Appendix B. Supplemental images to Delivery of Hydrophobic Small Molecule, Hydrophilic Small Molecule, and Protein Drugs from Novel 2-methylene-1,3,6-trioxocane (MTC) Hydrogels

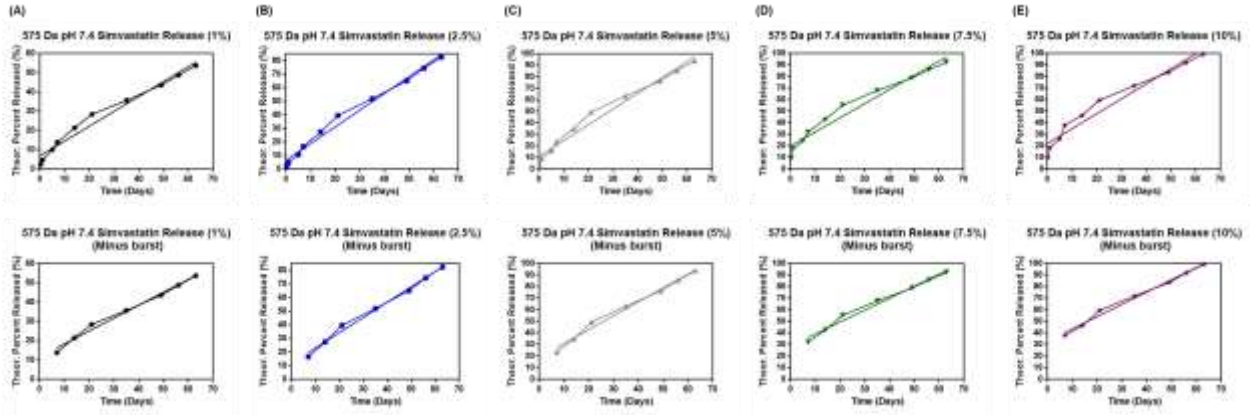

Figure B.1: Linear zero-order curve fitting for Simvastatin release from 575 Da samples at pH 7.4. Fitting shown with burst release (top) and without burst release (bottom). Columns: (A) 1% crosslinked samples, (B) 2.5% crosslinked samples, (C) 5% crosslinked samples, (D) 7.5% crosslinked samples, and (E) 10% crosslinked samples.

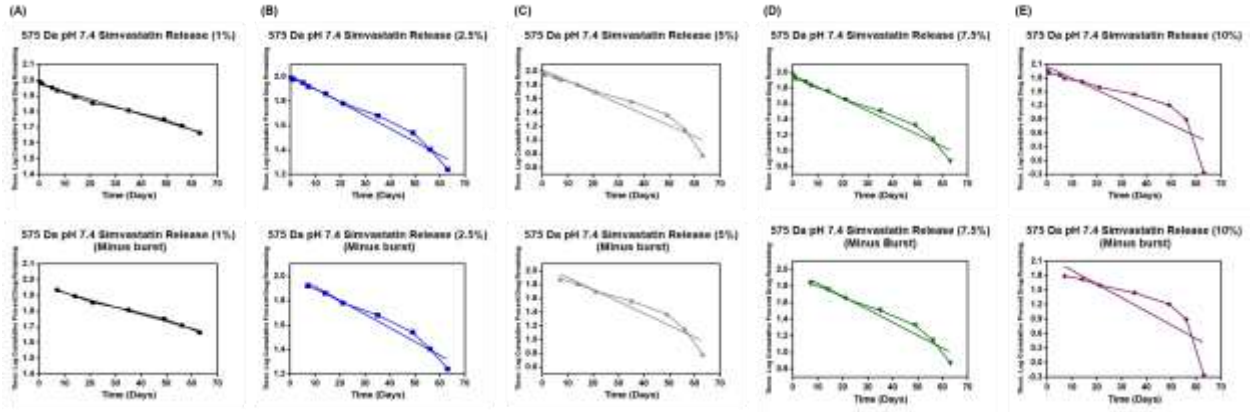

Figure B.2: Linear first order curve fitting for Simvastatin release from 575 Da samples at pH 7.4. Fitting shown with burst release (top) and without burst release (bottom). Columns: (A) 1% crosslinked samples, (B) 2.5% crosslinked samples, (C) 5% crosslinked samples, (D) 7.5% crosslinked samples, and (E) 10% crosslinked samples.

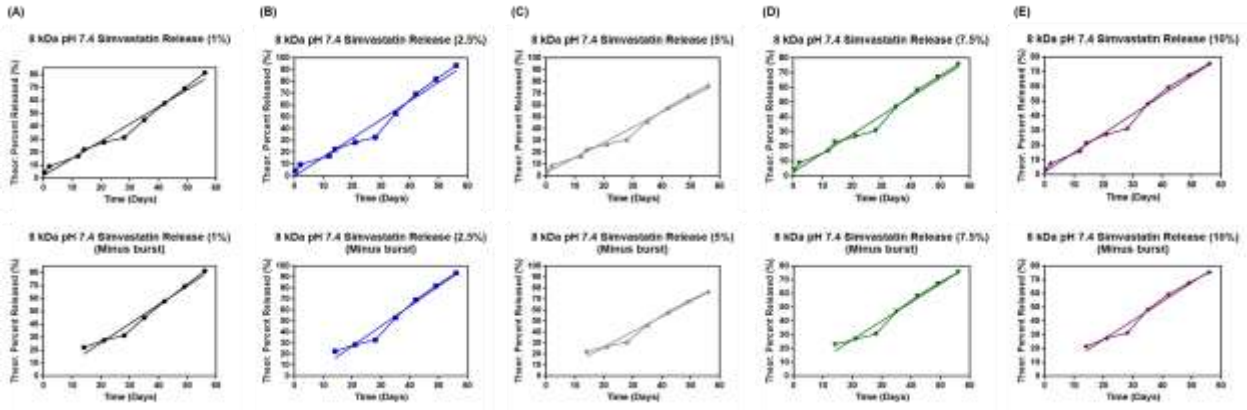

Figure B.3: Linear zero-order curve fitting for Simvastatin release from 8 kDa samples at pH 7.4. Fitting shown with burst release (top) and without burst release (bottom). Columns: (A) 1% crosslinked samples, (B) 2.5% crosslinked samples, (C) 5% crosslinked samples, (D) 7.5% crosslinked samples, and (E) 10% crosslinked samples.

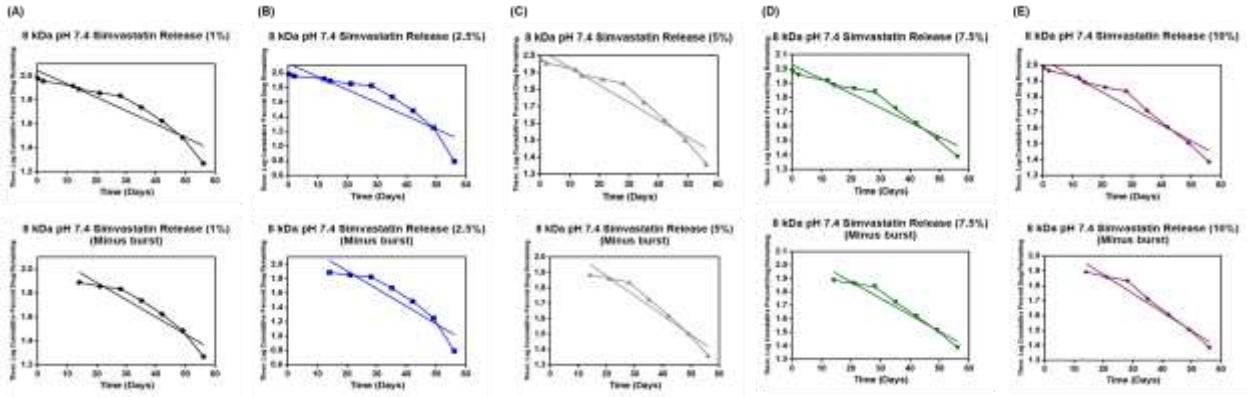

Figure B.4: Linear first order curve fitting for Simvastatin release from 8 kDa samples at pH 7.4. Fitting shown with burst release (top) and without burst release (bottom). Columns: (A) 1% crosslinked samples, (B) 2.5% crosslinked samples, (C) 5% crosslinked samples, (D) 7.5% crosslinked samples, and (E) 10% crosslinked samples.

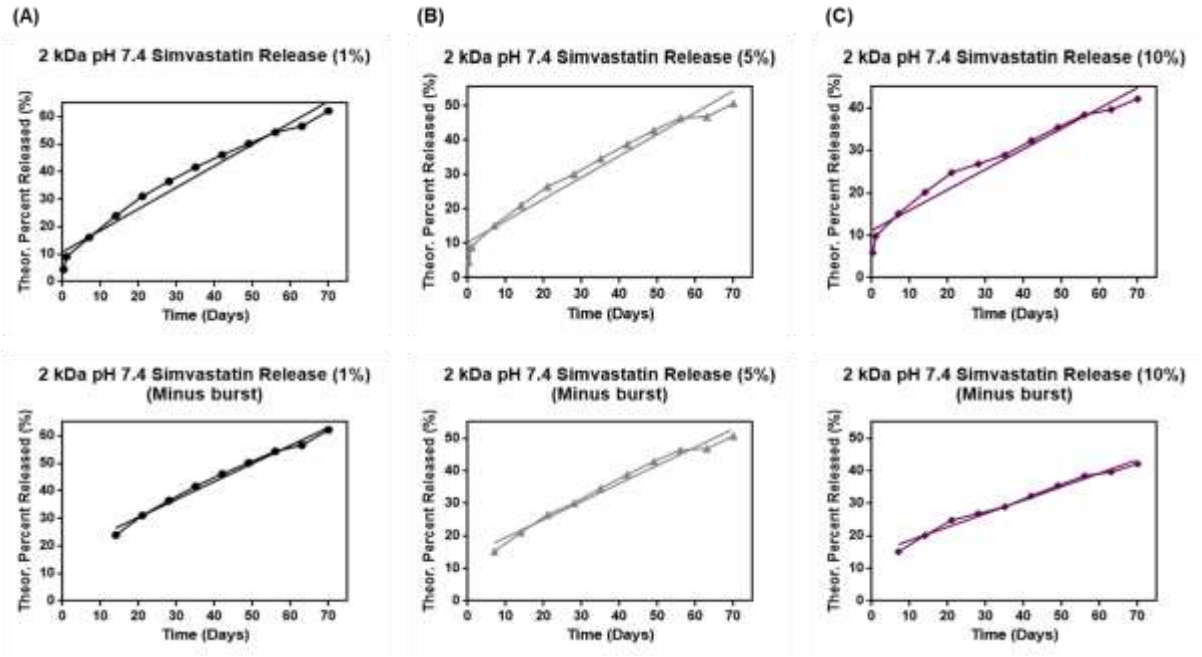

Figure B.5: Linear zero-order curve fitting for Simvastatin release from 2 kDa samples at pH 7.4. Fitting shown with burst release (top) and without burst release (bottom). Columns: (A) 1% crosslinked samples, (B) 5% crosslinked samples, and (C) 10% crosslinked samples.

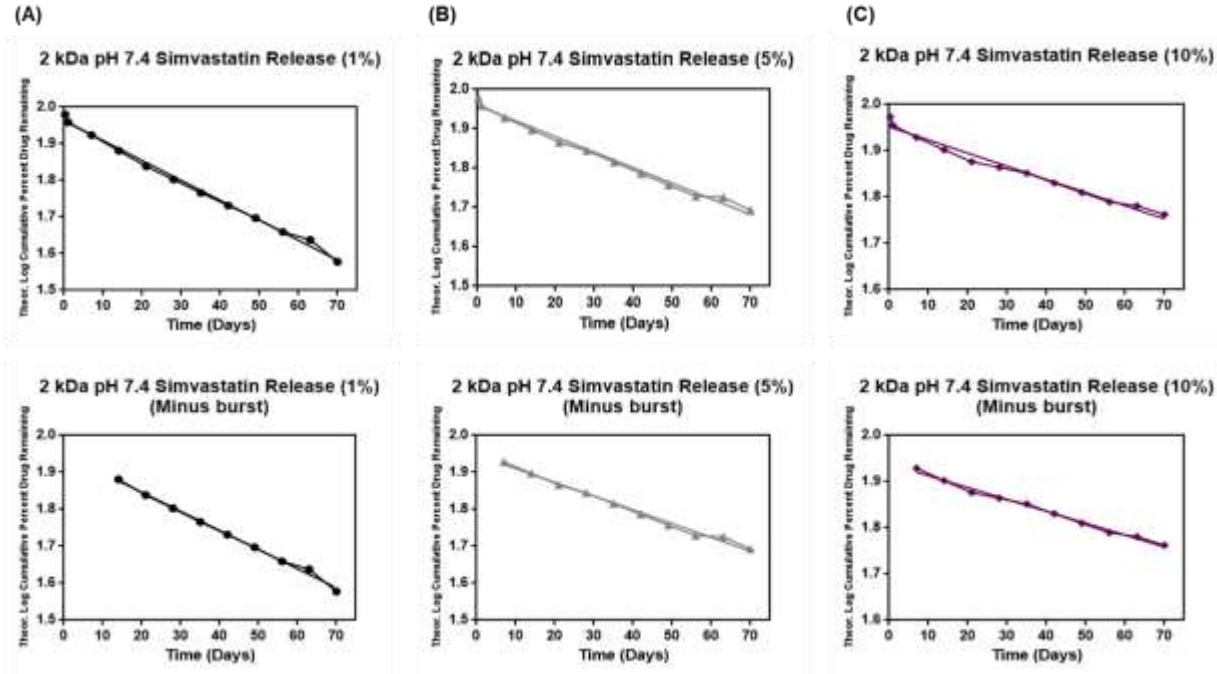

Figure B.6: Linear first order curve fitting for Simvastatin release from 2 kDa samples at pH 7.4. Fitting shown with burst release (top) and without burst release (bottom). Columns: (A) 1% crosslinked samples, (B) 5% crosslinked samples, and (C) 10% crosslinked samples.

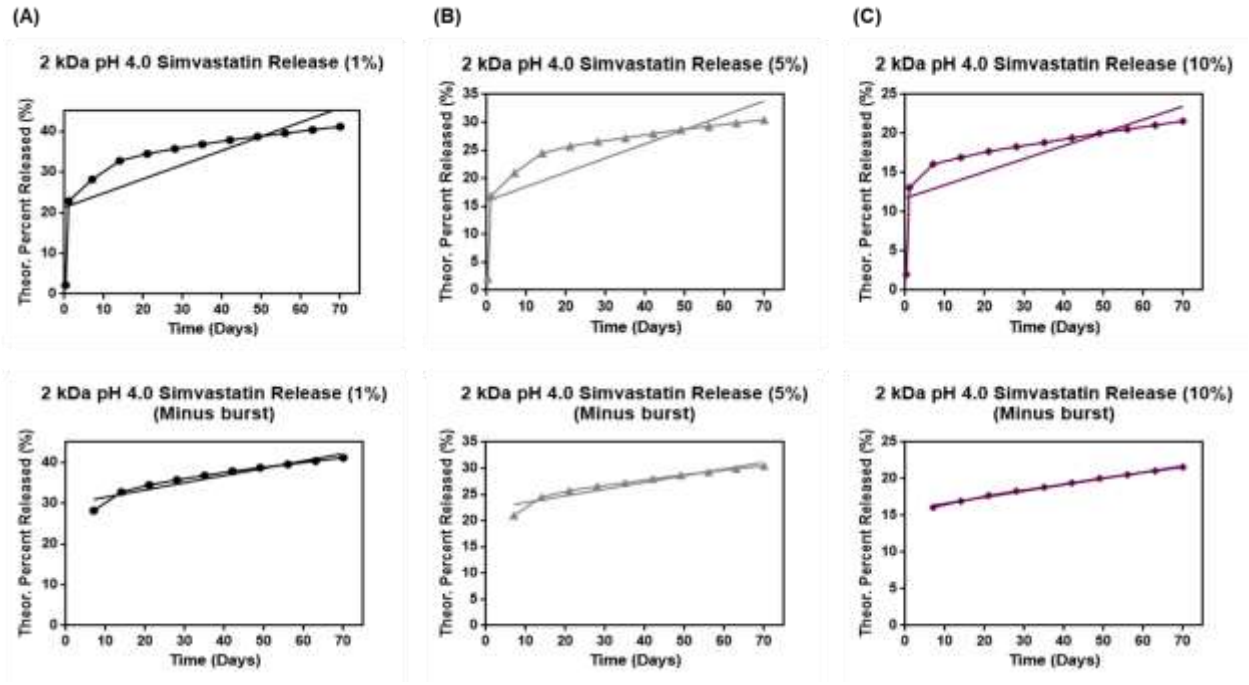

Figure B.7: Linear zero-order curve fitting for Simvastatin release from 2 kDa samples at pH 4.0. Fitting shown with burst release (top) and without burst release (bottom). Columns: (A) 1% crosslinked samples, (B) 5% crosslinked samples, and (C) 10% crosslinked samples.

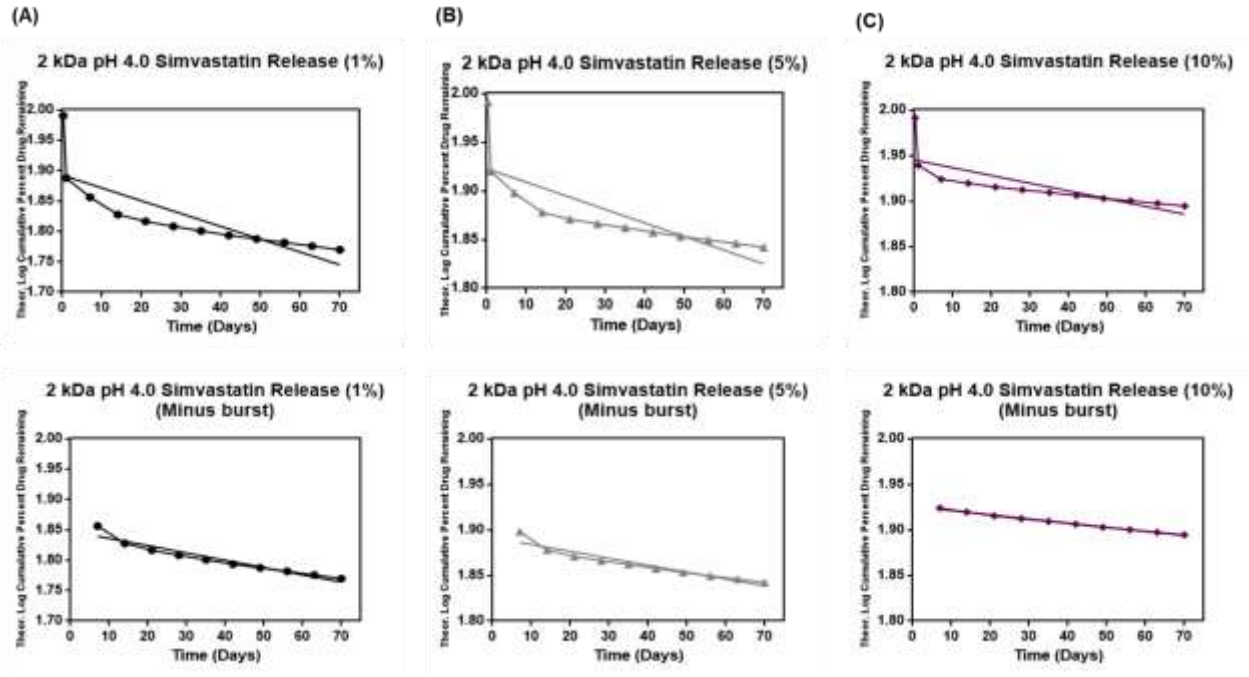

Figure B.8: Linear first order curve fitting for Simvastatin release from 2 kDa samples at pH 4.0. Fitting shown with burst release (top) and without burst release (bottom). Columns: (A) 1% crosslinked samples, (B) 5% crosslinked samples, and (C) 10% crosslinked samples.

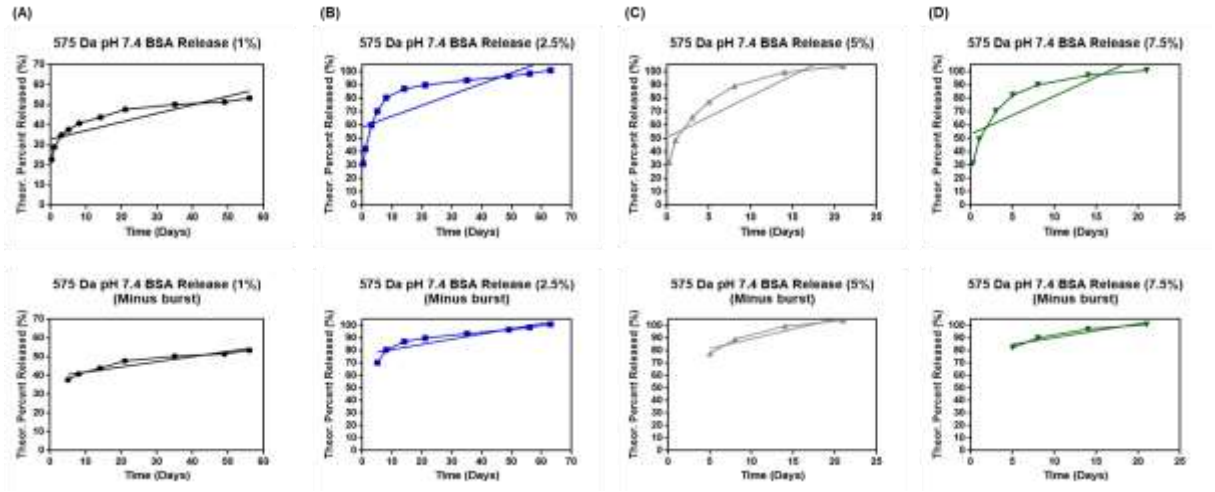

Figure B.9: Linear zero-order curve fitting for BSA release from 575 Da samples at pH 7.4. Fitting shown with burst release (top) and without burst release (bottom). Columns: (A) 1% crosslinked samples, (B) 2.5% crosslinked samples, (C) 5% crosslinked samples, and (D) 7.5% crosslinked samples.

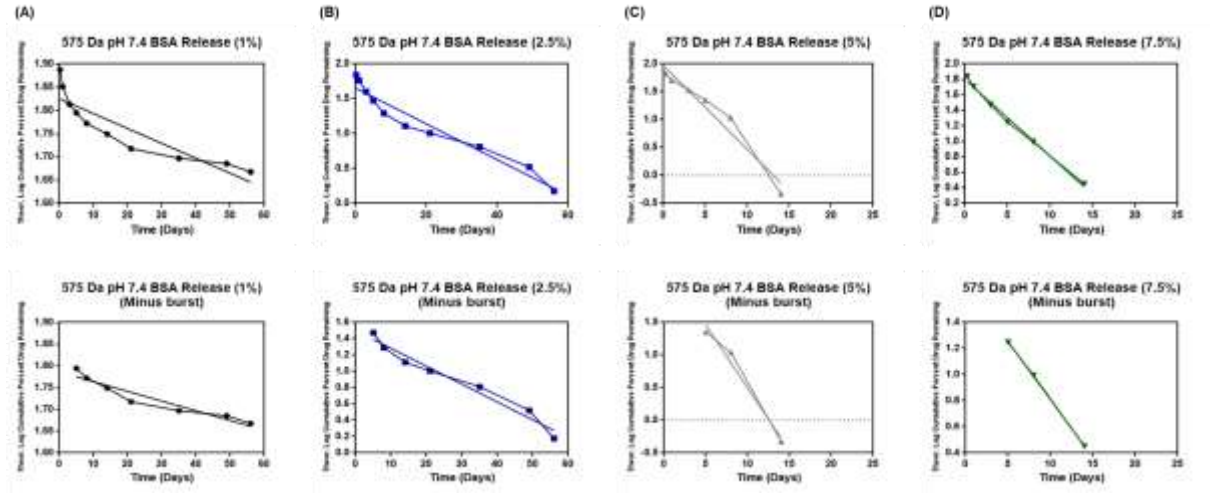

Figure B.10: Linear first order curve fitting for BSA release from 575 Da samples at pH 7.4. Fitting shown with burst release (top) and without burst release (bottom). Columns: (A) 1% crosslinked samples, (B) 2.5% crosslinked samples, (C) 5% crosslinked samples, and (D) 7.5% crosslinked samples.

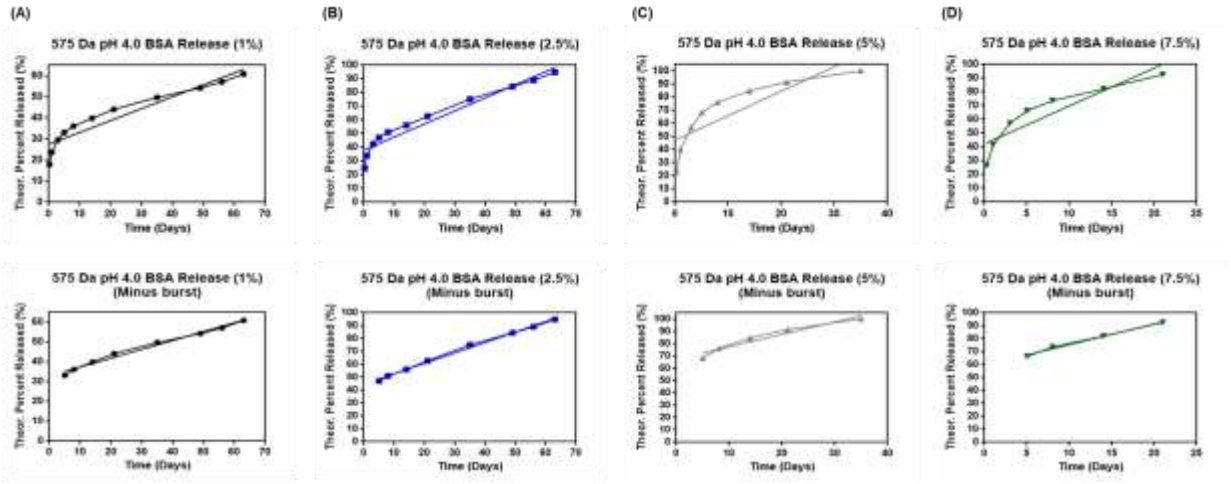

Figure B.11: Linear zero-order curve fitting for BSA release from 575 Da samples at pH 4.0. Fitting shown with burst release (top) and without burst release (bottom). Columns: (A) 1% crosslinked samples, (B) 2.5% crosslinked samples, (C) 5% crosslinked samples, and (D) 7.5% crosslinked samples.

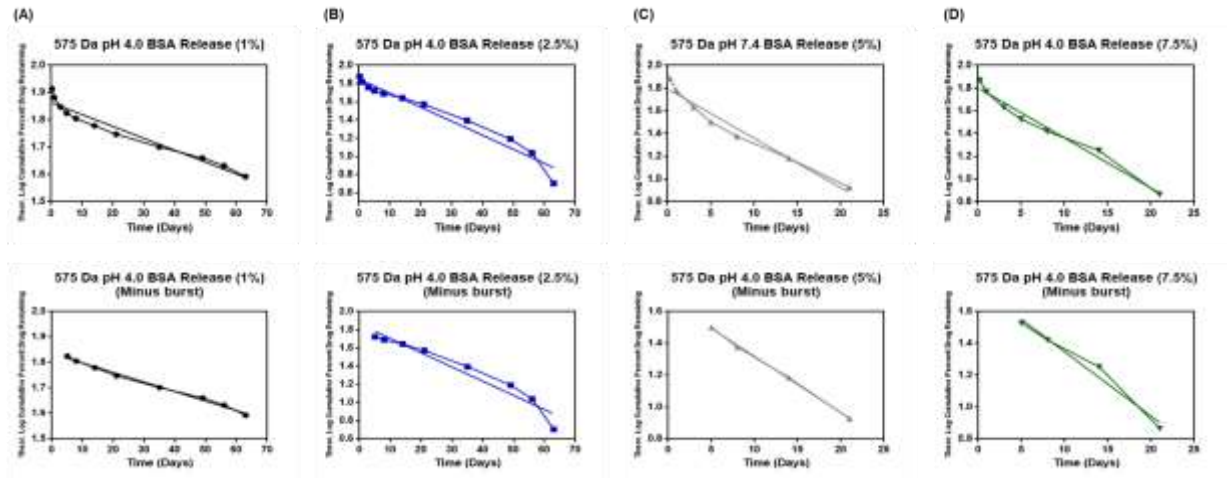

Figure B.12: Linear zero-order curve fitting for BSA release from 575 Da samples at pH 7.4. Fitting shown with burst release (top) and without burst release (bottom). Columns: (A) 1% crosslinked samples, (B) 2.5% crosslinked samples, (C) 5% crosslinked samples, and (D) 10% crosslinked samples.

Appendix C. Supplemental images to Targeting of HER2+ SKBR3 cells with Novel Conjugated Targeting Peptides on "Single" versus "Palm-tree" PEG-PLGA Nanoparticles

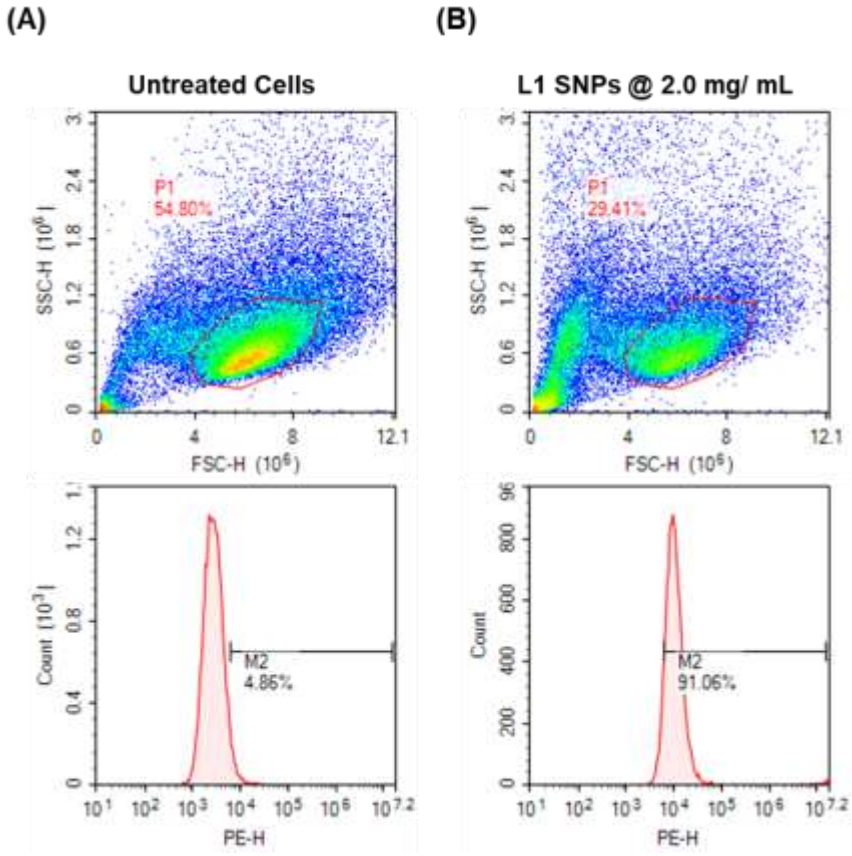

Figure C.1: Flow cytometry of increased L1 conjugated PEGMA-PLGA particles against HER2+ SKBR3 cells negatively affects cell viability and leads to fluorescence oversaturation.

Bibliography

1. Yang L, Zhang L, Webster TJ. Nanobiomaterials: State of the art and future trends. Adv. Eng. Mater. 2011;13(6):197–217.
2. Mershin A, Cook B, Kaiser L, Zhang S. A classic assembly of nanobiomaterials. Nat. Biotechnol. 2005;23(11):1379–80.
3. Hasirci V, Vrana E, Zorlutuna P, Ndreu A, Yilgor P, Basmanav FB, Aydin E. Nanobiomaterials: A review of the existing science and technology, and new approaches. J. Biomater. Sci. Polym. Ed. 2006;17(11):1241–68.
4. De Stefano D, Carnuccio R, Maiuri MC. Nanomaterials Toxicity and Cell Death Modalities. J. Drug Deliv. 2012;2012:1–14.
5. Prakash Sharma V, Sharma U, Chattopadhyay M, Shukla VN. Advance Applications of Nanomaterials: A Review. Mater. Today Proc. [Internet]. Elsevier Ltd; 2018;5(2):6376–80. Available from: https://doi.org/10.1016/j.matpr.2017.12.248
6. Thein-Han W, Xu HHK. Collagen-calcium phosphate cement scaffolds seeded with umbilical cord stem cells for bone tissue engineering. Tissue Eng. - Part A. 2011;17(23–24):2943–54.
7. Jungreuthmayer C, Donahue SW, Jaasma MJ, Al-Munajjed AA, Zanghellini J, Kelly DJ, O'Brien FJ. A comparative study of shear stresses in collagen-glycosaminoglycan and calcium phosphate scaffolds in bone tissue-engineering bioreactors. Tissue Eng. - Part A. 2009;15(5):1141–9.
8. Li J, Baker BA, Mou X, Ren N, Qiu J, Boughton RI, Liu H. Biopolymer/calcium phosphate scaffolds for bone tissue engineering. Adv. Healthc. Mater. 2014;3(4):469–84.
9. Parmar PA, Chow LW, St-Pierre JP, Horejs CM, Peng YY, Werkmeister JA, Ramshaw JAM, Stevens MM. Collagen-mimetic peptide-modifiable hydrogels for articular cartilage regeneration. Biomaterials [Internet]. Elsevier Ltd; 2015;54:213–25. Available from: http://dx.doi.org/10.1016/j.biomaterials.2015.02.079
10. Armiento AR, Stoddart MJ, Alini M, Eglin D. Biomaterials for articular cartilage tissue engineering: Learning from biology. Acta Biomater. [Internet]. Acta Materialia Inc.; 2018;65:1–20. Available from: https://doi.org/10.1016/j.actbio.2017.11.021
11. Atmanli A, Domian IJ. Recreating the Cardiac Microenvironment in Pluripotent Stem Cell Models of Human Physiology and Disease. Trends Cell Biol. [Internet]. Elsevier Ltd; 2017;27(5):352–64. Available from: http://dx.doi.org/10.1016/j.tcb.2016.11.010
12. Khang D, Carpenter J, Chun YW, Pareta R, Webster TJ. Nanotechnology for regenerative medicine. Biomed. Microdevices. 2010;12(4):575–87.
13. Wei G, Jin Q, Giannobile W V., Ma PX. Nano-fibrous scaffold for controlled delivery of recombinant human PDGF-BB. J. Control. Release. 2006;112(1):103–10.
14. Liu X, Jin X, Ma PX. Nanofibrous hollow microspheres self-assembled from star-shaped polymers as injectable cell carriers for knee repair. Nat. Mater. [Internet]. Nature Publishing Group; 2011 May [cited 2013 Oct 25];10(5):398–406. Available from: http://www.pubmedcentral.nih.gov/articlerender.fcgi?artid=3080435&tool=pmcentrez&rendertype=abstract

15. Zhang Z, Gupte MJ, Jin X, Ma PX. Injectable peptide decorated functional nanofibrous hollow microspheres to direct stem cell differentiation and tissue regeneration. Adv. Funct. Mater. 2015;25(3):350–60.
16. Discher DE, Janmey P, Wang YL. Tissue cells feel and respond to the stiffness of their substrate. Science (80-.). 2005;310(5751):1139–43.
17. Lo CM, Wang HB, Dembo M, Wang YL. Cell movement is guided by the rigidity of the substrate. Biophys. J. [Internet]. Elsevier; 2000;79(1):144–52. Available from: http://dx.doi.org/10.1016/S0006-3495(00)76279-5
18. Ren YJ, Zhang H, Huang H, Wang XM, Zhou ZY, Cui FZ, An YH. In vitro behavior of neural stem cells in response to different chemical functional groups. Biomaterials [Internet]. Elsevier Ltd; 2009;30(6):1036–44. Available from: http://dx.doi.org/10.1016/j.biomaterials.2008.10.028
19. Dalby MJ, Riehle MO, Johnstone HJH, Affrossman S, Curtis ASG. Polymer-demixed nanotopography: Control of fibroblast spreading and proliferation. Tissue Eng. 2002;8(6):1099–108.
20. Dulgar-Tulloch AJ, Bizios R, Siegel RW. Human mesenchymal stem cell adhesion and proliferation in response to ceramic chemistry and nanoscale topography. J. Biomed. Mater. Res. - Part A. 2009;90(2):586–94.
21. Chen F-M, Liu X. Advancing biomaterials of human origin for tissue engineering. Prog Polym Sci [Internet]. 2016;53:86–168. Available from: https://www.ncbi.nlm.nih.gov/pmc/articles/PMC4808059/pdf/nihms680686.pdf
22. Yun MH. Changes in regenerative capacity through lifespan. Int. J. Mol. Sci. 2015;16(10):25392–432.
23. Feinberg AW. Engineered tissue grafts: Opportunities and challenges in regenerative medicine. Wiley Interdiscip. Rev. Syst. Biol. Med. 2012;4(2):207–20.
24. Shieh SJ, Vacanti JP. State-of-the-art tissue engineering: From tissue engineering to organ building. Surgery. 2005;137(1):1–7.
25. Heidary Rouchi A, Mahdavi-Mazdeh M. Regenerative medicine in organ and tissue transplantation: Shortly and practically achievable? Int. J. Organ Transplant. Med. 2015;6(3):93–8.
26. Ma PX. Scaffolds for tissue fabrication. Mater. Today [Internet]. Elsevier Ltd; 2004;7(5):30–40. Available from: http://dx.doi.org/10.1016/S1369-7021(04)00233-0
27. O'Brien FJ. Biomaterials & scaffolds for tissue engineering. Mater. Today [Internet]. Elsevier Ltd; 2011;14(3):88–95. Available from: http://dx.doi.org/10.1016/S1369-7021(11)70058-X
28. Ma PX, Eyster TW, Doleyres Y. Tissue Engineering Biomaterials. Encycl. Polym. Sci. Technol. [Internet]. 2002. Available from: http://dx.doi.org/10.1002/0471440264.pst471.pub2
29. Wen JH, Vincent LG, Fuhrmann A, Choi YS, Hribar KC, Taylor-Weiner H, Chen S, Engler AJ. Interplay of matrix stiffness and protein tethering in stem cell differentiation. Nat. Mater. 2014;13(10):979–87.
30. Mao AS, Shin JW, Mooney DJ. Effects of substrate stiffness and cell-cell contact on mesenchymal stem cell differentiation. Biomaterials [Internet]. Elsevier Ltd; 2016;98:184–91. Available from: http://dx.doi.org/10.1016/j.biomaterials.2016.05.004
31. Guo B, Ma PX. Synthetic biodegradable functional polymers for tissue engineering: A brief review. Sci. China Chem. 2014;57(4):490–500.

32. Gultekinoglu M, Öztürk Ş, Chen B, Edirisinghe M, Ulubayram K. Preparation of poly(glycerol sebacate) fibers for tissue engineering applications. Eur. Polym. J. [Internet]. Elsevier; 2019;121(October):109297. Available from: https://doi.org/10.1016/j.eurpolymj.2019.109297
33. Chu TMG, Halloran JW, Hollister SJ, Feinberg SE. Hydroxyapatite implants with designed internal architecture. J. Mater. Sci. Mater. Med. 2001;12(6):471–8.
34. Ma PX, Choi JW. Biodegradable polymer scaffolds with well-defined interconnected spherical pore network. Tissue Eng. 2001;7(1):23–33.
35. Chen VJ, Ma PX. Nano-fibrous poly(L-lactic acid) scaffolds with interconnected spherical macropores. Biomaterials. 2004;25(11):2065–73.
36. Liu X, Smith LA, Hu J, Ma PX. Biomimetic nanofibrous gelatin/apatite composite scaffolds for bone tissue engineering. Biomaterials [Internet]. Elsevier Ltd; 2009;30(12):2252–8. Available from: http://dx.doi.org/10.1016/j.biomaterials.2008.12.068
37. Wei G, Ma PX. Macroporous and nanofibrous polymer scaffolds and polymer / bone-like apatite composite scaffolds generated by sugar spheres. J. Biomed. Res. Part A. 2006;306–15.
38. Mooney DJ, Baldwin DF, Suh NP, Vacanti JP, Langer R. Novel approach to fabricate porous sponges of poly(D,L-lactic-co-glycolic acid) without the use of organic solvents. Biomaterials. 1996;17(14):1417–22.
39. Whang K, Thomas CH, Healy KE, Nuber G. A novel method to fabricate bioabsorbable scaffolds. Polymer (Guildf). 1995;36(4):837–42.
40. Agrawal CM, Ray RB. Biodegradable polymeric scaffolds for musculoskeletal tissue engineering. J. Biomed. Mater. Res. 2001;55(2):141–50.
41. El-Sherbiny IM, Yacoub MH. Hydrogel scaffolds for tissue engineering: Progress and challenges. Glob. Cardiol. Sci. Pract. 2013;2013(3):38.
42. Hoffman AS. Hydrogels for biomedical applications. Adv. Drug Deliv. Rev. [Internet]. Elsevier B.V.; 2012;64:18–23. Available from: http://dx.doi.org/10.1016/j.addr.2012.09.010
43. Spicer CD. Hydrogel scaffolds for tissue engineering: the importance of polymer choice. Polym. Chem. Royal Society of Chemistry; 2019;11:184–219.
44. Catoira MC, Fusaro L, Di Francesco D, Ramella M, Boccafoschi F. Overview of natural hydrogels for regenerative medicine applications. J. Mater. Sci. Mater. Med. [Internet]. Springer US; 2019;30(10). Available from: http://dx.doi.org/10.1007/s10856-019-6318-7
45. Dhandayuthapani B, Yoshida Y, Maekawa T, Kumar DS. Polymeric scaffolds in tissue engineering application: A review. Int. J. Polym. Sci. 2011;2011(ii).
46. Lee KY, Mooney DJ. Hydrogels for Tissue Engineering. Chem. Rev. 2001;101(7).
47. Bailey WJ, Ni Z, Wu S-R. Synthesis of Poly-e-Caprolactone via a Free Radical Mechanism. Free Radical Ring-Opening Polymerization of 2-Methylene-1,3-Dioxepane. J. Polym. Sci. Polym. Chem. Ed. 1982;20:3021–30.
48. Bailey WJ, Zhou L-L. A New Elimination with Phase-Transfer Catalysis for Cyclic Ketene Acetals. Tetrahedron Lett. 1991;32(12):1539–40.
49. Agarwal S. Chemistry, chances and limitations of the radical ring-opening polymerization of cyclic ketene acetals for the synthesis of degradable polyesters. Polym. Chem. 2010;1:953–64.
50. Hiraguri Y, Katase K, Tokiwa Y. Biodegradability of Poly (ester - ether) and Poly (ester

) Obtained from a Radical Ring - Opening Polymerization of Cyclic Ketene Acetals Biodegradability of Poly (ester-ether) and Poly (ester) Obtained from a Radical Ring-Opening Polymerization of. J. Macromol. Sci. Part A Pure Appl. Chem. 2007;42(7):901–7.
51. Undin J, Plikk P, Finne-wistrand A, Albertsson A. Synthesis of Amorphous Aliphatic Polyester-Ether Homo- and Copolymers by Radical Polymerization of Ketene Acetals. J. Polym. Sci. Part A Polym. Chem. 2010;48:4965–73.
52. Hiraguri Y, Tokiwa Y. Syntheses of Biodegradable Functional Polymers by Radical Ring-Opening Polymerization of 2-Methylene-1,3,6-trioxocane. J. Polym. Environ. 2010;18:116–21.
53. Hiraguri Y, Tokiwa Y. Synthesis of Photodegradable Polymers Having Biodegradability and Their Biodegradations and Photolysis. Macromolecules. 1997;30(12):3691–3.
54. Redaelli F, Sorbona M, Rossi F. Synthesis and processing of hydrogels for medical applications [Internet]. Bioresorbable Polym. Biomed. Appl. From Fundam. to Transl. Med. Elsevier Ltd; 2017. Available from: http://dx.doi.org/10.1016/B978-0-08-100262-9.00010-0
55. Patra JK, Das G, Fraceto LF, Campos EVR, Rodriguez-Torres MDP, Acosta-Torres LS, Diaz-Torres LA, Grillo R, Swamy MK, Sharma S, Habtemariam S, Shin HS. Nano based drug delivery systems: Recent developments and future prospects. J. Nanobiotechnology [Internet]. BioMed Central; 2018;16(1):1–33. Available from: https://doi.org/10.1186/s12951-018-0392-8
56. DiMasi JA, Grabowski HG. The cost of biopharmaceutical R&D: Is biotech different? Manag. Decis. Econ. 2007;28:469–79.
57. Watkins R, Wu L, Zhang C, Davis RM, Xu B. Natural product-based nanomedicine: Recent advances and issues. Int. J. Nanomedicine. 2015;10:6055–74.
58. Langer R. Biomaterials for Drug Delivery and Tissue Engineering. MRS Bullentin. 2006;31(June):477–85.
59. Srinivasan M, Rajabi M, Mousa SA. Nanobiomaterials in cancer therapy [Internet]. Seventh Ed. Nanobiomaterials Cancer Ther. Appl. Nanobiomaterials. Elsevier Inc.; 2016. Available from: http://dx.doi.org/10.1016/B978-0-323-42863-7.00003-7
60. Rajabi M, Srinivasan M, Mousa SA. Nanobiomaterials in drug delivery [Internet]. Nanobiomaterials Drug Deliv. Appl. Nanobiomaterials. Elsevier Inc.; 2016. Available from: http://dx.doi.org/10.1016/B978-0-323-42866-8.00001-0
61. Upadhyay RK. Drug delivery systems, CNS protection, and the blood brain barrier. Biomed Res. Int. Hindawi Publishing Corporation; 2014;2014.
62. Kinoshita M. Targeted drug delivery to the brain using focused ultrasound. Top. Magn. Reson. Imaging. 2006;17(3):209–15.
63. Han H. The effect of nanoparticle size on in vivo pharmacokinetics and cellular interaction. Nanomedicine (Lond). 2016;11(6):673–92.
64. Kumari A, Yadav SK, Yadav SC. Biodegradable polymeric nanoparticles based drug delivery systems. Colloids Surfaces B Biointerfaces. 2010;75(1):1–18.
65. Yoo HS, Park TG. Biodegradable polymeric micelles composed of doxorubicin conjugated PLGA-PEG block copolymer. J. Control. Release [Internet]. 2001 Jan 29;70(1–2):63–70. Available from: http://www.ncbi.nlm.nih.gov/pubmed/11166408
66. Yoo HS, Park TG. Folate receptor targeted biodegradable polymeric doxorubicin micelles. J. Control. Release [Internet]. 2004 Apr 28 [cited 2014 Jan 22];96(2):273–83. Available

from: http://www.ncbi.nlm.nih.gov/pubmed/15081218
67. Cho HK, Cheong IW, Lee JM, Kim JH. Polymeric nanoparticles, micelles and polymersomes from amphiphilic block copolymer. Korean J. Chem. Eng. 2010;27(3):731–40.
68. Lale S V., Kumar A, Prasad S, Bharti AC, Koul V. Folic acid and trastuzumab functionalized redox responsive polymersomes for intracellular doxorubicin delivery in breast cancer. Biomacromolecules. 2015;16(6):1736–52.
69. Hu M, Shen Y, Zhang L, Qiu L. Polymersomes via Self-Assembly of Amphiphilic β-Cyclodextrin-Centered Triarm Star Polymers for Enhanced Oral Bioavailability of Water-Soluble Chemotherapeutics. Biomacromolecules. 2016;17(3):1026–39.
70. Dykes GM. Dendrimers: a review of their appeal and applications. J. Chem. Technol. Biotechnol. 2001;76:903–18.
71. Lai P, Lou P, Peng C, Pai C, Yen W. Doxorubicin delivery by polyamidoamine dendrimer conjugation and photochemical internalization for cancer therapy. J. Control. Release. 2007;122:39–46.
72. Hui Zhong, He Z-G, Zheng Li, Li G-Y, Shen S-R, Li X-L. Studies on polyamidoamine dendrimers as efficient gene delivery vector. J. Biomater. Appl. [Internet]. 2008 May [cited 2015 Jun 22];22(6):527–44. Available from: http://www.ncbi.nlm.nih.gov/pubmed/17623709
73. Noriega-Luna B, Godínez LA, Rodríguez FJ, Rodríguez A, Zaldívar-Lelo De Larrea G, Sosa-Ferreyra CF, Mercado-Curiel RF, Manríquez J, Bustos E. Applications of dendrimers in drug delivery agents, diagnosis, therapy, and detection. J. Nanomater. 2014;2014.
74. Liu M, Kono K, Fréchet JMJ. Water-soluble dendritic unimolecular micelles: Their potential as drug delivery agents. J. Control. Release. 2000;65(1–2):121–31.
75. Lin CC, Metters AT. Hydrogels in controlled release formulations: Network design and mathematical modeling. Adv. Drug Deliv. Rev. 2006;58(12–13):1379–408.
76. Lin C, Anseth KS. PEG Hydrogels for the Controlled Release of Biomolecules in Regenerative Medicine. Pharm. Res. 2009;26(3):631–43.
77. Hoare TR, Kohane DS. Hydrogels in drug delivery : Progress and challenges. Polymer (Guildf). [Internet]. Elsevier Ltd; 2008;49(8):1993–2007. Available from: http://dx.doi.org/10.1016/j.polymer.2008.01.027
78. Peppas NA. Hydrogels and drug delivery. Curr. Opin. Colloid Interface Sci. [Internet]. Current Chemistry Ltd.; 1997;2(5):531–7. Available from: http://dx.doi.org/10.1016/S1359-0294(97)80103-3
79. Kim SW, Bae YH, Okano T. Hydrogels: Swelling, Drug Loading, and Release. Pharm. Res. An Off. J. Am. Assoc. Pharm. Sci. 1992. p. 283–90.
80. E. Uhrich K, M. Cannizzaro S, S. Langer R, M. Shakesheff K. Polymeric Systems for Controlled Drug Release. Chem. Rev. American Chemical Society; 1999 Oct 26;99(11):3181–98.
81. Larrañeta E, Stewart S, Ervine M, Al-Kasasbeh R, Donnelly RF. Hydrogels for hydrophobic drug delivery. Classification, synthesis and applications. J. Funct. Biomater. 2018;9(1).
82. Steichen SD, Caldorera-Moore M, Peppas NA. A review of current nanoparticle and targeting moieties for the delivery of cancer therapeutics. Eur. J. Pharm. Sci. [Internet]. 2013;48(3):416–27. Available from: http://dx.doi.org/10.1016/j.ejps.2012.12.006

83. Wang M, Thanou M. Targeting nanoparticles to cancer. Pharmacol. Res. [Internet]. Elsevier Ltd; 2010;62(2):90–9. Available from: http://dx.doi.org/10.1016/j.phrs.2010.03.005
84. Suri SS, Fenniri H, Singh B. Nanotechnology-based drug delivery systems. J. Occup. Med. Toxicol. [Internet]. 2007 Jan [cited 2015 Jun 21];2:16. Available from: http://www.pubmedcentral.nih.gov/articlerender.fcgi?artid=2222591&tool=pmcentrez&rendertype=abstract
85. Danhier F, Ansorena E, Silva JM, Coco R, Le Breton A, Préat V. PLGA-based nanoparticles: an overview of biomedical applications. J. Control. Release [Internet]. Elsevier B.V.; 2012 Jul 20 [cited 2013 May 27];161(2):505–22. Available from: http://www.ncbi.nlm.nih.gov/pubmed/22353619
86. Bertrand N, Wu J, Xu X, Kamaly N, Farokhzad OC. Cancer nanotechnology : The impact of passive and active targeting in the era of modern cancer biology. Adv. Drug Deliv. Rev. [Internet]. Elsevier B.V.; 2014;66:2–25. Available from: http://dx.doi.org/10.1016/j.addr.2013.11.009
87. Phillips MA, Gran ML, Peppas NA. Targeted nanodelivery of drugs and diagnostics. Nano Today [Internet]. Elsevier Ltd; 2010;5(2):143–59. Available from: http://dx.doi.org/10.1016/j.nantod.2010.03.003
88. Lu RM, Chen MS, Chang DK, Chiu CY, Lin WC, Yan SL, Wang YP, Kuo YS, Yeh CY, Lo A, Wu HC. Targeted Drug Delivery Systems Mediated by a Novel Peptide in Breast Cancer Therapy and Imaging. PLoS One. 2013;8(6).
89. Steichen SD, Caldorera-moore M, Peppas NA. A review of current nanoparticle and targeting moieties for the delivery of cancer therapeutics. Eur. J. Pharm. Sci. [Internet]. 2013;48(3):416–27. Available from: http://dx.doi.org/10.1016/j.ejps.2012.12.006
90. Wilhelm S, Tavares AJ, Dai Q, Ohta S, Audet J, Dvorak HF, Chan WCW. Analysis of nanoparticle delivery to tumours. Nat. Rev. Mater. 2016;1:1–12.
91. Temming K, Schiffelers RM, Molema G, Kok RJ. RGD-based strategies for selective delivery of therapeutics and imaging agents to the tumour vasculature. Drug Resist. Updat. 2005;8(6):381–402.
92. Hersel U, Dahmen C, Kessler H. RGD modified polymers: Biomaterials for stimulated cell adhesion and beyond. Biomaterials. 2003;24:4385–415.
93. Ruoslahti E. Rgd and Other Recognition Sequences for Integrins. Annu. Rev. Cell Dev. Biol. 1996;12(1):697–715.
94. Bellmann-Sickert K, Beck-Sickinger AG. Peptide drugs to target G protein-coupled receptors. Trends Pharmacol. Sci. [Internet]. Elsevier Ltd; 2010;31(9):434–41. Available from: http://dx.doi.org/10.1016/j.tips.2010.06.003
95. Huang S, Li J, Han L, Liu S, Ma H, Huang R, Jiang C. Dual targeting effect of Angiopep-2-modified, DNA-loaded nanoparticles for glioma. Biomaterials [Internet]. Elsevier Ltd; 2011;32(28):6832–8. Available from: http://dx.doi.org/10.1016/j.biomaterials.2011.05.064
96. Engel RH, Kaklamani VG. HER2-Positive Breast Cancer: Current and Future Treatment Strategies. Drugs [Internet]. Springer International Publishing; 2007 [cited 2016 Dec 19];67(9):1329–41. Available from: http://link.springer.com/10.2165/00003495-200767090-00006
97. Female Breast Cancer - Cancer Stat Facts [Internet]. [cited 2020 Feb 26]. Available from: https://seer.cancer.gov/statfacts/html/breast.html

98. Figueroa-Magalhães MC, Jelovac D, Connolly RM, Wolff AC. Treatment of HER2-positive breast cancer. The Breast [Internet]. Elsevier Ltd; 2014;23(2):128–36. Available from: http://linkinghub.elsevier.com/retrieve/pii/S0960977613003007
99. Korkaya H, Paulson a, Iovino F, Wicha MS. HER2 regulates the mammary stem/progenitor cell population driving tumorigenesis and invasion. Oncogene [Internet]. 2008 Oct 16 [cited 2015 May 12];27(47):6120–30. Available from: http://www.pubmedcentral.nih.gov/articlerender.fcgi?artid=2602947&tool=pmcentrez&rendertype=abstract
100. Carlson RW, Allred DC, Anderson BO, Burstein HJ, Carter WB, Edge SB, Erban JK, Farrar WB, Lori J, Gradishar WJ, Hayes DF, Hudis CA, Kiel K, Ljung B, Marcom PK, Mayer IA, Mccormick B, Nabell LM, Pierce LJ, Reed EC, Lou M, Somlo G, Theriault RL, Topham NS, Ward JH, Winer EP, Wolff AC. Breast Cancer. J. Natl. Compr. Cancer Netw. 2009;7(2):121–91.
101. Bryant SJ, Anseth KS. Controlling the spatial distribution of ECM components in degradable PEG hydrogels for tissue engineering cartilage. 2002;
102. Ullah F, Bisyrul M, Javed F, Akil H. Classification, processing and application of hydrogels: A review. Mater. Sci. Eng. C. 2015;57:414–33.
103. Ahmed EM. Hydrogel : Preparation , characterization , and applications : A review. J. Adv. Res. [Internet]. Cairo University; 2015;6(2):105–21. Available from: http://dx.doi.org/10.1016/j.jare.2013.07.006
104. Hoffman A., Schmer G, Harris C, Kraft W. Covalent Binding of Biomolecules to Radiation-Grafted Hydrogels on Inert Polymer Surfaces. ASAIO J. 1972;18:10–6.
105. Ratner BD, Hoffman AS. Synthetic Hydrogels for Biomedical Applications. Hydrogels Med. Relat. Appl. 1976;31:1–36.
106. Marler JJ, Guha A, Rowley J, Koka R, Mooney D, Ph D, Upton J, Vacanti JP. Soft-Tissue Augmentation with Injectable Alginate and Syngeneic Fibroblasts. Plast. Reconstr. Surg. 2000;105(6):2049–58.
107. Yamamoto M, Tabata T, Ikada Y. Growth Factor Release from Gelatin Hydrogel for Tissue Engineering. J. Bioact. Compat. Polym. 1999;14:474–89.
108. Stile RA, Burghardt WR, Healy KE. Synthesis and Characterization of Injectable Poly (N -isopropylacrylamide)-Based Hydrogels That Support Tissue Formation in Vitro. Macromolecules. 1999;32:7370–9.
109. Burdick JA, Anseth KS. Photoencapsulation of osteoblasts in injectable RGD-modified PEG hydrogels for bone tissue engineering. Biomaterials. 2002;23:4315–23.
110. Bryant SJ, Bender RJ, Durand KL, Anseth KS. Encapsulating Chondrocytes in Degrading PEG Hydrogels With High Modulus : Engineering Gel Structural Changes to Facilitate Cartilaginous Tissue Production. 2004;
111. Hiraguri Y, Katase K, Tokiwa Y. Synthesis of Biodegradable Hydrogel by Radical Ring - Opening Polymerization of 2-Methylene-1,3,6-Trioxocane. J. Macromol. Sci. Part A Pure Appl. Chem. 2006;43:1021–7.
112. Hiraguri Y, Tokiwa Y. Synthesis of Copolymers Composed of 2-Methylene- 1 , 3 , 6-trioxocane and Vinyl Monomers and Their Enzymatic Degradation. J. Polym. Sci. Part A Polym. Chem. 1993;331:3159–61.
113. Hiraguri Y, Tokiwa Y. Synthesis of a new gel with enzymatic degradability. J. Mater. Sci. Lett. 2002;21(23):1875–6.
114. Raeber GP, Lutolf MP, Hubbell JA. Molecularly Engineered PEG Hydrogels : A Novel

Model System for Proteolytically Mediated Cell Migration. Biophys. J. [Internet]. Elsevier; 2005;89(2):1374–88. Available from: http://dx.doi.org/10.1529/biophysj.104.050682
115. Zhao J, Guo B, Ma PX. Injectable alginate microsphere/PLGA-PEG-PLGA composite hydrogels for sustained drug release. RSC Adv. 2014;4(34):17736–42.
116. Lin C, Raza A, Shih H. PEG hydrogels formed by thiol-ene photo-click chemistry and their effect on the formation and recovery of insulin-secreting cell spheroids. Biomaterials [Internet]. Elsevier Ltd; 2011;32(36):9685–95. Available from: http://dx.doi.org/10.1016/j.biomaterials.2011.08.083
117. Miller JS, Shen CJ, Legant WR, Baranski JD, Blakely BL, Chen CS. Bioactive hydrogels made from step-growth derived PEG–peptide macromers. Biomaterials [Internet]. Elsevier Ltd; 2010;31(13):3736–43. Available from: http://dx.doi.org/10.1016/j.biomaterials.2010.01.058
118. Engebretson B, Sikavitsas VI. Long-Term In Vivo Effect of Peg Bone Tissue Engineering Scaffolds. Joournal Long-Term Eff. Med. Implant. 2012;22(3):211–8.
119. Rehmann MS, Skeens KM, Kharkar PM, Ford EM, Maverakis E, Lee KH, Kloxin AM. Tuning and Predicting Mesh Size and Protein Release from Step Growth Hydrogels. Biomacromolecules. 2017;18(10):3131–42.
120. Boccaccini AR, Blaker JJ. Bioactive composite materials for tissue engineering scaffolds. Expert Rev. Med. Devices. 2014;2(3):303–17.
121. Freed LE, Vunjak-novakovic G, Biron RJ, Eagles DB, Lesnoy DC, Barlow SK, Langer R. Biodegradable Polymer Scaffolds for Tissue Engineering. Nat. Biotechnol. 1994;12:689–93.
122. Woo KM, Chen VJ, Ma PX. Nano-fibrous scaffolding architecture selectively enhances protein adsorption contributing to cell attachment. J. Biomed. Mater. Res. Part A. 2003;67.2:531–7.
123. Holzwarth JM, Ma PX. Biomimetic nanofibrous scaffolds for bone tissue engineering. Biomaterials [Internet]. Elsevier Ltd; 2011 Dec [cited 2014 May 23];32(36):9622–9. Available from: http://www.pubmedcentral.nih.gov/articlerender.fcgi?artid=3195926&tool=pmcentrez&rendertype=abstract
124. Hu J, Feng K, Liu X, Ma PX. Chondrogenic and osteogenic differentiations of human bone marrow-derived mesenchymal stem cells on a nanofibrous scaffold with designed pore network. Biomaterials. Elsevier Ltd; 2009 Oct;30(28):5061–7.
125. Toepke MW, Impellitteri NA, Theisen JM, Murphy WL. Characterization of thiol-ene crosslinked PEG hydrogels. Macromol. Mater. Eng. 2013;298(6):699–703.
126. Gorgieva S, Kokol V. Preparation, characterization, and in vitro enzymatic degradation of chitosan-gelatine hydrogel scaffolds as potential biomaterials. J. Biomed. Mater. Res. Part A. 2012;100(7):1655–67.
127. Pascault JP, Williams RJJ. Glass transition temperature versus conversion relationships for thermosetting polymers. J. Polym. Sci. Part B Polym. Phys. 1990;28(1):85–95.
128. Stejny J. The effect of crosslinking on the glass transition temperature and the density of diethylene glycol bis(allylcarbonate) polymer networks. Polym. Bull. 1996;36(5):617–21.
129. Smith MJ, Peppas NA. Effect of the degree of crosslinking on penetrant transport in polystyrene. Polymer (Guildf). 1985;26(4):569–74.
130. Madaghiele M, Maffezzoli A, Ambrosio L, Nicolais L. Crosslinking of cellulose

derivatives and hyaluronic acid with water-soluble carbodiimide. Polymer (Guildf). 2005;46:11206–12.
131. Jiang H, Su W, Mather PT, Bunning TJ. Rheology of highly swollen chitosan / polyacrylate hydrogels. Polymer (Guildf). 1999;40:4593–602.
132. Young JL, Holle AW, Spatz JP. Nanoscale and mechanical properties of the physiological cell-ECM microenvironment. Exp. Cell Res. [Internet]. Elsevier; 2016;343(1):3–6. Available from: http://dx.doi.org/10.1016/j.yexcr.2015.10.037
133. Liang X. Biomechanical Properties of In Vivo Human Skin From Dynamic Optical Coherence Elastography. IEEE Trans Biomed Eng. 2013;57(4):953–9.
134. Handorf AM, Zhou Y, Halanski MA, Li WJ. Tissue stiffness dictates development, homeostasis, and disease progression. Organogenesis. 2015;11(1):1–15.
135. Wei G, Jin Q, Giannobile W V, Ma PX. The enhancement of osteogenesis by nano-fibrous scaffolds incorporating rhBMP-7 nanospheres. Biomaterials. 2007;28(12):2087–96.
136. Kim JK, Kim HJ, Chung JY, Lee JH, Young SB, Kim YH. Natural and synthetic biomaterials for controlled drug delivery. Arch. Pharm. Res. 2014;37(1):60–8.
137. Gupta P, Vermani K, Garg S. Hydrogels : from controlled release to pH-responsive drug delivery. Drug Discov. Today. 2002;7(10):569–79.
138. Fahr A, Liu X. Drug delivery strategies for poorly water-soluble drugs. Expert Opin. Drug Deliv. 2007;4(4):403–16.
139. Pérez P, Gallardo A, Corrigan OI, Román JS. Thermosensitivity of N-isopropylacrylamide hydrogels cross-linked with degradable cross-linker. J. Biomater. Sci. Polym. Ed. 2008;19(6):769–83.
140. Aspirin | HC9H7O4 - PubChem [Internet]. [cited 2020 Mar 19]. Available from: https://pubchem.ncbi.nlm.nih.gov/compound/Aspirin#section=Octanol-Water-Partition-Coefficient
141. Simvastatin | C25H38O5 - PubChem [Internet]. [cited 2020 Mar 19]. Available from: https://pubchem.ncbi.nlm.nih.gov/compound/Simvastatin#section=Octanol-Water-Partition-Coefficient
142. Yang L, Fassihi R. Zero-order release kinetics from a self-correcting floatable asymmetric configuration drug delivery system. J. Pharm. Sci. 1996;85(2):170–3.
143. Bruschi ML. Mathematical models of drug release. Strateg. to Modify Drug Release from Pharm. Syst. 2015. p. 63–86.
144. Bruschi ML. Main mechanisms to control the drug release. Strateg. to Modify Drug Release from Pharm. Syst. 2015. p. 37–62.
145. Dash S, Murthy PN, Nath L, Chowdhury P. Kinetic modeling on drug release from controlled drug delivery systems. Acta Pol. Pharm. - Drug Res. 2010;67(3):217–23.
146. He X, Li J, An S, Jiang C. pH-Sensitive drug-delivery systems for tumor targeting. Ther. Deliv. 2013;4(12):1499–510.
147. Pinto JF. Site-specific drug delivery systems within the gastro-intestinal tract: From the mouth to the colon. Int. J. Pharm. 2010;395:44–52.
148. Bierbrauer F. Hydrogel Drug Delivery: Diffusion Models.
149. Karvinen J, Ihalainen TO, Calejo MT, Jönkkäri I, Kellomäki M. Characterization of the microstructure of hydrazone crosslinked polysaccharide-based hydrogels through rheological and diffusion studies. Mater. Sci. Eng. C [Internet]. Elsevier; 2019;94:1056–66. Available from: https://doi.org/10.1016/j.msec.2018.10.048
150. Sandrin D, Wagner D, Sitta CE, Thoma R, Felekyan S, Hermes HE, Janiak C, De Sousa

Amadeu N, Kühnemuth R, Löwen H, Egelhaaf SU, Seidel CAM. Diffusion of macromolecules in a polymer hydrogel: From microscopic to macroscopic scales. Phys. Chem. Chem. Phys. 2016;18:12860–76.
151. Small Molecule [Internet]. 2020 [cited 2020 Apr 1]. Available from: https://www.astrazeneca.com/what-science-can-do/drug-modalities/small-molecule.html
152. Mellot MB, Searcy K, Pishko M V. Release of protein from highly cross-linked hydrogels of poly(ethylene glycol) diacrylate fabricated by UV polymerization. Biomaterials. 2001;22:929–41.
153. Van Tomme SR, Hennink WE. Biodegradable dextran hydrogels for protein delivery applications. Expert Rev. Med. Devices. 2007;4(2):147–64.
154. Zustiak SP, Boukari H, Leach JB. Solute diffusion and interactions in cross-linked poly(ethylene glycol) hydrogels studied by Fluorescence Correlation Spectroscopy. Soft Matter. 2010;6(15):1–24.
155. Hennink WE, Talsma H, Borchert JCH, De Smedt SC, Demeester J. Controlled release of proteins from dextran hydrogels. J. Control. Release. 1996;39(1):47–55.
156. Dimatteo R, Darling NJ, Segura T. In situ forming injectable hydrogels for drug delivery and wound repair. Adv. Drug Deliv. Rev. [Internet]. Elsevier B.V.; 2018;127:167–84. Available from: http://dx.doi.org/10.1016/j.addr.2018.03.007
157. Ma J, Jemal A. Breast Cancer Statistics. In: Ahmad A, editor. Breast Cancer Metastasis Drug Resist. Prog. Prospect. [Internet]. New York, NY: Springer New York; 2013. p. 1–18. Available from: http://dx.doi.org/10.1007/978-1-4614-5647-6_1
158. Yezhelyev M V., Gao X, Xing Y, Al-Hajj A, Nie S, O'Regan RM. Emerging use of nanoparticles in diagnosis and treatment of breast cancer. Lancet Oncol. 2006;7(8):657–67.
159. Sharma G, Anabousi S, Ehrhardt C, Ravi Kumar MNV. Liposomes as targeted drug delivery systems in the treatment of breast cancer. J. Drug Target. 2006;14(5):301–10.
160. Firer M a, Gellerman G. Targeted drug delivery for cancer therapy: the other side of antibodies. J. Hematol. Oncol. [Internet]. Journal of Hematology & Oncology; 2012 Jan [cited 2013 Mar 9];5(1):70. Available from: http://www.pubmedcentral.nih.gov/articlerender.fcgi?artid=3508879&tool=pmcentrez&rendertype=abstract
161. Webster DM, Sundaram P, Byrne ME. Injectable nanomaterials for drug delivery : Carriers, targeting moieties, and therapeutics. Eur. J. Pharm. Biopharm. [Internet]. Elsevier B.V.; 2013;84(1):1–20. Available from: http://dx.doi.org/10.1016/j.ejpb.2012.12.009
162. Mu Q, Kievet FM, Kant RJ, Lin G, Jeon M, Zhang M. Anti-HER2/neu Peptide-Conjugated Iron Oxide Nanoparticles for Targeted Delivery of Paclitaxel to Breast Cancer Cells. Nanoscale. 2015;7(43):18010–4.
163. Yoo HS, Park TG. Folate-receptor-targeted delivery of doxorubicin nano-aggregates stabilized by doxorubicin-PEG-folate conjugate. J. Control. Release [Internet]. 2004 Nov 24 [cited 2014 Jan 17];100(2):247–56. Available from: http://www.ncbi.nlm.nih.gov/pubmed/15544872
164. Zwicke GL, Ali Mansoori G, Jeffery CJ. Utilizing the folate receptor for active targeting of cancer nanotherapeutics. Nano Rev. 2012;3(1):18496.
165. Geng L, Wang Z, Jia X, Han Q, Xiang Z, Li D, Yang X, Zhang D, Bu X, Wang W, Hu Z, Fang Q. HER2 targeting peptides screening and applications in tumor imaging and drug

delivery. Theranostics. Ivyspring International Publisher; 2016;6(8):1261–73.
166. Ding H, Gangalum PR, Galstyan A, Fox I, Patil R, Hubbard P, Murali R, Ljubimova JY, Holler E. HER2-positive breast cancer targeting and treatment by a peptide-conjugated mini nanodrug. 2016 [cited 2020 Mar 26]; Available from: http://dx.doi.org/10.1016/j.nano.2016.07.013
167. Abbineni G, Modali S. Evolutionary selection of new breast cancer cell-targeting peptides and phages with the cell-targeting peptides fully displayed on the major coat and their effects on actin dynamics during cell internalization. Mol. Pharm. [Internet]. 2010 [cited 2013 May 4];7(5):1629–42. Available from: http://pubs.acs.org/doi/abs/10.1021/mp100052y
168. Gandra N, Abbineni G, Qu X, Huai Y, Wang L, Mao C. Bacteriophage bionanowire as a carrier for both cancer-targeting peptides and photosensitizers and its use in selective cancer cell killing by photodynamic therapy. Small [Internet]. 2013 Jan 28 [cited 2013 May 4];9(2):215–21. Available from: http://www.ncbi.nlm.nih.gov/pubmed/23047655
169. Heitz F, Morris MC, Divita G. Twenty years of cell-penetrating peptides : from molecular mechanisms to therapeutics. Br. J. Pharmacol. 2009;157(October 2008):195–206.
170. Ruseska I, Zimmer A. Internalization mechanisms of cell-penetrating peptides. Beilstein J. Nanotechnol. 2020;11:101–23.
171. Wu H, Zhuang Q, Xu J, Xu L, Zhao Y, Wang C, Yang Z, Shen F, Liu Z, Peng R. Cell-Penetrating Peptide Enhanced Antigen Presentation for Cancer Immunotherapy. Bioconjug. Chem. American Chemical Society; 2019;30(8):2115–26.
172. Hamley IW. PEG-peptide conjugates. Biomacromolecules [Internet]. 2014 May 12;15(5):1543–59. Available from: http://www.ncbi.nlm.nih.gov/pubmed/24720400
173. Singh R, Lillard JW. Nanoparticle-based targeted drug delivery. Exp. Mol. Pathol. [Internet]. Elsevier Inc.; 2009;86(3):215–23. Available from: http://dx.doi.org/10.1016/j.yexmp.2008.12.004
174. Peracchia MT, Fattal E, Desmaële D, Besnard M, Noël JP, Gomis JM, Appel M, D'Angelo J, Couvreur P. Stealth(®) PEGylated polycyanoacrylate nanoparticles for intravenous administration and splenic targeting. J. Control. Release. 1999;60(1):121–8.
175. Wei Y, Ji Y, Xiao LL, Lin QK, Ji J. Different complex surfaces of polyethyleneglycol (PEG) and REDV ligand to enhance the endothelial cells selectivity over smooth muscle cells. Colloids Surfaces B Biointerfaces [Internet]. Elsevier B.V.; 2011;84(2):369–78. Available from: http://dx.doi.org/10.1016/j.colsurfb.2011.01.028
176. Suga T, Fuchigami Y, Hagimori M, Kawakami S. Ligand peptide-grafted PEGylated liposomes using HER2 targeted peptide-lipid derivatives for targeted delivery in breast cancer cells: The effect of serine-glycine repeated peptides as a spacer. Int. J. Pharm. [Internet]. Elsevier B.V.; 2017;521(1–2):361–4. Available from: http://dx.doi.org/10.1016/j.ijpharm.2017.02.041
177. McKinney R, Thacker L, Hebert GA. Conjugation methods in immunofluorescence. J. Dent. Res. 1976;55(A):38–44.
178. Fluorescein (FITC) | Thermo Fisher Scientific - US [Internet]. [cited 2020 Apr 7]. Available from: https://www.thermofisher.com/us/en/home/life-science/cell-analysis/fluorophores/fluorescein.html#
179. Kondo E, Saito K, Tashiro Y, Kamide K, Uno S, Furuya T, Mashita M, Nakajima K, Tsumuraya T, Kobayashi N, Nishibori M, Tanimoto M, Matsushita M. Tumour lineage-homing cell-penetrating peptides as anticancer molecular delivery systems. Nat. Commun.

[Internet]. Nature Publishing Group; 2012;3:913–51. Available from: http://dx.doi.org/10.1038/ncomms1952
180. Théry C, Zitvogel L, Amigorena S. Exosomes: Composition, biogenesis and function. Nat. Rev. Immunol. 2002;2(8):569–79.
181. Simons M, Raposo G. Exosomes - vesicular carriers for intercellular communication. Curr. Opin. Cell Biol. 2009;21(4):575–81.
182. Wang SH, Lu L, Fan Y, Wicha MS, Cao Z, Chang AE, Xia J, Jr JRB, Li Q. Characterization of a Novel Transgenic Mouse Tumor Model for Targeting HER2 + Cancer Stem Cells. Int. J. Biol. Sci. 2014;10(1):25–32.